TURUN
YLIOPISTO
UNIVERSITY
OF TURKU

NOVEL INSIGHTS INTO FILOPODIA FUNCTION

A focus on integrin and F-actin regulation

Mitro Miihkinen

TURUN YLIOPISTON JULKAISUJA – ANNALES UNIVERSITATIS TURKUENSIS
SARJA – SER. D OSA – TOM. 1585 | MEDICA – ODONTOLOGICA | TURKU 2021

TURUN
YLIOPISTO
UNIVERSITY
OF TURKU

NOVEL INSIGHTS INTO FILOPODIA FUNCTION

A focus on integrin and F-actin regulation

Mitro Miihkinen

TURUN YLIOPISTON JULKAISUJA – ANNALES UNIVERSITATIS TURKUENSIS
SARJA – SER. D OSA – TOM. 1585 | MEDICA – ODONTOLOGICA | TURKU 2021

University of Turku

Faculty of Medicine
Anatomy and Cell Biology
Drug Research Doctoral Programme

Supervised by

Professor, Johanna Ivaska
Turku Bioscience Centre,
University of Turku and Åbo Akademi
Turku, Finland

Docent, PhD, Guillaume Jacquemet
Turku Bioscience Centre,
Åbo Akademi
Turku, Finland

Reviewed by

PhD, Jenny Gallop
University of Cambridge
Cambridge, United Kingdom

Professor Vesa Hytönen
University of Tampere
Tampere, Finland

Opponent

Professor Staffan Strömblad
Karolinska Institutet
Stockholm, Sweden

ISBN 978-951-29-8626-2 (PRINT)
ISBN 978-951-29-8627-9 (PDF)
ISSN 0355-9483 (Print)
ISSN 2343-3213 (Online)
Painosalama, Turku, Finland 2021

To all my friends and family.
To people who make life meaningful.

UNIVERSITY OF TURKU
Faculty of medicine
Cell biology and anatomy
Drug research doctoral programme
Turku Bioscience Centre
MITRO MIIHKINEN: Novel insights into filopodia function – A focus on integrin and F-actin regulation
Doctoral dissertation 236 p, November 2021

ABSTRACT

Filopodia are actin-rich cell protrusions that are extended from the plasma membrane by different cell types in order to sense the surrounding environment. In cancer cells, the emergence of filopodia supports metastasis, while in neuronal cells filopodia help to form synapses by probing adjacent cells for suitable presynaptic partners. Filopodia can make contact with the extracellular matrix with small, integrin-mediated adhesions located at their tips. During cancer invasion, recognition of the extracellular matrix by filopodia not only supplies migrating cells with guidance cues but has also been linked with increased colony growth at the metastatic site. In neuronal cells, inhibition of integrin activity has been shown to negatively impact synapse formation. Although both filopodia and integrin-positive adhesions have roles in metastasis or in synaptogenesis, filopodial adhesions remain under-studied cellular structures and there exists minimal literature on how these adhesions are regulated or how they function. The objective of this study was to reveal novel regulatory mechanisms of filopodia by studying two integrin and filopodia linked proteins: myosin-X and SHANK3. The work presented here provides fundamental information on how 1) integrins are activated at filopodia tips, 2) which integrin-linked proteins are recruited to adhesions at filopodia providing a road-map to classify these adhesions and 3) how SHANK3, an F-actin network organizer and filopodia regulator, modulates the crosstalk between integrin and F-actin via direct and conformationally regulated binding with F-actin. The thesis also provides novel methodology in the form of a high-end biochemical binding assay (4) where protein binding to integrin tails can be interrogated in the presence of a lipidic membrane.

KEYWORDS: Filopodia, integrins, myosin-X, SHANK3, assay development

TURUN YLIOPISTO
Lääketieteen tiedekunta
Solubiologia ja anatomia
Lääketutkimuksen tohtoriohjelma
Turku Bioscience
MITRO MIIHKINEN: Solun filopodien toiminta
Väitöskirja 236 sivua, lokakuu 2021

TIIVISTELMÄ

Filopodit ovat solukalvon pullistumia, joita täyttää sisältäpäin solun aktiinitukiranka. Filopodit syntyvät solukalvon pullistuessa ulospäin aktiinitukirangan vaikutuksesta ja solut käyttävät niitä ympäristönsä aistimiseen käyttämällä filopodien kärjissä sijaitsevia tarttumisreseptoreja - integriinejä. Syövän leviämisen aikana solujen kyky tunnistella ympäröivää soluväliainetta tarjoaa solulle tarkkaa tietoa sen ympäristöstä, ohjaten solun kulkua vaikeassa 3-ulotteisessa soluväliaineen verkostossa. Toisaalta hermosolut käyttävät filopodeja naapurisolujensa (tai ympäröivän kudoksen) tarkasteluun hermoliitosten muodostusprosessissa. Vaikka filopodit ja integriini-reseptorit ohjaavat sekä syövän leviämistä ja aivojen normaalia toimintaa, filopodien välittämien integriini-positiivisten soluadheesioiden synty tunnetaan huonosti. Lisäksi filopodien soluadheesioiden säätely sekä vaikutukset solun toiminnalle ovat heikosti ymmärrettyjä tapahtumasarjoja. Tämän väitöskirjatyön tarkoituksena oli ymmärtää filopodien solullisia säätelyketjuja paremmin tutkimalla kahta integriineihin ja filopodeihin aiemmin liitettyä proteiinia: myosiini-X ja SHANK3. Tässä väitöskirjatyössä esitetyt tulokset tuovat täysin uutta tietoa seuraavista tapahtumista: 1) miten filopodit muodostavat adheesioita soluväliaineen kanssa 2) mitkä solun adheesioproteiinit sijoittuvat filopodien kärkiin adheesiomuodostus-prosessin aikana sekä 3) kuinka SHANK3 proteiini säätelee samanaikaisesti solun aktiinitukirankaa ja integriiniaktiivisuutta. Lisäksi väitöskirja sisältää menetel-mällisen julkaisun uudesta biokemiallisesta koeasetelmasta, jonka avulla voidaan paremmin tutkia solun proteiinien sitoutumista integriinireseptoreihin solukalvon läheisyydessä.

AVAINSANAT: filopodi, integriinit, myosiini-X, SHANK3, uudet koeasetelmat.

Table of Contents

Abbreviations

IPTG	Isopropyl-β-D-thiogalactoside
TCEP	Tris(2-carboxyethyl)phosphine hydrochloride
PMSF	Phenylmethanesulfonyl fluoride
AEBSF	4-(2-aminoethyl)benzenesulfonyl fluoride hydrochloride
DNAse	Deoxyribonuclease
DDM	n-dodecyl-β-D-maltoside
ECM	Extracellular matrix
VEGF-A	Vascular endothelial growth factor A
EMT	Epithelial to mesenchymal transition
2D	2-dimensional
3D	3-dimensional
MAT	Mesenchymal to amoeboid transition
Arp2/3 complex	Actin related protein 2/3 complex
F-actin	Filamentous actin
WH2	Wiskott-aldrich homology 2
NPF	Nucleating promoting factor
WASP	Wiskott–Aldrich syndrome protein
GTP	Guanosine-5'-triphosphate
Rac1	Ras-related C3 botulinum toxin substrate 1
Cdc42	Cell division control protein 42 homolog
RhoA	Transforming protein RhoA
WAVE	Wiskott-Aldrich syndrome protein family member
Rap1	Ras-related protein Rap1
IAC	Integrin-mediated adhesion complex
BioID	Proximity-dependent biotin identification
iPALM	Interferometric photoActivated localization microscopy
VASP	Vasodilator-stimulated phosphoprotein
RIAM	Rap1-Interactive Adaptor Molecule
FAK	Focal adhesion kinase 1
PC	Phosphatidylcholine
PS	Phosphatidylserine

PE	Phosphatidylethanolamine
PI	Phosphatidylinositol
DAG	Diacylglycerol
PH	Pleckstrin homology
PI3K	Phosphoinositide 3-kinase
Akt	Protein kinase B
mTOR	The mechanistic target of rapamycin
FMNL	Formin-like protein
IRSP53	Insulin-resistance substrate 53 kDa
BMP	Bone morphogenetic protein
CXCL12	C-X-C motif chemokine 12
cAMP	Cyclic AMP
AMP	Adenosine monophosphate
PIP	Phosphoinositide phosphate
NF-kb	Nuclear Factor kappa B
TGFβ	Transforming growth factor beta
EGFP	Enhanced green fluorescent protein
DMEM	Dulbecco's modified Eagle's medium
FBS	Fetal bovine serum
PEI	Polyethylenimine
HBSS1	Hank's Balanced Salt Solution
DIV	Days in vitro
TBS	Tris buffered saline
PBS	Phosphate buffered saline
RNA	Ribonucleic acid
DNA	Deoxyribonucleic acid
cDNA	Complementary DNA
RT-PCR	Real time polymerase chain reaction
mRNA	Messenger RNA
GST	Glutathione S-transferase
DBP	Vitamin D binding protein
ATP	Adenosine triphosphate
MBP	Maltose-binding protein
PMT	Photomultiplier tube
FACS	Fluorescence-activated cell sorting
HPLC	High-performance liquid chromatography
MS	Mass spectrometry
FERM	F for 4.1 protein, E for ezrin, R for radixin and M for moesin
Lpd	Lamellipodin
SDS	Sodium dodecyl sulphate

FSC	Forward scatter
SSC	Side scatter
ProLIF	Protein-Liposome interactions by Flow cytometry
ARR	Ankyrin repeat region

List of Original Publications

This dissertation is based on the following original publications, which are referred to in the text by their Roman numerals:

I MIIHKINEN M, Grönloh MLB, Vihinen H, Jokitalo E, Goult B, Ivaska J, Jacquemet G. Myosin-X and talin modulate integrin activity at filopodia tips. *BioRxiv*. Manuscript.

II Jacquemet G, Stubb A, Saup R, MIIHKINEN M, Kremneva E, Hamidi H, Ivaska J. Filopodome mapping identifies p130Cas as a mechanosensitive regulator of filopodia stability. 2019. *Current biology*.

III Salomaa SI, MIIHKINEN M, Kremneva, E, Lilja, J, Jacquemet, G, Vuorio, J, Hassani-Nia, F, Hollos, P, Isomursu, A, Vattulainen, I, Coffey, E, Kreienkamp, HJ, Lappalainen, P, Ivaska, J. Conformational dynamics regulate SHANK3 actin and Rap1 binding. *BioRxiv*. Manuscript.

IV De Franceschi N*, MIIHKINEN M*, Hamidi H, Alanko J, Mai A, Picas L, Guzman C, Levy D, Mattjus P, Goult B, Goud B, Ivaska J. ProLIF - quantitative integrin protein-protein interactions and synergistic membrane effects on proteoliposomes. 2018. *Journal for Cell Science*. * indicates equal contribution.

1 Review of the literature

1.1 Cellular movement

1.1.1 Cellular movement in health and disease

Cell migration is one of the fundamental requirements for multicellular life. While the well-coordinated and balanced movement of cells and embryonic tissues completely restructures the developing embryo, pathological cell migration drives undesirable events such as cancer metastasis (Scarpa and Mayor 2016; Horwitz and Webb 2003). Early in embryonic development, the appearance of a small groove in the epiblast layer of the embryo marks the beginning of an event known as gastrulation. In gastrulation, the collective and individual movements of epiblast cells form a three-layered sandwich-like structure sealing the cell faith for each cell in a layer-specific manner. The cells in the three germ layers (called endo- meso- and ectoderm) will later give rise to different adult tissues predefined by their site of origin (Solnica-Krezel and Sepich 2012). To contrast the early cell migration events of an embryo, cell migration of nerve endings in the brain or in the body starts after 10–12 weeks of development but continues well into adulthood in restricted brain regions such as in the hippocampus (Ghashghaei, Lai, and Anton 2007). Axon pathfinding in the brain provides a stunning example of directional cell migration where the nerve fibers (axons) sent out by neuronal cells use external cues to navigate and reach their correct targets – sometimes crossing the midline to the opposite hemisphere of the brain (Stoeckli 2018).

Once cells start to differentiate into specific lineages, programs driving cell migration are turned off (F. Wu et al. 2020, 1). The immune system, however, offers the most striking example of dynamic cell migration in adult animals as leukocytes patrol the body for recognizable pathogens. Although most adult cells are mainly static, trauma or injury in a tissue can re-activate transcriptional programs driving coordinated movement of cells to seal wounds (Schäfer and Werner 2007), build blood vessels (Hashiya et al. 2004) or supply newly repaired tissue neuronal connections (Llorens-Bobadilla et al. 2015). Wound healing is one of the best-studied cell migration processes where both skin and blood vessel epithelium move as uniform sheets to close the wound and supply the newly generated tissue with sufficient blood

flow. Interestingly, one of the hallmarks of cancer is the tumour's ability to support angiogenesis – the formation of new blood capillaries - to supply the tumour with nutrients (Hanahan and Weinberg 2011). Angiogenesis, like wound healing, has been extensively studied for its physiological importance and distinct morphology where vascular endothelial growth factor (VEGF-A) causes characteristic morphological features of a migrating blood vessel where leader cell, studded with extensions called filopodia guide the cells in the vessel stalk (Gerhardt et al. 2003).

Whereas tumour cells can induce cell migration of their neighbouring cells, the invasion and metastasis of cancer cells themselves largely dictates the prognosis of the patient. Metastasis is a highly cell migration dependent event where cancer cells can re-activate some of the evolutionary programs gaining motility (Hanahan and Weinberg 2011). Thus, the mechanisms of cell migration and how cancer cells move are fundamental aspects in understanding cancer biology.

1.1.2 Collective versus single-cell migration

Cells during development and in cancer can move as individuals (McDole et al. 2018; Jacquemet et al. 2013) or as collective sheets (Omelchenko, Hall, and Anderson 2020; Jacquemet et al. 2017). Cells migrating collectively are less sensitive to cell intrinsic factors in their migration and the migration is rather defined by the interactions cells make with their neighbours. Thus, collectively migrating cells display many population-level characteristics, such as collective polarization, mechanical coupling and decision making (Ladoux and Mège 2017).

Although, most cell migration events *in vivo* during development or in patients samples are collective, cancer dissemination has been classically characterized as migrating single cells where carcinoma cells activate epithelial-to-mesenchymal transcriptional (EMT) program to promote E-cadherin downregulation while obtaining a spindle-like, pro-migratory, mesenchymal phenotype. Initially identified by developmental genetics, EMT is driven by a set of transcription factors (Snail, Slug, Twist, and Zeb1/2) and supported by frequently observed downregulation of E-cadherin in human carcinomas (Hanahan and Weinberg 2011). Lately, however, as collective cell migration has been recognized as a tumour invasion mechanism (Y. Yang et al. 2019) and cancer cells with varying levels of EMT have been reported to metastasize (Pastushenko et al. 2018), a hybrid EMT has been coined as a term to explain the spectra of mild to strong EMT phenotypes observed in cancer.

What defines collective migration has been a topic of extensive study. In some collectively migrating cell systems, such as during sprouting angiogenesis, leader cells localised at the tip of the sprouting vessel guide cell migration of the collective pack in a VEGF-dependent manner. The VEGF gradient has been shown to upregulate filopodial protrusions in leader cells and the loss of these protrusions

leads to defected blood-vessel formation. The leader-follower cell polarity is clearly observed in other systems as well, such as in invading lung cancer spheroids. Here, the epigenetic rewiring in leader cells during collective migration support the migration of the whole sheet as the leaders upregulate thin, pro-migratory protrusions such as filopodia and shape the ECM in front of the migrating cell sheet (Summerbell et al. 2020). Interestingly, and similar to leader cells, also individually migrating cells upregulate can upregulate filopodial protrusions as a response to chemokine gradients, indicating that filopodia formation can support both individual and collective migration (Meyen et al. 2021).

Leader cell position is not necessarily fixed. The cells that sense the highest chemotactic gradient will become leader cells but competition within the monolayer for the leader-cell position have been reported. In fact, exchange of leader cells at the tip of sprouting angiogenic endothelial cells have been thought to be a cooperative strategy to maximize cell interaction with the chemogradient (Jakobsson et al. 2010; Riahi et al. 2015). The expression of certain proteins such as Keratin-14 has been shown to give cells an advantage in the competition of the leader cell position as breast cancer cells with high Keratin-14 expression will polarize to the leading edge and guide collective migration (Hwang et al. 2019)

Even though the leader-follower identities can be observed during collective migration, the confinement-promoted collective migration of neural crest cells does not rely on actively functioning leader cells (Szabó et al. 2016; Szabó and Mayor 2016). Also seemingly unrelated cell types such as fibroblasts have been shown to situate themselves at the front of collectively migrating cell sheet guiding the migration. (Labernadie et al. 2017). Single cell and collective migration are schematically presented in Figure 1.

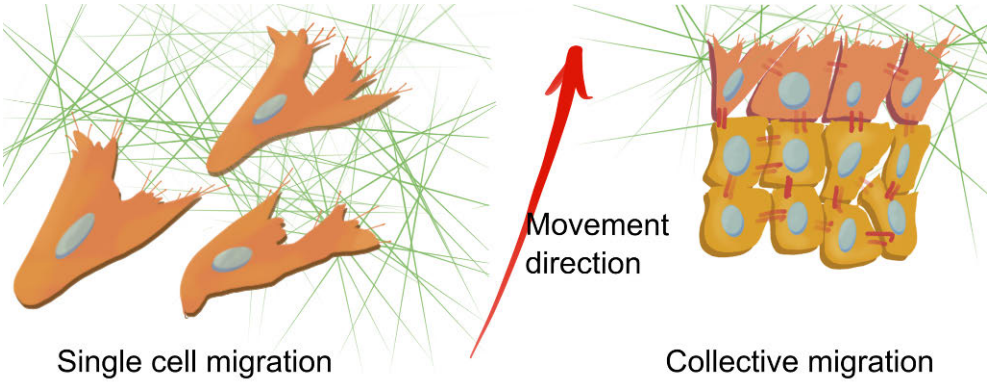

Figure 1. Cells can migrate in either single cells (left) or in collective fashion (right). Although increased cell-cell interaction can promote collective cell migration in some settings, it is not a general requirement for collective migration. Direction of migration is shown by the red arrow. Adapted from (Jiang et al. 2021).

1.1.3 Different modes of cell migration

Collective cell migration has implications in many areas in biology, but historically it has been easier to isolate and study systems that migrate as single cells. A lot of focus has thus been given to look at single cell migration systems. Although cells plated on 2D coverslips have revealed a multitude of conceptual advances into how cells traverse on top of a surface, it has become eminent that ECM and its dimensionality by large regulates cellular movement (Yamada and Sixt 2019; Rhee 2009). Single fibroblast cells on a 2D coverslip often display a stereotypical mode of migration that's characterized by repetitive cellular extension, contraction and release of the trailing edge where cells can extend their membrane using one of the four possible protrusions: lamellipodia, filopodia, membrane blebs or invadopodia (Ridley 2011). How cells extend their plasma membrane defines the different extremes of how migration modes are defined. Noteworthy, the existence of filopodia does not relate to any specific migration mode but filopodia can be detected in cells despite their mode of migration (Petrie and Yamada 2012). Different migration modes are depicted in figure 2.

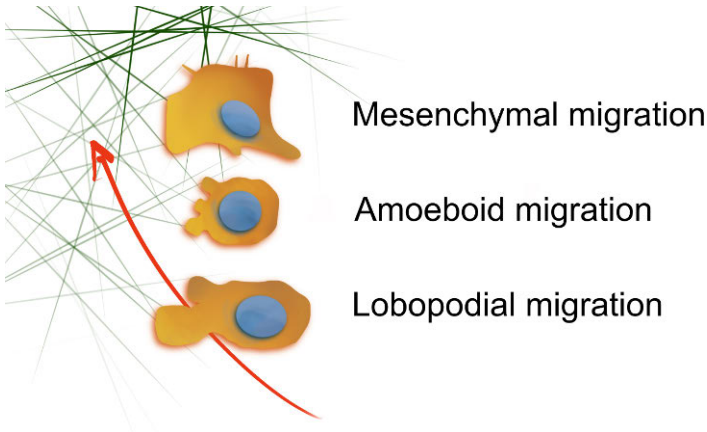

Figure 2. Examples of different migration modes used by cells. Whereas mesenchymal migration is heavily dependent on adhesion, amoeboid migration is characterized by weak adhesion with the surrounding ECM but depends on other factors such as compression of the ECM. Lobobodial protrusions are regulated by intracellular pressure. Adapted from (Conway and Jacquemet 2019).

Mesenchymal migration driven by lamellipodia extension is the classical mode of migration described first in microscopy studies in the 1970's (Abercrombie, Heaysman, and Pegrum 1970). Later studies have shown that it is also characterized by protease activity at the leading edge and reliance on integrin-mediated cell adhesion (Wolf et al. 2013). On the contrary, amoeboid migration is mostly

characterized by low adhesion to the surrounding substrate and named after high resemblance to the movement of protist unicellular amoebas (Y.-J. Liu et al. 2015). Although displaying low-adhesion properties, ameoboidally migrating cells rely on contractility but are only seen in 3D or under confinement (Wyckoff et al. 2006). During lopobodic movement, intracellular pressure driven membrane blebs propel the plasma membrane forward to exert pulling forces on the cell (Yamada and Sixt 2019). The complex structure of the non-cellular constituent of a tissue, the ECM, poses a challenge for the migrating cell. Depending on the composition and morphology of the ECM, cells have been known to adapt their migration accordingly (Wolf et al. 2013). In addition, setting restrictions for a cell, such as inhibition of protease activity, cells have been observed to change using more ameboid migration mode instead of mesenchymal in a process termed as mesenchymal to ameboid transition (MAT) (Wolf et al. 2003).

Although different protrusions can define locomotion modes used by a cell in simpler settings, In vivo, many cell types can rapidly and flexibly interconvert itself between these definitions or display multiple protrusion types. (T.-L. Liu et al. 2018; Petrie and Yamada 2012). Although definitions of distinct migration modes are useful, it can be difficult to classify *in vivo* migrating cell into only one of these categories. Figure 3 shows a sketch of an immune cell and its outer boundaries while it is navigating in a tissue.

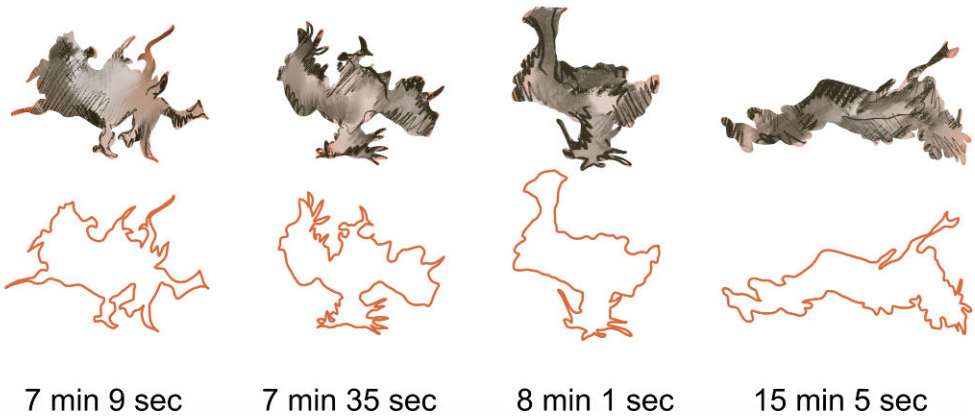

Figure 3. A sketch of an immune cell migrating in vivo. Although different protrusion types are well defined in simpler settings, in vivo migrating cells may flexibly use multiple protrusions while moving inside a tissue. Adapted from a microscopy study (Liu et al., 2018). Orange lines display the outlines of the moving cell. Also other cells, such as cancer cells, that navigate adult tissues do not strictly fit into just one classical migration modes.

1.1.4 Pathways driving pro-migratory protrusions

Most protrusions are driven via F-actin network assembly. In cellular protrusions and overall, the shape of cellular F-actin network is largely regulated by F-actin nucleating factors and the type of nucleator involved largely defines the morphological features of the actin network it nucleates (Rottner et al. 2017). The classical actin nucleators are Arp2/3 complex (branched network) and formin family of nucleators (linear bundles). In addition, proteins such as Spire or Cobl having WH2 domains in tandem repeats have been implicated in actin nucleation but it is also argued they only play auxiliary roles in these processes (Dominguez 2016). To regulate lamellipodial actin network formation, Arp2/3 complex needs to unite with nucleating promoting factors (NPF), mainly WASP (Wiskott–Aldrich syndrome protein) family proteins to stimulate Arp2/3 complex function (Padrick et al. 2011). Although Arp2/3 complex is a classical branched network nucleating factor, its association with Dip NPF has been reported to promote the formation of de novo linear filaments that could then function as mother filaments for branched network nucleation (Balzer et al. 2019). To contrast Arp2/3 complex-driven branched actin network formation, formin-family of actin nucleators nucleate linear actin bundles. Formins are shaped as a circular dimer that stays attached with the extending branched F-actin end protecting the end from de-polymerization and promoting further extension of the end from profilin-bound G-actin monomers (Breitsprecher and Goode 2013).

Upstream of most actin nucleating factors are a protein family of Rho-family GTPases. Although there are 20 Rho-family GTPases most of which can shape F-actin network, Rac1, Cdc42 and RhoA are the three most studied Rho-family GTPases in the context of cell migration (Ridley 2011). In a migrating cell, Rho GTPases form a complex signaling network but when expressed alone Rac1, Cdc42 or RhoA can induce the formation of lamellipodia, filopodia or stress fiber structures, respectively. Expression of Rac1 drives lamellipodia formation through its binding with WAVE complex leading to Arp2/3 complex activation whereas multiple pathways supporting filopodia formation by Cdc42 have been reported (J. Peng et al. 2003, 42; Krugmann et al. 2001, 42; Bohil, Robertson, and Cheney 2006). In summary, dozens of proteins are known to bind actin and control essentially every step of F-actin assembly and disassembly (Pollard 2016) and their dynamics are regulated by cell intrinsic and external factors via GTPases. Even though specialized labs have made massive progress in the field, systems view models of how actin binding proteins collectively orchestrate F-actin network assembly are lacking.

1.1.5 Integrin receptors as mediators of cell-ECM attachment

The extracellular matrix (ECM) is an intricate meshwork of fibrous and other proteins that together form a structurally stable scaffold for cells to adhere to (Yue et al. 2014). The core matrisome (proteins in the extracellular matrix) consists of ~300 proteins, some of which function as ligands for cell-ECM adhesion (Hynes et al. 2012). Collagen and fibronectin are two of such proteins (Yue et al. 2014, Hynes et al. 2012). Although cell-cell adhesion is often a defining factor for collectively migrating cells, cell-ECM adhesion drives cytoskeletal rearrangements and promotes cellular protrusions while maintaining friction between the cell and extracellular substrate. Integrins are key mediators of ECM and cytoplasmic F-actin networks owing to their ability to interact with ECM ligands outside of the cells and to connect to the actin cytoskeleton via proteins recruited to their intracellular domains (Bachmann et al. 2019). In addition to mediating cell adhesion, active integrin receptors control migration, survival and differentiation of cells via their downstream signaling pathways (Watt and Fujiwara 2011; Kechagia, Ivaska, and Roca-Cusachs 2019).

Integrin family of transmembrane receptors are key adhesion receptors to mediate cell-ECM attachment during cell migration. The family consists of multiple α and β subunits form obligate heterodimers with each other. In a tissue-specific manner human cells express a subset of 24 different integrin heterodimers with distinct preferences and affinities for different ECM ligands. Integrin receptors have a large extracellular head, a single-pass transmembrane receptor and a small carboxy-terminal tail where the extracellular head defines binding specificity toward ECM ligands while the tail recruits intracellular adaptor proteins to drive cell adhesion formation (Humphries, Byron, and Humphries 2006). For most integrin heterodimers, the conformation of the receptor and extracellular domains define the adhesive state of the molecule with inactive conformation having a low affinity towards the favourable ECM ligand (Sun, Costell, and Fässler 2019a). In addition, integrin receptors are constantly recycled between the plasma membrane and cytoplasmic pools which regulates their availability (Sahgal et al. 2019; Ratcliffe et al. 2016).

The conformation of an integrin receptor is dynamically controlled by both cytoplasmic adaptor proteins and ECM ligand availability (Takagi et al. 2002) where talin is the best studied cytoplasmic adaptor protein for integrin receptors. Talin binding to integrins induces conformational activation of the receptor (Shattil, Kim, and Ginsberg 2010). Talin is recruited to the plasma membrane through direct or indirect interactions with small GTPase Rap1 where its binding to β-integrin tails promotes separation of α-β integrin tails with the simultaneous extension of the extracellular integrin domains (Shattil, Kim, and Ginsberg 2010; Lagarrigue, Kim,

and Ginsberg 2016; Gingras et al. 2019, 1). Once activated by talin, a versatile group of cytoplasmic proteins are recruited to talin/integrin complex coupling the ECM-bound receptor with cellular F-actin network (Humphries et al. 2007). Individual receptors are also clustered together forming adhesive plaques (Welf, Naik, and Ogunnaike 2012). During cell migration, new adhesions form at the very front of the cell in lamellipodia or filopodia. Named as nascent adhesions, the newly formed adhesions will stay attached to the ECM and maturate over time while the cell simultaneously crawls forward (Geiger and Yamada 2011). While the cell moves forward, the integrin-tail binding complex changes and individual receptors are clustered together to form focal adhesions and in some cases fibrillar adhesions (Welf, Naik, and Ogunnaike 2012; Georgiadou et al. 2017). The maturation of these adhesions is not orchestrated by cytoplasmic integrin tail adaptors alone but requires cell-generated forces (actomyosin contraction) as Blebbistatin treatment prevents focal adhesion formation (Pasapera et al. 2010). The disassembly of focal adhesions is perhaps a less-studied phenomenon but seems to be calcium and microtubule dependent (D'Souza et al. 2020; Yue et al. 2014). Also proteolysis of talin via calpain is implicated to contribute to adhesion disassembly (Dourdin et al. 2001; A. Huttenlocher et al. 1997). Adhesion turnover can be increased in a FAK-mediated manner by transiently decreasing Rho activity or decreased by inhibiting microtubule polymerization leading to large adhesions (X. Wu, Kodama, and Fuchs 2008; Ren et al. 2000; Schober et al. 2007)

1.1.6 Integrin adhesome

The dynamic complex assembled around activated integrin cytoplasmic tails is called the adhesome, or integrin-mediated adhesion complex (IAC), and consists of potentially hundreds of cytosolic proteins. There exists curated mass-spectrometry and literature-based network models of the integrin adhesome (Winograd-Katz et al. 2014; Horton et al. 2016; 2015). To simplify this, efforts towards mapping the "core" adhesome has been done. These core adhesome components are proteins that are linked to fibronectin-bound integrin tails over a wide range of conditions in a cell type nonspecific way and consist of a list of 60 proteins (Horton et al. 2015). Whereas the adhesome work was done by purifying the ECM-bound adhesion complexes, lately proximity proteomics has been employed to study integrin-associated protein networks in intact cells. By using already validated IAC proteins as bait, recent work using BioID (Roux et al. 2018) has provided more depth into structure and composition of integrin-associated protein networks (Chastney et al. 2020). Proximity-biotinylation offers a toolkit for integrin biology to restrict mass spectrometry into a single type of adhesion in a cell - a major advantage over other adhesion purification methods.

Recent work has shown that filopodial adhesions are distinct from any other adhesions in a cell when classified based on the core adhesome components (Jacquemet et al. 2019, 130). Because integrin adhesome is dependent on the type of ECM and integrin receptor, future research will likely map integrin adhesome for specific integrin receptors or specific adhesions under changing conditions, such as on different ECM matrices (Horton et al. 2016).

Microscopy has been used to generate spatial models of an integrin adhesion. iPALM microscope based in interference as a physical phenomenon, can obtain images with a z-resolution in tens of nanometers and by imaging integrin, known cytosolic adhesome proteins (FAK, paxillin, talin, vinculin, zyxin, VASP, α-actinin) and actin, the distance of each component from the underlying glass-surface and from each other has been mapped in a "vertical" integrin adhesion model for different cell types. Comparison of the studies show how differences in adhesion architecture translate into differences in integrin adhesion function. How unique adhesions such as adhesions in filopodia are vertically organized is not understood (Stubb et al. 2019; Kanchanawong et al. 2010).

1.1.7 Integrin conformational switch: regulatory mechanisms governed by intracellular regulators

Integrin conformation affects the adhesiveness of the majority of integrin heterodimers and is under strict regulation. In the absence of activating signals, many key adhesome proteins adopt an autoinhibited form to prevent premature integrin activation (Khan and Goult 2019). Integrin activation, i.e. obtaining the highly-adhesive conformation, is a result of multiple signaling pathways integrated down to talin and kindlin whose binding to β-integrin tail constitutes the final steps of integrin activation (Shattil, Kim, and Ginsberg 2010; Bachmann et al. 2019). Both talin and kindlin are known to adopt a autoinhibitory conformation. Talin adopts a head-to-tail autoinhibited conformation where its membrane and integrin binding domains are embedded inside the molecule while binding sites for Rap1 adapter RIAM, remain accessible supporting Rap1/RIAM-mediated membrane localization of inactivated talin (Dedden et al. 2019). Release of talin head-to-tail inhibitory clasp reveals integrin binding FERM domain of the molecule and the opening of the clasp together with stretching of molecule reveals binding sites for adaptor proteins such as vinculin (Goult et al. 2009; Atherton et al. 2019). Integrin co-activator kindlin forms a trimeric autoinhibition complex when not bound with integrins (Li et al. 2017). Also many other integrin adhesion molecules such as vinculin have been known to obtain auto-inhibited conformation (X. Peng et al. 2011, Khan and Goult 2019)).

Advanced microscopy studies reveal that autoinhibited proteins such as talin and vinculin can be first recruited to the sites of nascent adhesions by paxillin, where the release of talin auto-inhibition and subsequent binding to integrin and vinculin leads to engagement of integrin receptors to actomyosin traction machinery (Atherton et al. 2019). Interestingly, talin is observed to be a core component of the filopodia-tip complex and suggested to activate integrin receptors at filopodia tips (Lagarrigue et al. 2015). However, talin's role in filopodia tip adhesions remains to be poorly characterized. Furthermore, Rap1-interacting adapter molecule RIAM also adopts a switchblade type of auto-inhibition where an inhibitory sequence at its N-terminus masks the Rap1-binding and potentially restricts integrin activity. The opening of the structure has not been well characterized but has been thought to be relieved via phosphorylation by FAK kinase (Chang et al. 2019). Talin autoinhibition can also be relieved via proteolytic cleavage. For example, recent work shows that talin undergoes calpain-mediated proteolysis that's important for adhesion maturation and growth signaling (Saxena et al. 2017). Finally, post-translational modifications are likely to contribute to regulation of autoinhibition. For example, talin head has a long loop which regulates integrin binding and integrin activation and is likely controlled via phosphorylation (Kukkurainen et al. 2020).

Integrin cytoplasmic tails are important hubs of regulation as the binding of cytoplasmic adaptors such as talin regulates integrin active-inactive conformation. The cytoplasmic tails are short sequences of tens of amino acids and share conserved motifs for protein-protein interactions. The differences in cytoplasmic tail sequences result in recruitment of diverse molecular complexes between different integrin heterodimers and facilitate heterodimer specific integrin signaling (Morse, Brahme, and Calderwood 2014). The short and conserved motifs in both α and β-integrin tails have been a focus of intensive studies as they recruit key proteins that regulate integrin function across the integrin family. Whereas most β-integrin tails contain two NPxY motifs for talin and kindlin binding, the α-tail GFFKR motif recruits adaptors that either support integrin inactivation (Rantala et al., 2011) or regulate integrin endocytosis (De Franceschi et al. 2016; Pellinen et al. 2006). Figure 4 shows how different cytoplasmic proteins bind integrin tails. The phosphorylation of tyrosine or threonine residues in β-integrin tails adds to the complexity as phosphorylation has been shown to alter the binding of subsets of integrin tail binding proteins by e.g. increasing Dok1 binding 100-fold (Oxley et al. 2008, 1; Takala et al. 2008; J. Liu et al. 2015). Although, the functional consequences of negatively charged lipid membrane in talin-mediated integrin activation are appreciated, how the plasma membrane supports integrin-receptor function after its activation remains understudied.

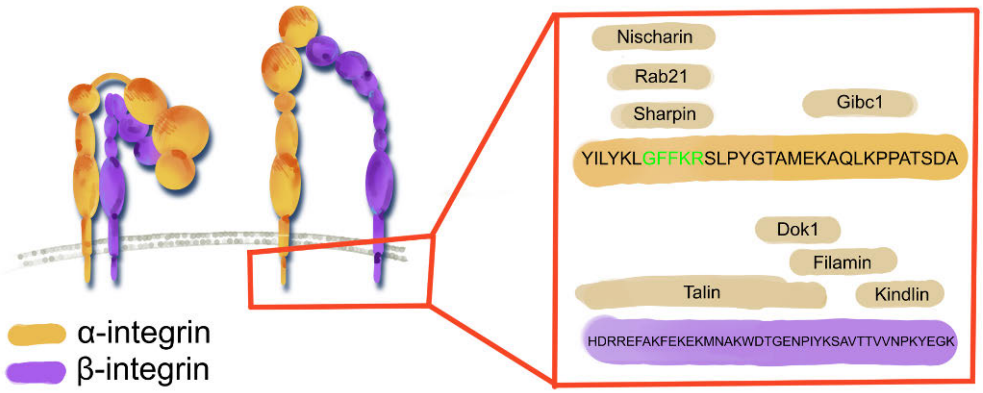

Figure 4. Integrins can adopt a closed bent conformation (right) or an elongated active conformation, where the movement of ectodomains is accompanied by a separation of both transmembrane domains and intracellular tails (left). The activation status is regulated by integrin tail binding proteins. Because of the small size of integrin tails and large number of interactors, there exists competition between cytoplasmic proteins binding to integrin tails. Red box on the right displays some of the integrin tail interactors and their respective binding sites in α5 (yellow) of β1 (purple) integrin tails. Important motifs for integrin function have been highlighted in green and red colour. Adapted from (Morse et al., 2014). A more recent review about integrin mediated cell adhesion lists a large number of established cytoplasmic proteins which directly interact with integrin cytoplasmic tails (Bachmann et al. 2019).

1.2 Lipid-membranes as a signaling platform

1.2.1 Cellular lipids

The plasma membrane sets the outer boundaries for cells across all domains of life. In addition to maintaining essential differences between the inside and outside of a cell, the plasma membrane and other membrane compartments are important signaling platforms essential for many elementary cell signaling pathways. By concentrating otherwise soluble signaling pathway components together, different cellular membranes can increase cell signaling kinetics while also compartmentalizing functionalities (Casares, Escribá, and Rosselló 2019). Cells use significant amount of their genes and resources to synthesize thousands of different lipid molecules and the related metabolic pathways (van Meer, Voelker, and Feigenson 2008; Han 2016)

Despite having different functions, all biological membranes have a common structure of a very thin (~5 nm in thickness) double layered film composed of lipids and embedded or otherwise attached proteins. As the majority of lipids in cell membranes are amphiphilic, the bilayer structure is attributable to this special property of membrane lipids that causes lipids to spontaneously assemble bilayered structures even in isolation and *in vitro*. Bilayer lipidic membranes in eukaryotic

cells are composed of a mixture of different phospholipids. Whereas the bulk of lipid membranes are constituted by phosphatidylcholine, sphingomyelin, phosphatidylserine, and phosphatidylethanolamine, other lipids such as inositol phospholipids have important signaling roles in cells (van Meer, Voelker, and Feigenson 2008, 20).

Although bilayered membranes can form spontaneously, living cells have protein machinery to sort their membranes leading to asymmetrical bilayers where (in the case of the plasma membrane) the outside leaflet differs from the inner membrane leaflet. Since phospholipid head groups are hydrophilic, phospholipids hardly ever transfer between leaflets spontaneously - rather, they are transferred by ATP consuming flippases, floppases and via energy independent mechanisms by scramblases that promote bidirectional movement of lipids and thus the collapse of lipid asymmetry (Hankins et al. 2015). Resulting of the collective function of lipid transferring proteins is an inner-outer leaflet segregation of phospholipids where the bulk of phosphatidylcholine (PC) and sphingolipids are contained in the exoplasmic leaflet, whereas phosphatidylserine (PS), phosphatidylethanolamine (PE), phosphatidylinositol (PI), and phosphoinositides are predominantly located in the cytosolic leaflet (Ikeda, Kihara, and Igarashi 2006; Hankins et al. 2015). This lipid asymmetry regulates many aspects of cellular behaviour from apoptosis where the loss of membrane asymmetry is recognized by phagocytes (Manno, Takakuwa, and Mohandas 2002) to cell migration supported by phosphoinositide species and second messengers either located at or generated from the inner leaflet of the plasma membrane (Senning et al. 2014; Howe, Baldor, and Hogan 2005).

Although phosphoinositides comprise less than 1 % of total lipid mass, they have key regulatory roles in many fundamental cell biological processes such as cell migration. At the plasma membrane they are concentrated at the inner leaflet where they function as docking sites for numerous different signaling cascades and as a source for soluble second messengers, IP_3 and diacylglycerol (DAG) (Berridge 2016). Their reversible head group phosphorylation gives rise to different PI isoforms with distinct functions in eukaryotic cells (Prestwich 2004). Cytosolic proteins are known to interact with phosphoinositides in multiple ways that differ in their specificity for different phosphoinositide species. PH (pleckstrin homology) domain is the most studied phosphoinositide binding domain with a cleft to bind phosphoinositides with high specificity. For example, the PH domain of myosin-X binds PtdIns(3,4,5)P_3 with high specificity, but exhibits little to none binding towards PI3P (Plantard et al. 2010). In addition to PH domains as lipid binding entities, variety of other lipid binding domains exist creating a versatile machinery for cellular proteins to interact with different phosphoinositide isoforms. These domains are shown in Table 1.

Table 1. Examples of lipid-binding domains.

Domain	Example protein	Reference
C2	Syndecan2	Corbin et al 2007
PH	Myosin-X	Plantard et al 2010
PX	SNX9	Yarar et al 2008
FYVE	PIKfyve	Sbrissa et al 2002
PTB	Dab2	Alajlouni et al 2011
FERM	Talin	Bouaouina et al 2012
BAR	IRSP53	Prevost et al 2015
PHD	ING2	Gozani et al 2003
C1	PKC	Giorgione et al 2006
ANTH	Sla2p	Sun et al 2005
ENTH	Epsin	Rozovsky et al 2012

1.2.2 Lipid environments inside a cell

Distinct lipidic environments coexist inside a cell. Animal cells have tens of different membrane-limited organelles, each with their distinct lipid composition (Aguilera-Gomez and Rabouille 2017). Different lipid environments together with the versatile repertoire of lipid-binding domains compartmentalize cellular proteins and resulting signaling pathways (Gagnoux-Palacios et al. 2003; Meer and Kroon 2011). Disturbing lipid equilibrium by e.g. inhibiting phosphoinositide kinases or phosphatases has major effects on cellular function as proper membrane recognition by cellular proteins is interrupted. As an example, interfering with PtdIns(3,4,5)P_3 levels at the plasma membrane by targeting PTEN or PI3K family kinases affects cell migration and, again, energy balance by affecting PI3K-Akt-mTOR pathway (Lee, Loh, and Yap 2015; Matsuoka and Ueda 2018)

On the other hand, the deletion or inhibition of PIKfyve, an endosomally located phosphoinositide kinase (1-phosphatidylinositol 3-phosphate 5-kinase) prevents endocytic traffic into lysosomes and formation of autolysosomes thus preventing cellular energy metabolism by restricting autolysis (Kim et al. 2016).

To contrast lipid segregation between organelles, lipids in single membrane leaflets can partition forming distinct domains termed lipid rafts that affect signaling, trafficking and lateral sorting of proteins. Due to this spontaneous organisation inside a single membrane leaflet, lipid rafts can offer cells an energetically free way of organising and compartmentalizing signaling. Integrin family receptors have been

shown to be recruited into lipid raft domains via cell adhesion molecule CD24 where it likely activates Src signaling (Baumann et al. 2012; Gagnoux-Palacios et al. 2003; Runz et al. 2008). According to the lipid raft hypothesis, preferential interaction between sterols and certain phospholipids laterally induce formation of packed lipids. Endocytic vesicle pathways between Golgi/ER and the plasma membrane are thought to present a gradient in raft forming ability due to their membrane composition (Levental, Levental, and Heberle 2020). The plasma membrane is highly enriched in the components needed for lipid raft formation having 30–40 mol% cholesterol and 10–30% sphingolipids. Lipid segregation in artificial membranes can be seen, they likely don't recapitulate every aspect in cellular membranes as these can incorporate hundreds of different lipids. Although lipid rafts have also been seen in isolated membrane blebs (Baumgart et al. 2007, 20), they have been largely elusive to visualize under a microscope (Levental, Levental, and Heberle 2020). Fundamental understanding of how lipids organize inside a membrane has been hindered by the lack of experimental model systems that could capture the essence of cellular membrane together with cellular proteins. However, recent advances in creating membranes with e.g. robust asymmetry will likely pave the way for understanding lateral lipid segregation and its underlying chemico-physical properties

1.3 Filopodia

1.3.1 Filopodia formation and function

Filopodia are sensory organelles that extend from the plasma membrane of a cell. Their ability to sense the surrounding matrix or the surfaces of neighbouring cells is underlain by the set of plasma membrane receptors that they harbour. Among the receptors that localize to filopodia tips are integrins that create a special integrin-positive adhesion type that is different from other cell-ECM adhesions cells make by shape and function (Galbraith, Yamada, and Galbraith 2007). The activation of filopodial adhesions have been described to affect both filopodial function but also biological outcomes such as muscle-tendon attachment where integrin activation downregulates filopodia leading to proper muscle-tendon bonding (Richier et al. 2018). Whereas a single actin filament is unable to deform the plasma membrane, filopodia are created through an extension of intracellular F-actin bundle, the forces of which are large enough. An elongating F-actin bundle can generate forces larger than 50 pN to create membrane curvature (Mogilner and Rubinstein 2005). This leads to a characteristic slender outlook of these protrusion with only 0.1–0.3 μm in diameter.

Classically, two models explaining filopodia formation have been proposed: In the first model, the convergent elongation model, Arp2/3 complex nucleated branched actin network at the lamellipodia is reorganized by oligomeric proteins that can bring together several actin filaments. In the second model, the tip nucleation model, filopodia are formed directly from formin mediated actin nucleation. In this model, formins induce filopodia via their ability to both nucleate and promote elongation of linear actin networks. The two models, however, are not mutually exclusive and both Arp2/3 complex and formin driven actin nucleation can under the right conditions lead into formation of filopodia (C. Yang and Svitkina 2011). Past reviews discuss how the full arsenal of actin bundling proteins should be assessed when predicting the versatility functions of filopodia in epithelial cells (Khurana and George 2011). To build up on this ideology, thorough experimental studies arrived at a model where a combination of multiple actin-regulatory proteins are stochastically recruited to filopodia tips to ensure stringent filopodia formation and where the stochasticity likely underlies much of the heterogeneity observed around filopodia (Dobramysl et al. 2021). Contrary to normal situations where a multi-component system likely organises actin network in order to favor filopodia formation, high expression of a handful of proteins have been known to efficiently induce filopodia formation. Fascin and myosin-X are perhaps the most widely studied due to their upregulation in invasive carcinomas (Machesky and Li 2010; Arjonen et al. 2014; Cao et al. 2014). However, whether these proteins require accessory components to support their filopodia formation potential has not been thoroughly investigated.

Although similar elements such as the existence of plasma membrane receptors that mediate the substrate recognition exist in filopodia in different cell lines (Mao et al. 2018; Hongquan Zhang et al. 2004), depending on the cell and the context, the activation of filopodial receptors will likely have very different consequences: Whereas migrating cells use filopodia for making contacts with the underlying ECM, neuronal cells use filopodia to sense neighbouring cells and act as precursors for neuronal dendrites during synaptogenesis (Fiala et al. 1998). Still separate from synaptogenesis, axon pathfinding during development is highly dependent on filopodia structures as indicated by both their abundance in migrating growth cones and knock-out studies proving the importance of filopodia regulators in neural development. Taken together, an accumulating body of evidence suggests that filopodia are sensory organelles for different cell types that mediate sensory information leading to different outcomes depending on the context and cell type. The similarities in pathways between cell types indicate partly conserved mechanisms in the downstream signaling from filopodia protrusions.

1.3.2 Filopodia as synaptic precursors

Neuronal cells are an interesting cell type as they form at least two types of filopodia along their plasma membrane: During embryonic development, the extending axons form highly dynamic filopodia at their leading edge while the axon navigates the forming brain tissue for synaptic partners (Leondaritis et al. 2015). In addition to axonal filopodia, filopodia forming at the dendrites of neuronal cells will form a basis for new nerve connections before and after birth (Spence et al. 2019). The rapid synaptogenesis that reaches its pinnacle at 2-3 years of age in humans facilitates the development of complex cognitive tasks and adaptation to environment (Huttenlocher 1979). While both axonal and dendritic filopodia have a stick-like morphology, the F-actin networks they extend from are very different. Whereas axonal filopodia originate from a lamellipodial F-actin network (very similar to cancer cells or epithelial cells), dendritic filopodia do not have this type of F-actin mesh at their base but rather extend directly from the fairly linear dendrite base. Before synaptogenesis, neuronal cells respond to cellular activation by upregulating dendritic filopodia that will then sense the surrounding space for presynaptic terminals. Upon contact, dendritic filopodia get stabilized by local calcium signaling leading to synaptogenesis (Maletic-Savatic et al. 1999). Calcium signaling has been shown to be important for filopodia stabilization in cancer cells as well, although the exact calcium-dependent pathways seem not to be exactly the same (Jacquemet et al. 2016). Transient dendritic filopodia have been classically hard to study, however, electron microscopy studies of a developing hippocampus *in vivo* have been supporting a role for filopodia in synapse formation early on (Fiala et al. 1998). Since this, sensory-dependent synapse forming filopodia have been characterized at least in the fly brain (Sheng et al. 2018). Although some of the factors needed for dendritic filopodia formation and stability have been mapped (Kayser et al. 2008, Chen et al. 2010, Wu et al. 1998), how the recognition of a neighbouring neuron leads to formation of a synapse is still obscure. In particular, how the F-actin network completely reshapes itself from linear bundles in filopodia into shapes present in a chemical synapse is not completely understood. It has been shown, however, that removal of F-actin or some of the known F-actin binding proteins expressed in these cells are essential for re-shaping the network during synaptogenesis (Zhang et al. 2001, Nelson et al. 2013). Knowledge of the molecular components involved in shaping the chemical synapse are essential in understanding how synapse formation takes place after cell-cell recognition between correct neurons. Although not covered here in depth, it is to be noted that neuro-muscular junctions likely resemble regular synapses in their need for F-actin restructuring. Similar to post-synaptic neurons, muscle cells have been reported to bear numerous filopodia on their cell surface - capable of intimate interaction with innervating motoneuron axons (Ritzenthaler et al. 2000).

1.3.3 Filopodia regulation

It has been long recognized that the majority of GTPases have profound effects on the F-actin architecture. As filopodia protrusiveness depends on the F-actin bundle elongation at the vicinity of the cell edge, signaling events that support this type of linear bundling of F-actin can upregulate filopodia. More specifically, activation of Cdc42 GTPase has been linked with increased filopodia formation and considered as one of the most important hubs in filopodia regulation. Other GTPases that affect filopodia formation do exist: for example small GTPase Rif has been shown to increase filopodia formation via its binding with mDia1/2 formins (Goh et al. 2011; Pellegrin and Mellor 2005). Since Cdc42 has been under an extensive scrutiny due to its effects on cell polarization, filopodia formation and migration, a few pathways how Cdc42 supports filopodia function have been reported. Multiple formin proteins such as mDia2/3, FMNL1 and Daam1 have been reported to function as Cdc42 effectors (Kühn and Geyer 2014). In addition, Cdc42 contributes to filopodia formation from branched actin mesh via its binding with N-Wasp (Rohatgi, Ho, and Kirschner 2000). Molecular motor myosin-X promotes F-actin convergence at the cell edge to initiate filopodia formation from branched actin network (Tokuo, Mabuchi, and Ikebe 2007). Interestingly, also myosin-X has been shown to be a Cdc42 effector extending the downstream effector network for Cdc42 but whether the two proteins interact has not been studied (Bohil, Robertson, and Cheney 2006). Membrane deformation is a crucial aspect of filopodia formation. I-BAR domain containing proteins such as IRSP53 are well known to sense membrane curvature and tubulate membranes. The activity of IRSP53 is reciprocally regulated by 14-3-3 scaffold and Cdc42 (Kast and Dominguez 2019). In addition to allosteric changes to IRSP53 induced by Cdc42 binding, Cdc42 promotes formation of IRSP53:Mena loci (Krugmann et al. 2001) and IRSP53:VASP complex formation at the leading edge supporting actin polymerization in filopodia (Disanza et al. 2013). Other GTPases such as TC10 and RhoT have also been reported regulating filopodia-like process formation, although these proteins lack in depth validation (Abe et al. 2003).

Upstream of GTPases, plasma membrane receptors can signal filopodia formation. Developmentally, perhaps the best studied filopodia-system *in vivo* has been sprouting morphogenesis where soluble factors such BMP or VEGF can stimulate filopodia formation in the tip cells of migrating epithelium where filopodia seem to increase migration velocity (Gerhardt et al. 2003). In addition to sprouting morphogenesis, in long-range, filopodia-dependent migration by single primordial germ cells where external Cxcl12 gradient regulates filopodia distribution and dynamics (Meyen et al. 2021) providing examples where soluble external stimuli can both induce and regulate filopodia via a cell surface receptor. Other cellular receptors such as integrins have been shown to regulate filopodia formation as blocking integrin function with an antibody leads to short and distorted filopodia

(Arjonen et al. 2014). Opposite to integrin blockage, integrin signalling has been shown to regulate filopodia functions (Jacquemet et al. 2016). Interestingly, a trimeric G-protein G_s, previously only associated with cAMP signaling, has been only lately shown to work upstream of Cdc42 in filopodia induction in a competitive manner with the cAMP signaling. G_s protein links filopodia formation with G-protein linked receptors indicating that filopodia function is a result of integrated signal from multiple receptors (Castillo-Kauil et al. 2020). While phosphoinositide lipid species residing in the plasma membrane affect much of receptor function, curved membranes with phosphoinositide species have been shown to stimulate actin polymerization and filopodia formation in in vitro systems (Jennifer L. Gallop et al. 2013). Given that many filopodia localizing proteins do have a phosphoinositide binding PH domain (Jacquemet et al. 2019, 130), the plasma membrane likely affects much of the biology related to filopodia. While this remains largely unexplored, phosphoinositides have been reported to activate myosin-X as defective PIP binding by myosin-X localizes the protein inside the cell in Rab7-positive vesicles (Plantard et al. 2010).

Although many proteins have been studied in the context of filopodia initiation and function, there are a handful of proteins whose overexpression is known to efficiently induce filopodia formation. In addition, these proteins are mechanistically well defined in how they act to support filopodia structures. Myosin-X, IRSP53 and fascin are three of the most widely studied filopodia-inducing proteins. However, due to the small size and fast dynamics, determining the filopodia proteome in full has been historically challenging. There have, however, been attempts to assess filopodial proteins using mass spectrometry using: 1) Exploitation of high-affinity ligand-receptor interaction to pull down dendritic filopodia, 2) dendritic filopodia localizing BioID, 3) Removal of protruded areas for mass spectrometry (Choi et al. 2018) and using laser microdissection to isolate filopodia for mass spectrometry (Gordon and Gousset 2021). Also, other high-throughput set-ups such as phenotypic screens or microscopy screens to identify new filopodia-linked proteins (Jacquemet et al. 2019; Jarsch et al. 2020) have been made. The realisation that filopodia from different origins might have different proteomes and functions calls for better strategies to classify filopodia by their function or by the proteins localised in them.

1.3.4 Myosin superfamily in filopodia formation and function

Myosin superfamily is a large family of actin binding molecular motor proteins with wide-ranging functions. Myosins can be divided into subclasses based on their structure of functionality (Hartman et al. 2012). Myosins classified as unconventional myosins (i.e. having a FERM domain) are especially linked with filopodia or stereocilia – a cellular protrusion necessary for hearing and highly

analogous with filopodia. Myosin-X is the archetype of an unconventional myosin and its mere expression has been linked with filopodia formation. Other unconventional myosins do exist: Recessive mutations in myosin-VII have been linked to deafness in humans and mice (X. Z. Liu et al. 1997). Also congenital profound deafness has been linked with myosin-XV (Anderson et al. 2000) suggesting that both these myosins are needed to support the unique actin network assembly at the inner ear stereocilia. Interestingly, myosin-X knockout is only semi-lethal suggesting that to some extent other myosins can replace for the lack of myosin-X but even alive pups exhibit birth defects in their digit formation and e.g. neural tube closure (Heimsath et al. 2017). Given that myosin-X is a filopodia-inducing protein and neural tube closure is a filopodia intensive event (Pyrgaki et al. 2010), defects in neural tube closure upon myosin-X knockout are not surprising. All myosin motors are unidirectional in the sense that they processively walk toward branched ends of actin filaments. The only pointed-end directed motor, MYO6, can however induce filopodia formation when engineered with a branched-end directed motor (Masters and Buss 2017), indicating that myosin N-terminal domain coupled to myosin motor is enough to induce filopodia formation. However, since myosin-X does not have N-terminal domain (Sebé-Pedrós et al. 2014), it seems that a dimeric myosin head domain is sufficient to induce filopodia formation most likely according to the convergent elongation filopodia formation model where existing actin filaments are brought together by actin proteins capable of binding two actin filaments at the same time (Tokuo, Mabuchi, and Ikebe 2007). Because of their plus-end directed movement, multiple reports show myosin dependent cargo transport to filopodia tips. Myosin-X has been shown to transport VE-cadherin to filopodia tips via its FERM domain to support initial cell-cell contacts (Almagro et al. 2010). Also other cargo such as F-actin elongation factor Mena/VASP have been reported to bind myosin-X (Tokuo and Ikebe 2004). Importantly, all isolated unconventional myosins exist in a monomeric form but only one dimerization aiding protein for Myo7a has been reported (R. Liu et al. 2021, 7)

Intriguingly, not every myosin family member can induce filopodia formation but due to their +end directionality, other myosins such as Myo3a can contribute to filopodia-tip directed cargo transport (Salles et al. 2009). Interestingly, Myo3a belongs to a class-III myosins, characterized by an N-terminal kinase domain and IQ repeats (Sebé-Pedrós et al. 2014). Mutations in Myo3 have been linked to hearing loss defects due to its function in inner ear stereocilia. Like some unconventional myosins, Myo3 localizes to stereocilia tips where it regulates stereocilia length crucial for hearing (Ebrahim et al. 2016). How Myo3 supports filopodial function via its filopodia-tip localized kinase domain is not known. Altogether, excluding a few studies little is known how kinases phosphorylate proteins in filopodia tips (Robles, Woo, and Gomez 2005). It has been suggested however that starvation

induced phosphorylation would alter myosin-dependent cargo recruitment to filopodia tips (Shneyer et al. 2017). Another myosin, Myo5 does not affect filopodia formation but as a multipurpose transport myosin it has been reported to affect filopodia extension at least in chick neuronal cells (F. S. Wang et al. 1996). Lastly non-muscle myosin II does not localize to filopodia tips but it has been shown to be the responsible myosin to mediate force mediated cell-ECM attachment at filopodia tips (Alieva et al. 2019). Figure 5 shows the domain structures of different myosin proteins discussed in this chapter.

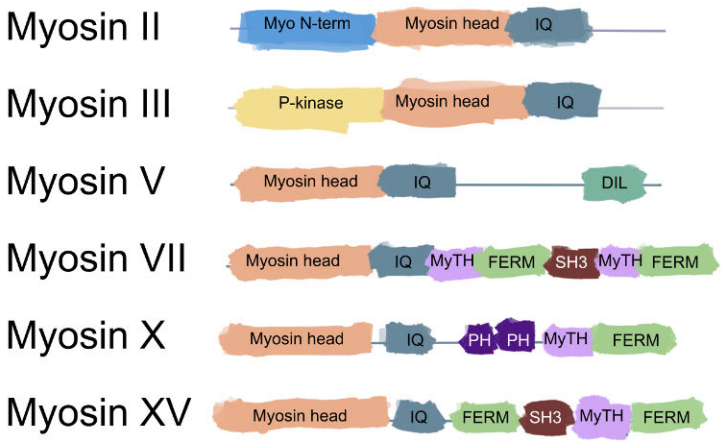

Figure 5. Domains of selected myosin superfamily members. Myosin head domain is the defining domain for the superfamily while other domains largely define much of the functional aspects of each myosin family member. FERM domain containing myosins (7, 10, 15) are considered as unconventional myosins. Adapted from (Sebé-Pedrós et al. 2014).

1.4 Cancer dissemination

1.4.1 Filopodia and cancer

Collective evidence of filopodia driving cancer progression exists and surprisingly many of the filopodia-regulating proteins have been linked to poor survival in different patient cohorts and the pivotal role for filopodia in cancer cell invasion is highlighted by loss-of-function studies of multiple filopodia regulators. While actin bundling protein fascin is expressed at low levels in a healthy epithelium, it is upregulated in many carcinomas (Machesky and Li 2010). High fascin expression often correlates with poor prognosis (Li et al., 2008; H. Zhang et al. 2006; Hashimoto et al. 2005). In addition, fascin is a part of a gene signature that positively correlates with lung metastasis in breast cancer (Arjonen, Kaukonen, and Ivaska 2011; Minn et al. 2005) and is regulated by Slug, a known EMT inducer (A. Li et al. 2014).

Interestingly, fascin expression is lost in metastatic colon cancer indicating that these tumours might undergo mesenchymal-to-epithelial transition upon metastasis (Vignjevic et al. 2007).

Another critical filopodia regulatory, myosin-X, is upregulated by mutant p53 and correlates with poor survival in breast and pancreatic cancer (Arjonen et al. 2014, Cao et al. 2014) The overexpression of myosin-X drives filopodia formation and increased invasion while silencing of myosin-X in mouse models prevents systemic cancer spread lowering metastatic burden (Arjonen et al. 2014). Similarly, fascin downregulation has been shown to increase survival and lower metastatic burden in pancreatic cancer (A. Li et al. 2014). Interestingly, downregulation of fascin or Myosin-X has been shown to prevent trans-mesothelial migration in ovarian cancer even though pharmaceutical inhibition of lamellipodia or invadopodia had no impact on trans-mesothelial migration indicating that filopodia are important protrusions overcoming anatomical barriers during cancer invasion (Yoshihara et al. 2020). The pivotal role for filopodia in cancer cell invasion is highlighted by loss-of-function studies of multiple filopodia regulators (A. Li et al. 2010; Arjonen et al. 2014; Zhong et al. 2018). In addition, the emergence of RhoA-dependent filopodia (here termed as microspikes) correlate with increased invasion in ovarian cancer (Jacquemet et al. 2013). In addition, a targeted inhibition of fascin inhibits invasion in different cancer cell models (F.-K. Huang et al. 2015)

Filopodia formation inducing formin family of proteins are also known to be upregulated by many cancers. FMNL2 formin is expressed in metastatic colorectal cancer but not in non-metastatic ones (Zhu, Liang, and Ding 2008). FMNL1 on the other hand is upregulated in renal cell carcinoma where its expression correlates with tumour stage and metastases (M.-F. Zhang et al. 2020). Although multiple formins regulate glioblastoma migration, only INF2 expression has been shown to correlate with poor prognosis (Heuser et al. 2020). Formin mediated filopodia have been also directly visualized in micrometastases where they support lung colonization via integrin signaling. The filopodia in these cells are upregulated via Rif-mDia axis and support micrometastatic growth likely through active β1-integrin distributed along filopodia shafts (Shibue et al. 2012). Also basal-like breast cancers express formin proteins that might contribute their invasiveness (Heuser et al. 2018)

It is likely that myosin-X, fascin or otherwise upregulated filopodia drive the progression in subsets of other cancer types as well. Better knowledge of filopodia function, implicated proteins and proper patient stratification will be a key in understanding filopodia-driven metastasis in its full breadth.

1.4.2 Mechanisms of cancer dissemination

Cancers of epithelial origin, carcinomas, invade the basement membrane to migrate into the surrounding tissue and intravasate into blood or lymphatic vessels. Entry into the blood circulation facilitates cancer cell dissemination to distant parts of the body where extravasated cancer cells enter the distant organ and colonize to give rise to metastasis. In addition to this, some cancers have been shown to disseminate along neurons (Amit, Na'ara, and Gil 2016). Although, anatomy of blood vessels does partly affect cancer dissemination, it does not fully explain the organotropism clinically evident for many cancers. For example, brain, liver and kidneys all receive 10–20% of total blood flow but display very different patterns of metastasis between each other (Budczies et al. 2015; Obenauf and Massagué 2015). For breast cancer, bone, liver, brain and lung are common sites for metastasis (Gerratana et al. 2015). Modeling approaches using humanoid blood circulation models suggest that blood flow would account for around 40% of where cancer metastasizes (Font-Clos, Zapperi, and La Porta 2020).

An extensive amount of clinical data shows that different tumours display organ tropism in their metastatic growth. Although some aggressive tumours are able to form secondary tumours virtually everywhere, there exists a preference for certain organs, where metastatic lesion growth is supported by suitable stroma and soluble factors. Also, bi-directional cross-talk with other cells in the metastatic niche is now recognized as a fundamental aspect of metastatic growth. A general overview of the metastatic cascade is given in Figure 6, where cells from primary tumour first invade locally, intravasate into blood vessels finally extravasating at the target organ. Active cell migration drives metastasis at multiple points before and after reaching to blood or lymph vasculature.

Breast cancer with its well defined subtypes offer a framework to scrutinise cancer dissemination as the cancers from the same tissue of origin display subtype-dependent organotropism (Chen et al. 2018). Besides a small fraction of non-metastatic in-situ tumours, most breast cancers will spread if left untreated. Invasive breast cancers can be roughly categorized by the part of the breast where the tumour is first initiated. More than 80% of invasive breast tumours start from the milk ducts (ductal carcinomas) where the rest of cancerous growth is initiated at milk producing lobules (lobular carcinoma) (Chen et al. 2018). Although predictions of the disease based on these histological differences can be made, breast cancers are further divided into categories by their gene expression profiles to sufficiently predict metastatic risk and select a treatment plan (Dai et al. 2015). As an example, HER2+ tumours have higher probabilities for brain metastasis than luminalA/B tumours (Chen et al. 2018).

Next-generation DNA sequencing and transcriptomic analyses comparing primary tumour with metastases at different sites have provided fundamental

knowledge of genetic alterations and gene expression changes during metastases. Importantly, metastasis at different sites show organ specific gene expression signatures that are fundamentally different between organs (Chen et al. 2018). Bone-guided NF-kb activated cancer cells upregulate osteoblast RANKL secretion and increase osteoclast-dependent bone resorption (Thomas et al. 1999; Casimiro et al. 2013; Monteiro et al. 2013). Different from bone metastases, CXCR4/CXCL12 signaling increases extravasation of cancer cells in the liver (Wendel et al. 2012) where claudin2-mediated a2β1 and α5β1 integrin upregulation supports cancer cell interaction with the fibrous liver tissue (Tabariès et al. 2012). Interestingly, αvβ3 integrin has been reported to support bone metastasis formation (Kwakwa and Sterling 2017) suggesting that integrin family receptors are essential not only for active cell migration processes but also for cell-ECM coupling at metastatic niche.

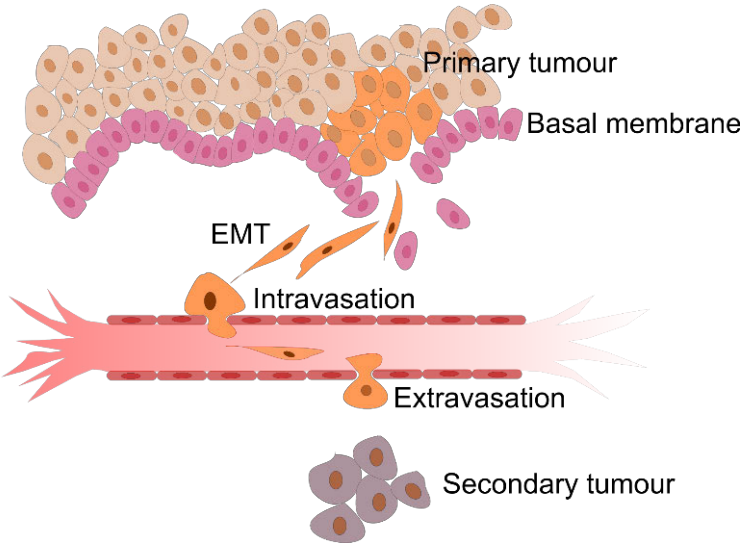

Figure 6. Illustration of a carcinoma invading through a basement membrane finally occupying distant organs and expanding in the new environment. Adapted from (Schroeder et al. 2012).

1.4.3 Integrin receptors in cancer

Integrin expression and function are frequently affected in cancer. Altered integrin expression patterns have been observed with many cancer types and integrins have been linked with metastatic progression of cancer at multiple steps (Anna Huttenlocher and Horwitz 2011; Hamidi and Ivaska 2018; Raab-Westphal, Marshall, and Goodman 2017). Different cancers display specifically altered integrin expression patterns and their cancer-subtype specific functions can even be opposite (De Arcangelis et al. 1999). For example, whereas α3β1 is required for breast

tumorigenesis, α2β1 is a tumour suppressor and increased recycling of α5β1 correlates with invasiveness in 3D. Thus, the mere expression of a single integrin gene is not a good measure for cancer aggressiveness.

It is also well recognized that integrin receptors cross-talk with growth factor receptors to support their oncogenic signaling (Ivaska and Heino 2011) and can activate TGFβ – a driver for EMT but also driver for immunological suppression (M. Liu et al. 2020; Xu, Lamouille, and Derynck 2009; Campbell et al. 2020).

Integrin trafficking between the plasma membrane and intracellular compartments is known to be dysregulated by cancer cells. Normally, integrin receptors are endocytosed via multiple mechanisms and routed to Rab5 positive endosomes to be recycled back to the plasma membrane via two individual routes known as the short and long loops (Franceschi et al. 2015; Hamidi and Ivaska 2018). Pathway components supporting integrin recycling along the long-loop pathway induce cancer cell invasion (Bridgewater, Norman, and Caswell 2012). For example, gain-of-function p53 mutant induces α5β1 integrin recycling correlating with cancer metastasis (Muller et al. 2009) and driving the formation of invasive protrusions (Jacquemet et al. 2013; Paul et al. 2015). Increased integrin recycling machinery has also been shown to predict lymph node metastasis and poor prognosis in patients at least in pancreatic cancer (Dozynkiewicz et al. 2012).

Although ligand-independent functions for integrins have been described (Petridou and Skourides 2016), integrin-ECM coupling is crucial for invasion and pro-survival signaling and thus integrin repertoire should most likely mirror the extracellular matrix at metastatic site. Breast cancer among others can metastasize in the brain which is known to be an ECM-poor tissue when compared to e.g. mammary tissue. From openly available RNA sequencing data comparing primary breast tumours with brain lesions, it is evident how breast cancer cells that successfully metastasize to brain, upregulate multiple collagen genes suggesting that breast cancer cells need to create a collagen rich metastatic niche for themselves in order to metastasize into ECM poor parts of the body, such as brain (Iwamoto et al. 2019).

Multiple reagents against integrin receptors have been developed: Antibodies that can block integrin function or detect their activation status (Byron et al. 2009), PET-tracers to visualize integrin upregulating tumours (Notni et al. 2017) or integrin function blocking peptides that compete with endogenous ligand binding (Reardon and Cheresh 2011). Even with a strong long-standing focus on integrin cancer biology and promising preclinical results, clinical trials have yet failed to show effectiveness of integrin function blockage in treating cancer. On top of the complex nature of integrin receptor function and regulation, poor pharmacological profile of integrin function blocking drugs and clinical trial design have been contemplated as potential explanations for negative results from clinical trials (Alday-Parejo, Stupp,

and Rüegg 2019). Despite massive promise, integrins still remain to be exploited pharmacologically in cancer although their inhibition clearly shows effect in other diseases such as pulmonary fibrosis (John et al. 2020).

1.4.4 Plasma membrane signaling in cellular movement and cancer

As previously discussed chapter 1.2, the ubiquitous plasma membrane not only limits the cells but functions as a signaling platform for many different signaling cascades. In cellular movement and cancer, different roles for different phosphoinositide isoforms have been posed. Many studies have pinpointed PtdIns(3,4,5)P_3 as key regulator for cellular movement but also for PI3K-Akt pathway, a nutrient sensing pathway often dysregulated in cancer, where PI3-kinase dependent PtdIns(3,4,5)P_3 upregulation drives Akt translocation from cytoplasm to the plasma membrane. Akt independently, invading cancer cells depend on integrin-mediated cell-matrix interactions where integrin activator talin is first recruited to the plasma membrane via Rap1/RIAM complex or directly via Rap1 (Lagarrigue, Kim, and Ginsberg 2016; Gingras et al. 2019). Following membrane recruitment, talin makes contact with negatively charged phosphoinositides with its positively charged patch increasing integrin binding avidity and likely positioning the molecule for efficient integrin activation (Chinthalapudi, Rangarajan, and Izard 2018). More broadly, the presence of phosphoinositides at the plasma membrane has been shown to support the function of all major plasma membrane receptor classes: 1) Integrin adhesions (Chinthalapudi, Rangarajan, and Izard 2018) 2) Cadherin adhesions (Wood et al. 2017) 3) growth factor receptor signaling 4) GRPC receptor signaling (Yen et al. 2018) 5) ion channels (Hille et al. 2015) and developing drugs for PtdIns(3,4,5)P_3 binding domains to treat cancer has been a topic of intensive study. PH domain inhibition of BRAG2 (nucleotide exchange factor) or Akt have been reported to inhibit cancer via lowered Arf GTPase or lowered Akt-pathway activation (Nawrotek et al. 2019), respectively. Interestingly, phosphoinositide PtdIns(3,4,5)P_3 is reported to be restricted at leading edge of migrating cells or alternatively, in neuronal cells, to the tips of growing axons (S.-H. Shi, Jan, and Jan 2003; Matsuoka and Ueda 2018). Even more specifically, pathways that regulate phosphoinositide formation, mainly PI3K-PTEN signaling axes, have been shown to regulate filopodia (J. L. Gallop 2020). Although the exact mechanism(s) of how phosphoinositides would regulate filopodia function are not known, the spatial restriction of PIP metabolism has been noted to drive the formation of pro-metastatic protrusions (Nacke et al. 2021) and axonal filopodia have been shown to extend from phosphoinositide-rich patches (Ketschek and Gallo 2010). Also the activity of key

filopodia regulators such as myosin-X does depend on their ability to bind phospholipids via their PH domain (Plantard et al. 2010).

Despite their central role supporting cancer related processes, no PH domain inhibitors have reached the clinics yet possibly due to suboptimal metabolics profile or due to off-target effects. Although the plasma membrane lipid composition has a pivotal role in signal transduction and cellular function, mechanistic understanding of this cross-talk is lagging behind largely because of lack in experimental systems where different components of the membrane could be modulated with ease.

To summarise the review, the existence of filopodia has been acknowledged around 100 years but due to the small size of these stick-like, thin protrusions, their research has been relatively slow. Still today, filopodia are defined morphologically, rather than by their function or proteome. Today's high-resolution optical imaging coupled with modern mass-spectrometry and biochemical approaches do offer means to study these organelles with an unprecedented accuracy but the field still remains under-studied. What is understood is that these protrusions can arise from very different cellular backgrounds. However, how different cells use filopodia and how variable filopodia are between different cell types are questions that still lack scientific rigor. In addition, more detailed questions, such as how (and which) different proteins at filopodia come together to regulate these protrusions. Finally, the plasma membrane is an ever crucial constituent creating boundaries for each cell but also for every filopodium. What roles does the plasma membrane have for filopodial function are big questions that likely intersect with many points at the filopodial life cycle.

2 Aims

1 Cells sense ECM using integrin receptors located in filopodia. Dissecting the pathways that regulate adhesion formation at filopodia via quantitative high-resolution microscopy and complementary approaches was the first aim of this thesis.

2 Different cell-ECM adhesion structures are defined by the intracellular proteins that they recruit to the adhesion site. Although the proteins (=proteome) that associate with integrin-positive adhesions have been under tight scrutiny, which adhesion molecules localize to filopodial adhesions has not been known. Defining filopodial adhesions by their cytoplasmic proteins was the second aim of this thesis.

3 Integrin mediated cell adhesion is a key regulator of cellular protrusion, including filopodia. SHANK3 was recently identified as a key regulator of integrin activity. Because of its key role in integrin regulation the second aim was to study the biological role of SHANK3 in the context of dendritic filopodia or filopodia extended by cancer cells.

4 The plasma membrane affects the function of all major classes of plasma membrane receptors, including integrins. Developing an *in vitro* assay to study plasma membrane effects on receptor biology was the third aim of this thesis.

3 Materials and Methods

3.1 Cells

Original publication I and III: CHO (Chinese hamster ovary) cells were grown in α-MEM medium (Sigma-Aldrich), supplemented with 5% fetal bovine serum (FBS, Gibco) and 2 mM L-glutamine (Sigma-Aldrich). 1% (vol/vol) penicillin/ streptomycin (pen/strep, Sigma-Aldrich) was added to prevent bacterial growth in original publication III. HEK293 (human embryonic kidney) and U2OS (human osteosarcoma) cells were grown in Dulbecco's modified Eagle's medium (DMEM, Sigma-Aldrich) supplemented with 10% FBS, 2 mM glutamine and in the case of original publication III, 1% pen/strep.

All cell lines except U2OS were purchased from ATCC. U2OS cell line was provided by DSMZ (Leibniz Institute DSMZ-German Collection of Microorganisms and Cell Cultures, Braunschweig DE, ACC 785)

3.2 Transient transfections

Original publication IV: To probe EGFP-tagged protein binding to (proteo-)liposomes, HEK293 cells in a 10 cm dish were transfected at ~70% confluency. For this, 12 μg of the plasmid was mixed with 250 μl of Opti-MEM (Gibco). After 5 minutes of incubation in a room temperature, a recently prepared pre-mix of polyethylenimine (PEI) and Opti-MEM (20 μg of PEI and 250 μl of Opti-MEM) was combined with the plasmid. The resulting 500 ul mixture was then incubated further for 30 minutes (still at room temperature). The transfection reagent added into the cell culture medium and cells expressing the plasmid of interest were used 24–48 hours later. In other original publications (I–III), transient transfections for cell lines CHO, HEK293, and U2OS were done using Lipofectamine 3000 (Thermo Fisher Scientific Inc, # L3000-015) and following manufacturer's instructions. Primary neurons were transfected using two methods: at DIV16 using Lipofectamine2000 (Thermo Fisher Scientific Inc, #11668019), or at DIV7-9 using calcium phosphate method. In the case of Lipofectamine, manufacturer's instructions were followed. In the calcium phosphate method, cOmplete Neurobasal medium was collected from wells one hour before transfection and replaced with pre-warmed transfection medium (MEM+GlutaMAX).

Plasmid DNA was diluted into a 2.5 M $CaCl_2$ solution (in MilliQ). While continuously mixing, an equal amount of 2x Hepes buffered salt solution was added drop by drop into the reaction tube. The reaction tube was incubated in a room temperature for 30 minutes and then divided into cells. After two hours, cells were washed seven times with 1×Hank's Balanced Salt Solution (HBSS) to remove $CaCl_2$ solution. Finally, neurobasal medium was added back on the cells. 2x Hepes buffered salt solution contains: NaCl 274 mM; KCl 10 mM; Na2HPO41.4 mM; D-Glucose 15 mM; Hepes 42 mM; adjusted to pH 7.05 with NaOH.

3.3 Mice and rats

Primary hippocampal neurons were isolated from Sprague-Dawley rats and Wistar Unilever outbred rats (strain HsdCpb:WU, Envigo, Horst, The Netherlands). Shank3 αβ-deficient mice have been described before (Schmeisser et al., 2012) and were provided by Tobias Boeckers (Univ. of Ulm, Germany).

Timed, pregnant animals were housed in individual cages, with access to food and water *ad libitum*. All animal experiments were approved by, and conducted in accordance with, the Turku Central Animal Laboratory regulations and followed national guidelines for Finnish animal welfare, or regulations of the Animal Welfare Committee of the University Medical Center (Hamburg, Germany) under permission number Org766.

3.4 Plasmids

Table 2. Plasmids used in original publications I–IV.

Plasmid	Application	Original publication	Source
Jun–α5 (pD441-HMBP)	Bacterial expression	IV	Original plasmid
Fos–β1 (pGEX-4T)	Bacterial expression	IV	Original plasmid
BTK-PH–EGFP	Mammalian expression	IV	Addgene 51463
PLC(δ1)-PH–EGFP	Mammalian expression	IV	Addgene 21179
EGFP-2xFYVE	Mammalian expression	IV	Addgene 140047
talin FERM–EGFP (mouse Talin 1-433)	Mammalian expression	IV	Ben Goult
His-tagged talin FERM	Bacterial expression	I, IV	Ben Goult
SHANK3-mRFP (in pmRFP-N3)	Mammalian expression	III	Hans-Jürgen Kreienkamp (University of Hamburg, GE)
GFP-SPN (Shank3)	Mammalian expression	III	Johanna Ivaska (University of Turku, FI)

Plasmid	Application	Original publication	Source
GFP-SPN (Shank3) Q37A/R38A	Mammalian expression	III	Original plasmid
GFP-SPN (Shank3) R12C	Mammalian expression	III	Johanna Ivaska (University of Turku, FI)
GST-SPN (Shank3)	Bacterial expression	III	Johanna Ivaska (University of Turku, FI)
GST-SPN (Shank3) Q37A/R38A	Bacterial expression	III	Original plasmid
SUMO-SPN-ARR	Bacterial expression	III	Johanna Ivaska (University of Turku, FI)
GST SPN-ARR WT	Bacterial expression	III	Johanna Ivaska (University of Turku, FI)
GST SPN-ARR N52R	Bacterial expression	III	Original plasmid
GFP-Shank3 (in pHAGE vector)	Mammalian expression	III	Hans-Jürgen Kreienkamp (University of Hamburg, GE)
GFP-Shank3 (in pHAGE vector) N52R	Mammalian expression	III	Original plasmid
GFP-Shank3 (in pHAGE vector) Q37A/R38A	Mammalian expression	III	Original plasmid
SPN-ARR N52R-mRFP	Mammalian expression	III	Original plasmid
SPN-ARR WT-mRFP	Mammalian expression	III	Hans-Jürgen Kreienkamp (University of Hamburg, GE)
RFP control plasmid	Mammalian expression	III	Clontech
pEGFP-C3-Rap1Q63E	Mammalian expression	III	Bass Baum and
Myo10-mCherry	Mammalian expression	III	Addgene 139780 / Staffan Strömblad
kindlin-2-GFP	Mammalian expression	III	Maddy Parsons (King's College London, UK)
mRuby-Lifeact	Mammalian expression	III	Addgene 54560
EGFP-C1	Mammalian expression	I–IV	Clontech
EGFP-FERM (Myo10)	Mammalian expression	I	Original plasmid
His-tagged FERM (Myo10)	Bacterial expression	I	Original plasmid
EGFP-FERM ITGBD (Myo10)	Mammalian expression	I	Original plasmid
EGFP-MYO10 ΔFERM	Mammalian expression	I	Original plasmid
mScarlet-I-MYO10 ΔFERM	Mammalian expression	I	Original plasmid
EGFP-MYO10TF	Mammalian expression	I	Original plasmid
EGFP-MYO10 ITGBD	Mammalian expression	I	Original plasmid
EGFP-MYO10 ΔF2F3	Mammalian expression	I	Original plasmid
EGFP-MYO10 ΔF3	Mammalian expression	I	Original plasmid

Plasmid	Application	Original publication	Source
eGFP-TNS1	Mammalian expression	II	Johanna Ivaska (University of Turku, FI)
eGFP-TNS2	Mammalian expression	II	Johanna Ivaska (University of Turku, FI)
eGFP-TNS3	Mammalian expression	II	Johanna Ivaska (University of Turku, FI)
eGFP-TNS4	Mammalian expression	II	Johanna Ivaska (University of Turku, FI)
GFP-Sharpin	Mammalian expression	II	Johanna Ivaska (University of Turku, FI)
GFP-MDGI	Mammalian expression	II	Johanna Ivaska (University of Turku, FI)
GFP-FAK-FAT	Mammalian expression	II	David D. Schlaepfer (UC San Diego Health, US)
GFP-FL-FAK	Mammalian expression	II	David D. Schlaepfer (UC San Diego Health, US)
EFHD2-GFP	Mammalian expression	II	Dirk Mielenz (University of Erlangen-Nuremberg, DE)
CAAX-GFP	Mammalian expression	II	Gregory Giannone (Bordeaux University, FR)
EGFP-Talin-1	Mammalian expression	II	Ben Goult (University of Kent, UK)
mCherry-Talin-2	Mammalian expression	II	Ben Goult (University of Kent, UK)
pDsRedC1-Kindlin-1	Mammalian expression	II	Ben Goult (University of Kent, UK)
FMNL2-GFP	Mammalian expression	II	Robert Grosse (University of Marburg, DE)
FMNL3-GFP	Mammalian expression	II	Henry Higgs (Geisel School of Medicine at Dartmouth, US)
PPFIA1-GFP	Mammalian expression	II	Guido Serini (University of Torino, IT)
pEGFP-C1-Lamellipodin	Mammalian expression	II	Matthias Krause (King's College London, UK)
pEGFP-C2-Myo15a	Mammalian expression	II	Jonathan Bird (NIH, Bethesda US)
GFP-ICAP-1	Mammalian expression	II	Daniel Bouvard (University of Grenoble, FR)
GFP-KANK1	Mammalian expression	II	Reinhard Fassler (Max Planck Institute of €

Plasmid	Application	Original publication	Source
			Biochemistry, Martinsried, DE)
GFP-KANK2	Mammalian expression	II	Reinhard Fassler (Max Planck Institute of € Biochemistry, Martinsried, DE)
GFP-KANK3	Mammalian expression	II	Reinhard Fassler (Max Planck Institute of € Biochemistry, Martinsried, DE)
GFP-KANK4	Mammalian expression	II	Reinhard Fassler (Max Planck Institute of € Biochemistry, Martinsried, DE)
BTK-PH-EGFP	Mammalian expression	II	Matthias Wymann (University of Basel, Switzerland)
PLC(d1)-PH-EGFP	Mammalian expression	II	Matthias Wymann (University of Basel, Switzerland)
EGFP-tagged tandem FYVE	Mammalian expression	II	Harald Stenmark (Oslo University Hospital)
GFP-Cas-wt	Mammalian expression	II	Daniel Rösel (Charles University in Prague, Czech Republic)
GFP-CasdeltaCCH	Mammalian expression	II	Daniel Rösel (Charles University in Prague, Czech Republic)
GFP-CasdeltaSH3	Mammalian expression	II	Daniel Rösel (Charles University in Prague, Czech Republic)
GFP-Cas-deltaCCH-deltaSH3	Mammalian expression	II	Daniel Rösel (Charles University in Prague, Czech Republic)
Kindlin-2-GFP	Mammalian expression	II	Maddy Parsons (King's College London, UK)
Ezrin-GFP	Mammalian expression	II	Maddy Parsons (King's College London, UK)
Vinculin-GFP	Mammalian expression	II	Maddy Parsons (King's College London, UK)
Moesin-GFP	Mammalian expression	II	Buzz Baum (University College London, UK)
Lifeact-mTurquoise2	Mammalian expression	II	Joachim Goedhart (University of Amsterdam, NL)
Integrin alpha5-GFP	Mammalian expression	II	Rick Horwitz (Allen

Plasmid	Application	Original publication	Source
			institute for cell science, US)
mEmerald-Alpha-Actinin-19	Mammalian expression	II	Addgene 53989
mEmerald-Fascin-C-10	Mammalian expression	II	Addgene 54094
pGFP Cas	Mammalian expression	II	Addgene 50729
mEmerald-Cofilin-C-10	Mammalian expression	II	Addgene 54047
mEmerald-Coronin1B-C-10	Mammalian expression	II	Addgene 54049
pGFP CrkII	Mammalian expression	II	Addgene 50730
mEmerald-Cortactin-C-12	Mammalian expression	II	Addgene 54051
mEmerald-mDia1-C-14	Mammalian expression	II	Addgene 54156
mEmerald-mDia2-C-14	Mammalian expression	II	Addgene 54158
mEmerald-Migfilin-C-14	Mammalian expression	II	Addgene 54181
pEGFP-IQGAP1	Mammalian expression	II	Addgene 30112
mEmerald-LASP1-C-10	Mammalian expression	II	Addgene 54141
EGFP-EPLIN alpha	Mammalian expression	II	Addgene 40947
EGFP-EPLIN beta	Mammalian expression	II	Addgene 40948
mEmerald-PINCH-C-14	Mammalian expression	II	Addgene 54229
mEmerald-MyosinIIA-C-18	Mammalian expression	II	Addgene 54190
mEmerald-MyosinIIB-C-18	Mammalian expression	II	Addgene 54192
mEmerald-Palladin-C-7	Mammalian expression	II	Addgene 54213
mEmerald-Parvin-C-14	Mammalian expression	II	Addgene 54214
GFP-PTEN	Mammalian expression	II	Addgene 13039
mEmerald-Paxillin-22	Mammalian expression	II	Addgene 54219
mEmerald-TES-C-14	Mammalian expression	II	Addgene 54276
mEmerald-VASP-N-10	Mammalian expression	II	Addgene 54297
mEmerald-Zyxin-6	Mammalian expression	II	Addgene 54319
E-cadherin-GFP	Mammalian expression	II	Addgene 28009
pEGFP C1-Eps8 WT	Mammalian expression	II	Addgene 74950
GFP-P4M-SidM	Mammalian expression	II	Addgene 51469
pcDNA3.1-6His-MyoX	Mammalian expression	II	Addgene 47607
ARP3-GFP	Mammalian expression	II	Addgene 8462
mScarlet-MYO10	Mammalian expression	II	Original plasmid
pEGFP-CasCCHD	Mammalian expression	II	Original plasmid
mEmerald-MYO7A	Mammalian expression	II	Original plasmid
mEmerald-BAIAP2	Mammalian expression	II	Original plasmid
mEmerald-PDLIM5	Mammalian expression	II	Original plasmid
mEmerald-FERMT2	Mammalian expression	II	Original plasmid

Plasmid	Application	Original publication	Source
mEmerald-FHL2	Mammalian expression	II	Original plasmid
mEmerald-FHL3	Mammalian expression	II	Original plasmid
mEmerald-PDLIM7	Mammalian expression	II	Original plasmid
mEmerald-PLS3	Mammalian expression	II	Original plasmid
mEmerald-TRIP6	Mammalian expression	II	Original plasmid
mEmerald-ALYREF	Mammalian expression	II	Original plasmid
mEmerald-ANXA1	Mammalian expression	II	Original plasmid
mEmerald-BRIX1	Mammalian expression	II	Original plasmid
mEmerald-DIMT1	Mammalian expression	II	Original plasmid
mEmerald-FAU	Mammalian expression	II	Original plasmid
mEmerald-HP1BP3	Mammalian expression	II	Original plasmid
mEmerald-PCOLCE	Mammalian expression	II	Original plasmid
mEmerald-POLDIP3	Mammalian expression	II	Original plasmid
mEmerald-SERPINE1	Mammalian expression	II	Original plasmid
mEmerald-SORBS1	Mammalian expression	II	Original plasmid
mEmerald-TGM2	Mammalian expression	II	Original plasmid
mEmerald-P4HB	Mammalian expression	II	Original plasmid
mEmerald-PDLIM1	Mammalian expression	II	Original plasmid
mEmerald-SYNCRIP	Mammalian expression	II	Original plasmid
mEmerald-NISCH	Mammalian expression	II	Original plasmid
mEmerald-PRSS23	Mammalian expression	II	Original plasmid

3.5 Antibodies, lipids and other reagents

Table 3. Antibodies used in original publications I–IV.

Antigen	(Clone) or (manufacturer, identifier)	Species	Application	Original publication
β1 integrin	clone 12G10	mouse	IF	I–II
β1 integrin	clone HUTS21	mouse	IF	I
β1 integrin	clone 9EG7	rat	IF	I
β1 integrin	clone 4B4	mouse	IF	I-II
β1 integrin	clone mab13	rat	IF	I
β1 integrin	clone P5D2	mouse	IF	I
β1 integrin	Abcam, Ab183666	rabbit	WB	IV
α5 integrin	clone PB1	hamster	IF	I, III
α5 integrin	Merck Millipore, AB1949	rabbit	WB	IV
TLN1	clone 97H6	mouse	WB	I
TLN2	clone 68E7	mouse	WB	I
TLN1	clone 8D4	mouse	IF	II
β-actin	antibody AC-15	mouse	WB	I, III
Paxillin	antibody 349	mouse	IF	I
AP2μ	clone EP2695Y	rabbit	WB	I
myosin-X	Novus Biologicals, 22430002	rabbit	WB	I
GFP	Abcam, Ab290	rabbit	WB	I
pan-kindlin	Abcam, ab68041	rabbit	WB	I
Non-muscle myosin IIA heavy chain	Poly19098	rabbit	IF	III
Phospho myosin light chain	Cell Signaling Technology, #3674	rabbit	IF	III
BCAR1	Santa Cruz Biotechnology, SC-20029	mouse	IF/WB	II
FAK1	clone 77	mouse	IF	II
Pxn	clone 349	mouse	IF	II
Phospho-p130Cas	Cell Signaling, 4011	rabbit	IF	II
ILK	clone EPR1592	rabbit	IF	II

Table 4. Lipid reagents used in original publication IV.

Name	Application	Original publication
PC (L-α-phosphatidylcholine)	ProLIF	IV
PA (L-α-phosphatidicacid)	ProLIF	IV
Cholesterol (5-cholestene-3α,20α-diol/20α-hydroxycholesterol)	ProLIF	IV
PI(4,5)P2 (L-α-phosphatidylinositol-4,5-bisphosphate)	ProLIF	IV
PI(3,4,5)P (1-stearoyl-2-arachidonoyl-sn-glycero-3-phospho-(1′-myo-inositol-3′,4′,5′-trisphosphate)	ProLIF	IV
PI(3)P (1,2-dioleoyl-sn-glycero-3-phospho-(1′-myo-inositol-3′-phosphate)	ProLIF	IV
Biotin conjugated PE (1-oleoyl-2-[12-biotinyl(aminododecanoyl)]-sn-glycero-3-phosphoethanolamine)	ProLIF	IV

3.6 siRNA-mediated gene silencing

Protein expression of selected proteins were suppressed by using 50–100 nM siRNA (Qiagen) together with Lipofectamine 3000 (Thermo Fisher Scientific) using Lipofectamine instructions. Control siRNA was Allstars negative control siRNA (Qiagen,Cat No./ID: 1027280).

Table 5. siRNA reagents used in original publications I.

Target gene	siRNA name	Manufacturer	Cat. #
Control siRNA	Allstars	Qiagen	1027280
ACTN1	Hs_ACTN1_5	Qiagen	SI00299131
ACTN1	Hs_ACTN1_2	Qiagen	SI00021917
TNS3	Hs_TENS1_1	Qiagen	SI00134372
TNS3	Hs_TNS3_2	Qiagen	SI02778643
TNS1	Hs_TNS_3	Qiagen	SI00134106
TNS1	Hs_TNS_4	Qiagen	SI00134113
siFERMT1	Hs_C20orf42_5	Qiagen	SI0426918
siFERMT1	Hs_C20orf42_7	Qiagen	SI04307219
siFERMT1	Hs_C20orf42_8	Qiagen	SI04352978

Target gene	siRNA name	Manufacturer	Cat. #
siFERMT2	Hs_FERMT2_1	Qiagen	SI04952542
siFERMT2	Hs_FERMT2_3	Qiagen	SI04952556
CIB1	Hs_CIB1_5	Qiagen	SI02657102
CIB1	Hs_CIB1_7	Qiagen	SI03164476
SHARPIN	Hs_SHARPIN_2	Qiagen	SI00140182
SHARPIN	Hs_SHARPIN_5	Qiagen	SI03067344
ITGB1BP1	Hs_ITGB1BP1_5	Qiagen	SI03129385
ITGB1BP1	Hs_ITGB1BP1_8	Qiagen	SI04332832
TLN1	Hs_TLN1_2	Qiagen	SI00086968
TLN1	Hs_TLN1_3	Qiagen	SI00086975
TLN2	Hs_TLN2_3	Qiagen	SI00109277
MYO10	Hs_MYO10_5	Qiagen	SI04158245
MYO10	Hs_MYO10_6	Qiagen	SI04252822
MYO10	Hs_MYO10_7	Qiagen	SI05085507
SDC4	Hs_SDC4_1	Qiagen	SI00046816
SDC4	Hs_SDC4_2	Qiagen	SI00046823
ANXA1	Hs_ANXA1_6	Qiagen	SI02624174
ANXA1	Hs_ANXA1_7	Qiagen	SI02776886
ANXA1	Hs_ANXA1_8	Qiagen	SI02780239
RAPH1	Hs_RAPH1_2	Qiagen	SI00698642
RAPH1	Hs_RAPH1_5	Qiagen	SI04300982
RAPH1	Hs_RAPH1_6	Qiagen	SI04348190
AHNAK1	Hs_AHNAK_1	Qiagen	SI03138954
AHNAK1	Hs_AHNAK_5	Qiagen	SI04157503
AHNAK1	Hs_AHNAK_6	Qiagen	SI04208498
EPB41L3	Hs_EPB41L3_10	Qiagen	SI05113668
EPB41L3	Hs_EPB41L3_5	Qiagen	SI03207491
EPB41L3	Hs_EPB41L3_6	Qiagen	SI04157629
FLNA	Hs_FLNA_5	Qiagen	SI02654722
FLNA	Hs_FLNA_8	Qiagen	SI04145428
FLNA	Hs_FLNA_9	Qiagen	SI04206468
BCAR1	Hs_BCAR1_5	Qiagen	SI02757734
BCAR1	Hs_BCAR1_6	Qiagen	SI02757741

3.7 Isolation and culture of primary hippocampal neurons

Newborn Sprague-Dawley rats were sacrificed by decapitation and their hippocampi were placed into media containing 1 M Na_2SO_4, 0.5 M K_2SO_4, 1 M MgCl2, 100 mM CaCl2, 1 M Hepes (pH 7.4), 2.5 M Glucose, 0.5% Phenol Red (dissection media). After the removal of meninges, hippocampal pieces were collected and placed into dissection media containing 10% KyMg. After washing hippocampal tissue was treated with papain for 15 minutes (10 U/ml, #3119, Worthington) at 37°C. The papain treatment was repeated two times after which papain was deactivated using 10 mg/ml trypsin inhibitor (Sigma, T9128). This was done for 2 × 5 min at 37ºC. The tissue was homogenized by gently pipetting up and down and the cultures were plated on poly-d-lysine coated coverslips in Neurobasal-A medium (Thermo Fisher Scientific). The Neurobasal-A medium was supplemented with 2 mM glutamine, 50 U/ml penicillin, 50 µM streptomycin and B27 Neuronal supplement (Gibco, Thermo Fisher Scientific).

4–5 month old, pregnant Wistar rats were sacrificed on day E18 of pregnancy using CO_2 anesthesia and followed by decapitation. Neuronal cultures were prepared from 14–16 embryos regardless of their gender. The cultures were prepared by dissection of hippocampal tissue, followed by enzymatic digestion (with trypsin) and mechanical dissociation. Primary cell cultures were maintained on a poly-D-lysine coated glass coverslips and in a Neurobasal medium supplemented with 2% B27 Neuronal Supplement, 1% GlutaMAX and 1% pen/strep (Gibco, Thermo Fisher Scientific).

Neuronal cultures from Shank3 αβ-deficient mice were prepared in a similar manner but since these neuronal cultures are more fragile *in vitro*, the pregnant mice were sacrificed at E17 and neuronal analyses were done at DIV 14.

3.8 SDS–PAGE, quantitative western blotting and coomassie-staining

Recombinant proteins, cell extracts or pulldown/immunoprecipitation samples were resuspended in reducing Laemmli sample buffer. Samples were run on a gradient gel with gel percentage of 4-20 % using precast Mini-PROTEAN® TGX™ protein gels (Bio-Rad, #456-1093, #456-1094, #456-1095, #456-1095). For western blotting purposes, protein were transferred from the gel to a nitrocellulose membrane using Trans-Blot Turbo Transfer Pack (Bio-Rad, #170-4158, #170-4159). Nitrocellulose-membrane with transferred protein were blocked using any blocking buffer or buffered milk: 1X TBS, 0.1% Tween-20 with 5% (TBST) w/v nonfat dry milk. Blocked membranes were incubated with primary antibodies overnight in +4°C in a tube roller and with secondary antibodies conjugated with a fluorescent dye in room

temperature for one hour. The membrane was washed for 15 minutes with TBST between and after adding the antibodies and imaged using Odyssey Li-cor imager. Alternatively to fluorescence detection, membranes stained with antibodies coupled to HRP-tag, signal was detected using WesternBright ECL Western Blotting detection kit (#K-12045-D20, Advansta) together with Bio-Rad Chemidoc imager. SDS-PAGE gels were stained using instant blue stain from Biotop (#ISB1L).

3.9 siRNA screen

Glass-bottom 96-well plates (Cellvis, P96-1.5H-N) were coated first with poly-D-lysine (10 ug/ml in PBS, overnight +4°C, Sigma-Aldrich, A-003-M) followed by bovine fibronectin (10 ug/ml in PBS, overnight +4°C). After washing the plate with PBS, EGFP-MYO10 expressing U2-OS cells that were siRNA silenced 48 hours before were seeded into fibronectin coated wells. Cells were let to adhere and spread for 2 hours in full culture medium before fixing the samples with 4% paraformaldehyde (PFA, Thermo Scientific, 28906). Cells not used for microscopy were subjected to lysis, RNA extraction and Taq-Man qPCR to quantify silencing efficiency. After washing the microscopy samples with PBS, autofluorescence was quenched using 1M Glycine in PBS followed by more washes and staining the samples with DAPI (0.5 µg/ml in PBS, Thermo Fisher Scientific, D1306) and phalloidin-Atto647N (1:400 in PBS, Thermo Fisher Scientific, 65906). Washed samples stored in PBS were then manually imaged using a spinning-disk confocal microscope using a 40x water objective. Image analysis was performed in an automated way using Fiji (Schindelin et al., 2012). After background subtraction and normalization, bright Myo10 puncta were detected by using a 'Findmaxima' plugin from Michael Schmid. Intracellular Myo10 spots were excluded from analysis by creating a mask based on F-actin staining. The remaining spots per field of view were included in the analysis.

3.10 RNA extraction, cDNA preparation and Taq-Man qPCR

Cellular RNA was extracted using a NucleoSpin RNA extraction kit from Macherey-Nagel (cat. no. 740955.240C). RNA was reverse transcribed into cDNA using a high-capacity reverse transcription kit from Applied Biosystems (Thermo Fisher Scientific, 43-688-14). Universal probe library (Roche) together with appropriate DNA primers for polymerase (designed using ProbeFinder, version 2.53, Roche) and ordered from IDT were used to detect amplification of mRNA molecules of interest. Taq-man master mix (Thermo Fisher Scientific, 4444557) was used to prepare qPCR reactions according to manufacturer's instructions. Reactions themselves were

analyzed using 7900HT fast RT-PCR System (Applied Biosystems). Relative mRNA expression of genes were calculated with the $2^{-\Delta\Delta CT}$ method by comparing genes of interest to GAPDH mRNA expression to normalize between conditions and experiments.

3.11 Generation of the filopodia maps

To image cells with structured illumination microscope, U2-OS cells expressing EGFP-Myo10 were seeded on MatTek glass-bottom dishes (MatTek Corporation, coverslip#1.7), precoated with fibronectin. After 2 hours of spreading the cells were fixed with 4% paraformaldehyde and 0.25 % of Triton X-100 for 10 minutes in room temperature. After washing and quenching the samples with 1 molar Glycine in PBS (30 min at room temperature), samples were incubated with the appropriate primary antibodies (1:100 dilution, 1 hour at room temperature). After washes the same treatment was repeated using a secondary antibody coupled to a fluorescent Alexa dye. Samples were washed three times with PBS before placing them in +4°C in 100 nM SiR-actin solution (in PBS; Cytoskeleton; catalogue number:CY-SC001). Prior to imaging, samples were washed three times and mounted in Vectashield (Vector Laboratories). After imaging the samples with a structured-illumination microscope, data was analyzed using scripting-packages described in Jacquemet et al., 2019. Briefly, brightness and contrast of each image was automatically adjusted and a 1-pixel width line intensity profile was manually drawn on each filopodia from base-to-tip fashion. The base of the filopodium was defined as an intersection between filopodium and lamellipodium. The line intensity profiles of each visible filopodia were exported from Fiji using Multi Plot function and further analyzed using R where the line intensity profiles were compiled and their lengths were normalized into 40 bins. In heat maps style plots the median value of each bin was used to display the brightness of staining at that point and using the percentage of filopodia whose tips were positive for active β1 integrin were quantified. Heat map style plots were created by compiling line intensity profiles from hundreds of filopodia. Filopodia length data were directly extracted from these line intensity profiles.

3.12 Quantification of filopodia numbers and dynamics

In both cases U2-OS cells expressing EGFP-MYO10 plasmid were seeded on glass-bottom dishes pre-coated with fibronectin (MatTek Corporation). Seeded cells were let to adhere and spread for 2 hours and to analyze the number of filopodia formed by each cell, samples were fixed (4% paraformaldehyde) and stained for F-actin using either SiR-actin (SiR-actin (100 nM; Cytoskeleton;catalogue number: CY-

SC001) or phalloidin-Atto647N (1:400 in PBS, Thermo Fisher Scientific, 65906). Images were acquired with a spinning-disk confocal microscope and the amount of extracellular MYO10 puncta were manually calculated from each image. To track filopodia dynamics, live cells were imaged with Zeiss LSM880 microscope in normal culture media supplemented with 50 mM HEPES. Imaging was done at 37°C in the presence of 5% CO_2 and pictures were taken every 5 seconds over the 20 minute time-frame. The lifetime of MYO10 puncta was tracked using a Fiji plugin TrackMate (Tinevez et al., 2017). There, the LoG detector (estimated bob diameter = 0.8 mm; thresh-old = 20; subpixel localization enabled) and the simple LAPtracker (linking max distance = 1 mm; gap-closing max distance = 1 mm; gap-closing max frame gap = 0) were used.

3.13 Sample preparation for light microscopy

Samples for light microscopy were prepared in different ways depending on the study and cell type

Primary neurons isolated from the brains of rats and mice were grown on glass coverslips and were fixed using 4% paraformaldehyde at DIV indicated in figure legends. Paraformaldehyde fixation was followed by permeabilization with 0.1–0.5% Triton X-100 and finally samples were blocked using 10% horse serum (in PBS). After blocking, the auto-fluorescence was quenched using 1 M glycine in PBS for 30 minutes. Samples were immuno-stained with primary antibodies (30 minutes at room temperature), followed by washes and 30 minute incubation with a fluorescently labelled secondary antibody. After washes samples were imaged using a confocal microscope.

To prepare light microscopy samples for other than primary cells, 35 mm #1.5 glass-bottom dishes (Cellvis, #D35-14-1.5-N) were coated with bovine plasma fibronectin (Merck-Millipore, #341631, diluted to 10 µg/ml in PBS) (Original publication III). In the case of original publication I-II, glass-bottom dishes were first coated with poly-d-lysine and then with bovine plasma fibronectin using 10 µg/ml fibronectin solution in PBS. Coating for either poly-d-lysine or fibronectin was always done over-night in +4°C. Cells were plated on coated dishes at a reasonable confluency in a media suitable for each cell line and fixed using 4% paraformaldehyde and 0.1–0.25% Triton X-100. 4% paraformaldehyde/0.1–0.25% Triton X-100 solution was either poured directly onto the cells or a stronger solution was added into the culture medium to reach the wanted end concentration. Cells were fixed for 5–10 minutes in a room temperature and quenched using 1 M glycine in PBS for 30 minutes. Samples were stained similarly with neuronal samples and imaged using a confocal of structural-illumination microscope.

3.14 Integrin activity assay

Integrin activity levels were recorded by probing the cell surface with a labelled fibronectin fragment as previously described (Bouaouina, M., et al., 2012). CHO cells transiently transfected with an expression construct were detached using Hyclone® HyQTase (Thermo Fisher Scientific Inc, #SV300.30.01). HyQTase was replaced with warm, serum-free CHO culture media and Alexa Fluor 647-labelled fibronectin 7–10 fragment was added with and without EDTA (negative control) was added. Cells were let to bind fibronectin fragments for 40 minutes in a room temperature. Tyrode's buffer (10 mM Hepes-NaOH pH 7.5, 137 mM NaCl, 2.68 mM KCl, 0.42 mM NaH_2PO_4, 1.7 mM $MgCl_2$, 11.9 mM $NaHCO_3$, 5 mM glucose, 0.1% BSA) was used for washing of the cells and the fibronectin bound cells were fixed using 4% paraformaldehyde (in PBS) for 10 minutes in room temperature. Total α5-integrin levels were measured either staining the same set of fibronectin bound samples (original publication IV), or a separate corresponding set with PB1 anti-α5 antibody that was later stained with an appropriate fluorescent secondary antibody. Fluorescence intensity of bound fibronectin and total α5 integrin was recorded using BD LSRFortessa™cell analyzer (BD Bioscience). Integrin activity index was defined as AI = (F–F0)/(FPB1), where F was the geometric mean fluorescence intensity of fibronectin 7–10 fragment and F0 the mean fluorescent intensity of fibronectin 7–10 fragment in EDTA-containing negative control. F_{PB1} was the total α5 integrin level measured also as a geometric mean fluorescence intensity.

3.15 Micropatterning

Creating micropatterning with a crossbow shape has been described earlier in publication (Azioune et al. 2009). Briefly, 50 µl/ml fibronectin and either 1:200 dilution of 555-labelled BSA or 647-labelled fibrinogen were then used to coat the micropatterns. Cells were plated on micropatterns and fixed after 3–4 hours of spreading as described above.

3.16 Microscopy based cell spreading assay

Cells transfected with fluorescent plasmids were detached using trypsin and plated on fibronectin coated imaging plates. Cells were fixed with 4% paraformaldehyde after a sufficient amount of spreading time (indicated in figure legends). The spreading of the cells was recorded by imaging the bottom plane of each cell. ImageJ was used manually to measure the area of each transfected cell.

3.17 Recombinant protein expression and purification of soluble proteins

Competent *E. coli* BL-21 was used as a production strain to express the recombinant proteins and all the expression plasmids had an IPTG-inducible promoter. Transformed bacteria were grown in 37°C in LB broth supplemented with selection antibiotics (ampicillin or kanamycin depending on the expression construct). After bacterial cultures reached large enough optical density at 600 nm ($1>OD_{600}>0.6$), protein expression was induced by adding 0.1–0.5 mM of IPTG into the culture medium. After induction, culture temperature was lowered to 18-23°C and kept there overnight. Bacteria were harvested by centrifugation at 6000 x g for 15–20 minutes and depending on the protein of interest, resuspended in either TBS buffer (original publication I) or 50 mM Tris-HCl buffer with 150-300 mM NaCl (original publication III). Both resuspension buffers also contained a small spoonful of lysozyme from chicken egg white (Sigma-Aldrich, #L6876-5G), 1x BugBuster (Merck Millipore, #70584-4), cOmplete™ protease inhibitor tablet (Roche, #5056489001) and 2 µl/ml DNAse (Sigma-Aldrich, #11284932001). In addition, buffer in original publication III contained 1% Triton X-100. After 30 minutes of rotation in 4°C, the lysate was cleared from debris by centrifugation at 20 000 x g for 1 hour in 4°C.

For His-tagged FERM domains in original publication I, the lysate was ran through an equilibrated Protino 2000 packed Ni-TED column (Macherey Nagel). After washing and elution steps indicated in the column manual, Imidazole was removed by dialyzing the protein with Thermo Scientific Slide-A-Lyzer™ Dialysis Cassettes. In case a non-tagged version of the protein was purified, a His-tagged TEV protease (Sigma) was used overnight (+4°C, rotation) to cleave the tag when protein was bound to the column beads. Subsequent purification step was then added to remove cut His-tag and the protease by again using Protino 2000 packed Ni-TED column.

For purification of other proteins (Original publication III), protein was first bound to either Glutathione Sepharose® 4B (for GST-tagged proteins, GE Healthcare, #17-0756-01) or Protino Ni-TED resin (for SUMO-tagged proteins, Macherey-Nagel, #745200.5) (1 hour in rotation, +4°C), before transferring the resin into a gravity column (Talon® 2 ml Disposable Gravity Column, Clontech, #635606-CLI). The resin was washed five times with an ice cold washing buffer containing 50 mM Tris-HCl and 150-300 mM NaCl. Wash buffers were derived from this buffer by adding 1 mM DTT (Sigma-Aldrich, #D0632-5G) and 0.1% triton-X. In addition either 250 mM imidazole (His-tagged protein) or 30 mM reduced glutathione (GST/SUMO tag) was added to elute the protein of interest. After elution the pH was adjusted to 7–7.5 and protein was dialyzed using Thermo

Scientific Slide-A-Lyzer™ Dialysis Cassettes. Protein purity was estimated using SDS-PAGE and InstantBlue Protein Stain (Expedeon, #ISB1L).

3.18 Whole-mount immuno-SEM

EGFP-Myo10 expressing U2-OS cells were plated on fibronectin coated coverslips and let to spread for 2 hours before fixing the samples using 4% paraformaldehyde (in 0.1 M HEPES, pH 7.3) for 30 minutes in room temperature. Samples were washed and autofluorescence was quenched using a buffer of 50 mM NH4Cl (in 0.1 M HEPES). Non-specific binding was blocked using 2% BSA in 0.1 M HEPES. After washing, samples were labelled for 30 minutes in room temperature using an appropriate primary antibody (1:10 antibody dilution in 0.1 M HEPES). Gold-conjugated secondary antibodies were used to stain the samples in 1:50 dilution (0.1 M HEPES, 30 nm gold particles, BBIsolutions, EM.GAF30, 30 minutes). After labelling samples with nano-gold antibodies, samples were washed and post-fixed using 2.5% glutaraldehyde and 1% buffered osmium tetroxide. Post-fixing, samples were dehydrated and dried using hexamethyldisilazane. Dried samples were mounted on scanning-electron microscope stubs and sputter-coated with carbon. FEI Quanta FEG 250 microscope with SE and vC detectors was used to acquire micrographs of the samples by using an acceleration voltage of 5.00 kV and a suitable working distance (from 7.7 to 10.9 mm).

3.19 Integrin tail pull-downs

Pre-washed streptavidin coupled magnetic beads (MyOne Streptavidin C1, Invitrogen,65001) were incubated on ice for 30 minutes with the appropriate biotin-tagged integrin-tail peptides (LifeTein). U2-OS cells were washed and subsequently lysed using a lysis buffer of 40 mM HEPES, 75 mM NaCl, 2 mM EDTA, 1% NP-40, a cOmplete™ protease inhibitor tablet(Roche, 5056489001) and a phosphatase-inhibitor tablet (Roche, 04906837001). Debris was removed by centrifugation at 13000 x g for 10 minutes at +4°C. Cleared samples were incubated with magnetic beads coupled to integrin-tail peptides in rotation for 2 hours at +4°C. Washing buffer of 50 mM Tris-HCl pH 7.5, 150 mM NaCl, 1% (v/v) NP-40 was used to wash magnetic beads 3–4 times before resuspending the beads to 4x Laemmli sample buffer and eluting bound complexes by heating the samples 3–10 minutes at +90°C. The following integrin tail peptides were used in the study: β1-integrin tail (KLLMIIHDRREFAK-FEKEKMNAKWDTGENPIYKSAVTTVVNPKYEGK), α2-integrin tail (WKLGFFKRKYEKM), α2-integrin tail mutant (WKLGAAKRKYEKM), α5-integrin tail (KLGFFKRSLPYG-TAMEKAQLKPPATSDA)

3.20 GFP pull-down

EGFP tagged FERM domain construct expressing U2-OS cells were lysed using a lysis buffer of 20 mM Hepes, 75 mM NaCl, 2mM EDTA, 1% NP-40, cOmplete™ protease inhibitor tablet (Roche, cat. no. 5056489001) and a phosphatase-inhibitor tablet (Roche cat. no. 04906837001). Samples were cleared with a centrifuge (13000 x g, 10 min +4°C) and GFP-Trap-A beads (Chromotek) were added. To bind GFP-tagged proteins, beads were rotated in +4°C for two hours followed by 3–4 washes with 50 mM Tris-HCl pH 7.5, 150 mM NaCl, 1% (v/v) NP-40. Dry beads were resuspended into 4x Laemmli sample-buffer and formed complexes were eluted by heating the samples 3–10 minutes at +90°C.

3.21 Microscale thermophoresis

Thermophoresis is a directed movement of a molecule along a temperature gradient which may become affected by any change (such as binding of another molecule) in the molecule's chemical microenvironment.

To measure binding between integrin tails and recombinant proteins, His-tagged proteins were labelled from the tag using Monolith His-Tag LabelingKit RED-tris-NTA (NanoTemper, MO-L008). While keeping the labelled protein at a 20 nM concentration and probing the labelled protein with a range of integrin tail peptides at increasing concentrations, thermophoresis of tagged proteins were analyzed by using Nanotemper NT.115 device. K_d values were derived from the data using quadratic equation where [AL] is the concentration of the formed complex:

$$[AL]=1/2*(([A0]+[L0]+ Kd)-(([A0]+[L0]+ Kd) 2 -4*[A0]*[L0])1/2)$$

Here, K_d is the dissociation constant, [A] the concentration of the free fluorescent molecule, [L] the concentration of the free ligand. [A0] is the known concentration of the fluorescent molecule and [L0] the known concentration of an added ligand.

Alternatively to the quadratic fit, binding was also expressed as a change in fluorescence. Normalized fluorescence was used as a measure of the binding and is defined as a ratio of MST signal (=fluorescence) before and after IR laser activation:

$$F_{norm}=F_1/F_0$$

3.22 Dendritic spine analysis

Maximum intensity projections of neuronal images were used to assess dendritic spine morphology from primary rat hippocampal cells and at least 16 spines per cell were randomly selected for analysis. The neck length was measured by drawing a line from the base of the neck to the stem of the spine head. Head diameter was

measured by drawing a line between the most distant points in the spine head. From these measurements, the ratio of head diameter:neck length was drawn. Either ImageJ or Neurolucida Explorer (MBF Bioscience, Williston, DC, USA) were used to assess spine density on the neuron. In an analysis of shank3 αβ full knockout neurons, spines were manually divided into classes depending on their morphological features and whether they had a visible neck and a separate bulbous head (spine) or no apparent head at all (filopodia).

3.23 Co-immunoprecipitation

A 1:1 equimolar mixture of purified, Fos–β1 and Jun–α5 membrane proteins were subjected to co-immunoprecipitation by incubating the protein mixture with antibodies recognizing β1 and α5 cytoplasmic tails. 1 μg of antibody was incubated with the protein mixture and at +4°C for 2 hours and in a buffer containing 50 mM Tris-HCl pH 7.5, 150 mM NaCl, 600 μM TCEP plus 0.1% DDM. The formed complexes between the protein and antibody were then isolated using Protein-G beads from GE healthcare. The complexes were let to bind to the beads over a time of 2 hours at +4°C, while keeping the samples in constant rotation. Bead-bound complexes were then washed with the buffer above, suspended into Laemmli sample buffer, heated, separated with SDS-gel electrophoresis, transferred to a nitrocellulose membrane and analyzed using standard western blotting techniques.

3.24 Pulldown using affinity beads

GFP and RFP-tagged proteins were pulled down from a cell lysate using GFP-Trap® agarose, RFP-Trap® agarose and RFP-Trap® magnetic agarose (ChromoTek, #GTA-100, RTA-100 and RTMA-100) beads. U2OS or HEK293 cells were transfected with a preferred GFP/RFP expression construct and 24-48 hours later were lysed using IP lysis buffer (40 mM HEPES-NaOH, 75 mM NaCl, 2 mM EDTA, 1% NP-40 and cOmplete protease (Roche) and phos-stop phosphatase inhibitor tablets (Roche)). After clearing the lysate by centrifugation, 20-30 μl of beads were added directly to the lysate and samples were rotated in +4°C for 1-2 hours. The formed complexes were washed 3–4 times with a buffer containing 20 mM Tris-Hcl (pH 7.5), 150 mM NaCl and 1% NP-40. Finally, samples were resuspended in a reducing 4X Laemmli sample buffer and heated for 3-10 min at 95°C.

GST or SUMO-tagged proteins were pulled down similarly to GFP/RFP-proteins and by using 20 mM Tris-HCl (pH 7.5), 150 mM NaCl and 1% NP-40 as a wash buffer. Depending on the application, samples were analyzed using SDS-PAGE and/or western blot.

3.25 Flotation assay

Fos–β1 and Jun–α5 were reconstituted in liposomes (equimolar amounts of both proteins) which were then combined with 1:1 ratio of 60% Sucrose solution. The resulting 30% solution was added to the bottom of an ultracentrifuge tube and decreasing amounts of sucrose layers were gently added on top of each other in the tube. The gradient formed this way was ultra-centrifuged overnight at 20 000 x g at +4°C. The gradient fractions were retrieved at the inverse order and analyzed using SDS-PAGE.

3.26 β/γ-actin disassembly assay

β/γ-actin disassembly assay has been described before (Kremneva et al., 2014). Briefly and with slight modifications, both 1 or 2 μM GST-tagged SPN domain and and 0.8 μM cofilin-1 were diluted in G-buffer (5 mM Hepes pH 8, 0.2 mM $CaCl_2$, 0.2 mM ATP, 1 mM DTT) and mixed with polymerized pyrene actin (4 μM). The reaction was initiated by adding 6 μM vitamin D binding protein [DBP] (Human DBP, G8764, Sigma). The final buffering conditions were 20 mM HEPES pH 8, 100 mM KCl, 1 mM EGTA, 0.2 mM ATP across all samples. Agilent Cary Eclipse Fluorescence Spectrophotometer with BioMelt Bundle System (Agilent Technologies) was used for measurements with excitation wavelength of 365 nm (Ex. Slit = 5 nm) and emission wavelength of 407 nm (Em. Slit = 10 nm).

3.27 Protein structure visualization and structure-based superimpositions

Pymol (The PyMOL Molecular Graphics System, Version 2.0 Schrödinger, LLC) was used for all protein visualizations with available protein structures from protein data bank (rcsb.org). Pymol's align function was used to perform sequence alignment followed by structural superimposition. In low-homology cases, Pymol's cealign function was used to perform structural superimpositions. Pymol was used under a professional licence for academics.

3.28 Multiple sequence alignment

Geneious R8 platform (https://www.geneious.com) and MUSCLE multiple sequence alignment algorithm embedded inside was used for aligning multiple protein sequences.

3.29 Zebrafish microinjections

To study the effects of shank3 mutagenesis in the fish, endogenous shank was silenced using with 3.5 ng of either control morpholino oligo, or an oligo targeting shank 3a and/or shank3b (shank 3a: 5'-AGAAAGTCTTGCGCTCTCACCTGGA, shank 3b: 5'-AGAAGCATCTCTCGTCACCTGAGGT). Morpholino oligos were injected into 1-4 cell stage embryos together with in vitro transcribed shank3 mRNA (WT and mutant). The injection was done by using a NanojectII microinjector (Drummond Scientific). Following the injections, embryos were placed +27.5°C in a E3 medium containing 5 mM NaCl, 0.17 mM KCl, 0.33 mM $CaCl_2$, 0.33 mM $MgSO_4$ and supplemented with penicillin and streptomycin.

3.30 Zebrafish motility assay

A day before injections, 30 μg of Pronase was added on embryos to facilitate hatching. Embryos were transferred into a 96-well plate (one per well) at two days post fertilization. Daniovision instrument (Noldus IT) was used to track embryo motility (30 fps for 60 minutes). First a baseline was recorded by measuring embryo motility throughout three light/dark cycles (5 min light/5 min dark). Then the program was run again with 20 mM pentylenetetrazole (PTZ, Sigma-Aldrich) added to the wells to stimulate embryo movement. EthoVision XT software from Noldus IT was used for quantification. The first 20 minutes of baseline measurements were removed and the remaining 40 minutes was used for analysis. Minimum and maximum movement filters were used to (0.2 mm minimum filter / 4 mm maximum filter) and total distance, average speed and fraction of time spent moving were quantified.

3.31 Zebrafish eye pigmentation assay

For eye pigmentation analysis of microinjected zebrafish embryos, 30 hpf embryos were dechorionated using forceps. Embryos were anaesthetized with 160 mg/ml Tricaine and a Zeiss AxioZOOM stereo-microscope was used for imaging. Eye pigmentation analysis was performed using ImageJ where images were inverted and the background was removed. Signal intensity from the eye was recorded after manual segmentation of the eye using a line selection tool.

3.32 Membrane protein purification

E. coli (Rosetta-strain) transformed with Jun–α5 and Fos–β1 protein expression vectors were grown at 25°C in LB broth containing ampicillin and chloramphenicol. After measuring that the optical density at 600 nm of the bacterial culture had

reached 0.6, protein expression was induced by adding a final concentration of 0,5 mM of Isopropyl-β-D-thiogalactoside. After this, the temperature was lowered to 25°C and bacteria were incubated for 5 hours to translate Jun–α5 and Fos–β1 proteins. Bacteria were harvested by centrifugation 4000 x g for 20 minutes and the pellets were snap-freezed using liquid nitrogen for storage. After storage, the pellets were let to thaw gently and then resuspended in a buffer containing 50 mM Tris-HCl pH 7.5, 150 mM NaCl, 600 µM TCEP, 500 µM PMSF, 2 mM AEBSF, a cOmplete protease inhibitor tablet (Roche), 0.1 mg/ml DNAse (Roche), 1 mM β-mercaptoethanol (Sigma), 5 mM $MgCl_2$ and lysozyme (Sigma). A cell disruptor was then used to lyse bacterial cells. Cell debris was removed by centrifugation at 27 000 x g (JA 25/50 rotor for 20 min at +4°C) and after collecting supernatant, cell membranes were harvested again by 1 hour centrifugation at 278 000 x g in +4°C using a Ti50.2 rotor. The membrane fraction was resuspended in a buffer containing 50 mM Tris-HCl pH 7.5, 150 mMNaCl, 600 µM TCEP, 500 µM PMSF, 1 mM AEBSF. After resuspending the fraction, a teflon homogenizer was on the sample followed by addition of 300 mM sucrose and flash freezing using liquid nitrogen. After storage in -70°C and in order to remove the membrane lipids, the homogenized membrane fractions were incubated with n-dodecyl-β-D-maltoside (DDM) (Anatrace) at a 5:1 (w:w)ratio for 2 h at +4°C. This was done in agitation and followed by a centrifugation at 244 000 x g (Ti50.2rotor for 50 min at +4°C) to remove any debris from lipid membranes. Supernatant was collected and incubated with Nickel Sepharose beads (GE healthcare, 2 hours in +4°C) followed by 1x with a buffer of 50 mM Tris-HCl pH 7.5, 150 mM NaCl, 600 µM TCEP, 1 mM AEBSF, +0.5% DDM. Second wash was performed using a buffer of 50 mM Tris-HCl pH 7.5, 150 mM NaCl, 600 µM TCEP, 1 mM AEBSF and either 0.05% DDM (for Fos–β1) or 0.1% DDM (for Jun–α5). Soluble membrane proteins were then eluted using an elution buffer consisting of 50 mM Tris-HCl pH 7.5, 150 mM NaCl, 1 mM AEBSF, 0.05% DDM and 250 mM imidazole. Eluted proteins underwent a second round of purification where GST-tagged Fos–β1 protein was incubated with glutathione–Sepharose beads (GE healthcare) and MBP-tagged Jun–α5 was incubated with Dextrin–Sepharose beads. Proteins were incubated with the beads for 60 min at +4°C and then washed with 50 mM Tris-HCl pH 7.5, 150 mM NaCl, 600 µM TCEP, 1 mM AEBSF. The buffer was also substituted with either 0.05% DDM (for Fos–β1) or 0.1% DDM (for Jun–α5). Then, a buffer with 50 mM Tris-HCl pH 7.5, 150 mM NaCl, 1 mM AEBSF, 0.05% DDM and either 30 mM glutathione (for Fos–β1) or 20 mM maltose (for Jun–α5) was used to elute bound membrane proteins which were finally snap-freezed using liquid nitrogen and stored in -80°C. A yield of approximately 1 mg of protein per 1 liter of culture volume was obtained using this technique.

3.33 Bio-Beads™ preparation and dosing

To prevent blocking flow cytometric devices, Bio-Beads™(Bio-Rad) were first sifted to remove small sized beads that would have been difficult to remove otherwise. Beads were subjected to 8 washes (5 times with methanol, 3 times with milliQ water) after which beads were left to sediment and used in added volumes of 15 µl when preparing (proteo-)liposomes. 15 µl of beads prepared this was corresponds to 3 milligrams in weight and the sedimented beads were collected from the bottom of the tube by using a 200 µl pipette tip with an increased opening (cut tip).

3.34 Liposome and proteoliposome reconstitution

Throughout the study, different lipid membranes were compared to a control membrane composed of 73% (w/w) Egg-PC, 10% (w/w) Egg-PA, 15% (w/w) cholesterol and 2% (w/w) of lipids with biotin-tag. In the cases where phosphoinositides were included in the lipid membrane, this was done with the expense of Egg-PA. By doing this the percentage of negatively charged lipids was kept at a constant 10%.

In the beginning the stock lipids were dissolved in an organic solvent which was removed under a stream of nitrogen to prevent oxidation of the lipids. The residual solvent was removed in a vacuum-drier for at least 20 minutes. The mix of lipids was resuspended in milliQ water at 10 mg/ml and vortexed heavily. The prepared lipid mixes were then aliquoted and stored in -20°C. 400 µg of total lipids were used for each liposome/proteoliposome reconstitution by solubilizing lipids in Triton X-100 (Triton X-100:lipid ratio of 2.5, w/w). This was done in a total volume of 400 µl and by using a reconstitution buffer (50 mM Tris-HCl pH 7.0, 150 mM NaCl and 600 µM TCEP). Constant stirring at room temperature was applied until the milky-white solution started to clear indicating total lipid solubilization. The solution was cooled down to +4°C and was supplemented with 1 mM EDTA, 5 mM AEBSF protease inhibitors as well as GST–Fos–β1 and/or MBP–Jun–α5 proteins in the case of proteoliposome preparation. The solution was stirred for 15 minutes in +4°C before gradual addition of pre-washed Bio-Beads:

Table 6. Gradual addition of Bio-Beads removes detergents leading to formation of (proteo)liposomes. Original publication III.

Bio-Beads (mg)	Time (min)
3	0
3	90
12	180
30	over-night

3.35 Isolation of detergent-free cell lysate

To obtain detergent-free cell lysate, HEK293 cells expressing a EGFP tagged protein of interest were washed three times with ice-cold PBS and 400 µl of detergent free buffer (10 mM Tris-HCl pH 7.5, 250 mM sucrose, 1 mM EDTA, 1 mM MgOAc, 20 µM ATP plus complete protease and PhosSTOP phosphatase inhibitor tablets, Roche) was added for every 10 cm dish. After scraping the cells, the cell extracts were passed through a 0.5 mm needle with a syringe (5x times) and sonicated on ice for 5 minutes. The sonicated cell extracts were further ultracentrifuged at 100 000 x g (1 hour at +4°C). The membrane depleted supernatant was then used for experimenting with liposomes and/or proteoliposomes.

3.36 Calculation of EGFP concentration within cell lysates

A serial dilution of fluorescein (1–256 nM) was measured using a BioTEK Synergy H1 hybrid plate reader to obtain a standard curve. Similarly, a serial dilution of EGFP-protein containing cell lysate was measured in relation with the fluorescein standard curve and EGFP-protein concentration was calculated using Equation 1. The majority of values for quantum yields and extinction coefficients have previously been analyzed and published (Song et al., 2000; Zhang et al., 2014) and the extinction coefficient values for EGFP-fusion proteins were calculated using the ExPASy ProtParam tool at http://web.expasy.org/protparam.

During a passage of light through a sample, the fluorescence intensity or number of excited molecules in that sample can be determined by Lambert-Beer law (Equation 1) and its derivatives:

$$\mathbf{Equation1}: \qquad I = I_0 \cdot e^{-ln(10)\cdot\epsilon_\lambda\cdot c\cdot l}$$

Here I corresponds to the light intensity passing through the sample and I_0 to the incident radiation. ε_λ is the excitation coefficient at a certain wavelength, c being the concentration and l the length of the light path (sample thickness). For samples with low concentration this can be expanded to equation 2:

$$\mathbf{Equation2}: \qquad I = I_0[1 - ln(10)\cdot\epsilon_\lambda\cdot c\cdot l]$$

The emission intensity ($F\lambda$) for a specific molecule at a given wavelength is given by Equation 3. Since the detection depends heavily on the detector and other factors contributing to a constant detection error, the fraction of the wavelength that is detected ($f\lambda$) is compensated by a factor j depending on the measurement set-up.

$$\mathbf{Equation3}:$$
$$F_\lambda = ln(10)\cdot\epsilon_\lambda\cdot c\cdot l\cdot I_0\cdot\phi_\lambda\cdot f_\lambda\cdot j$$

By solving the linear system of equations for both EGFP-labelled molecule and fluorescein standard we obtain the following expressions:

$$\textbf{Equation4}: \quad c_{GFP} = \frac{F_{GFP}}{ln(10) \cdot \epsilon_{GFP} \cdot l \cdot \phi_{GFP} \cdot f_{\lambda} \cdot j}$$

$$\textbf{Equation5}: \quad I_0 = \frac{F_{Ext}}{ln(10) \cdot \epsilon_{Ext} \cdot l \cdot c_{GFP} \cdot \phi_{Ext} \cdot f_{\lambda} \cdot j}$$

Here sub-indices indicate the sample. Using the calibration curve obtained from a Fluorescein titration series measurements we can now obtain the incident radiation I_o for our EGFP sample. Here the c_{Ext}/F_{Ext} is the inverse of the slope when F_{Ext} is linearly fitted against c_{Ext}.

3.37 Flow cytometry-based binding assay

By using Lambert-beer law and its derivatives (Equations 1–5) we calculated the concentration of EGFP-tagged protein in the cell lysate. By doing this, known amounts of EGFP-tagged protein binding to (proteo-)liposomes were measured. The concentration of EGFP-tagged protein was adjusted by addition of a detergent-free buffer (50 mM Tris-HCl pH 7.0, 150 mM NaCl and 600 µM TCEP). 150 µl of detergent-free cell lysate was added with 60 µl of (proteo-)liposomes and 90 µl of reconstitution buffer (50 mM Tris-HCl pH 7.0, 150 mM NaCl and 600 µM TCEP). For proteins to bind liposomal surfaces, the mixture was stirred in +4°C for 4 hours. After 4 hours 2 µl of SA beads were added into each sample and stirred for additional 30 minutes. Finally, EGFP-binding to (proteo-)liposomes was recorded using BD LSRFortessa™ cell analyzer (BD Bioscience).

3.38 Flow cytometry settings, data acquisition and analysis

When data-acquisition was performed all flow-cytometry settings were kept constant when measuring samples that would be compared between each other. Fluorescence-activated cell sorter LSRFortessa™flow cytometer (BD Biosciences) was used for data acquisition and operated with a dedicated BD FACSDiva™software.

EGFP has fluorescence properties of excitation/emission, 488/509. Thus, a 488 laser line together with a set of filters was used to detect excitation from EGFP-protein bound (proteo-)liposomes. The filter set used was composed of a 505 nm long-pass filter and a narrower 530/30 nm filter.

Cy5 dye has fluorescence properties of excitation/emission 565/670. To detect this dye, we employed a 532 nm laser line and a filter set composed of a 635 nm long-pass filter and a 670/30 nm filter.

Before starting the experiments, the population corresponding to the streptavidin bead/liposome/protein complex was made visible by adjusting photomultiplier (PMT) tube voltages. At the same time the cell population was fit into the linear range of the instrument. Both background fluorescence from beads and fluorescence from sample complex were fitted into a single detection window and evaluated as a FSC-A versus SSC-A scatter plot. Here the count rate was typically between 20-200 events/second.

For subsequent analysis, Flowing software (by Mr Perttu Terho, Turku Centre for Biotechnology, Finland; www.flowingsoftware.com) was used. In the analyses, the population corresponding to sample-complex (beads/liposomes/protein) were selected and this population was further assessed for its fluorescence intensity. Median values for fluorescence were used for data analysis and plotting of the fluorescence data.

3.39 Kd fitting for EGFP-tagged proteins isolated from cell lysates

Since PC lipids extracted from chicken eggs produced a high background, synthetic POPC was used for any quantitative measurements. A basal mix of POPC (80.5% w/w), cholesterol (15% w/w), biotinylated lipid (2% w/w) was spiked with either PI(3,4,5)P3 (2.5% w/w) (in the case of BTK-PH–EGFP) or with PI(3)P (2.5% w/w) (in the case of 2xFYVE-EGFP). These were prepared as described before. Control liposomes were used to assess the amount of non-specific binding that was then subtracted from the final result. In the control liposome mix, POPC amount was increased to 83% to compensate for the lack of any phosphoinositides in the forming liposomes. Serial dilutions of lysate with decreasing concentrations of EGFP-tagged protein were probed against liposomes. EGFP-tagged protein binding to phosphoinositide containing liposomes and control liposomes was assessed using flow cytometry and the non-specific binding from control liposomes was subtracted before the theoretical maximum fluorescence value (F_{max}) was estimated by curve-fitting using equation 6:

$$\textbf{Equation6}: \qquad F = \frac{F_{max} \cdot [P]}{[P] + K_d}$$

Here F is the background-subtracted fluorescence value and [P] protein concentration. The fluorescence values from different samples were then normalized to F_{max} to yield occupancy values as shown in equation 7:

$$\textbf{Equation7}: \qquad \theta = \frac{F}{F_{max}} = \frac{[P_{bound}]}{[PIP_{total}]}$$

Here [Pbound] marks the concentration of the protein bound to phosphoinositides and [PIPtotal] is the maximum available binding sites (molecules) in the liposome. Finally, the dissociation constant (K_d) for the molecular interaction between EGFP-protein and phosphoinositide was calculated using the following equation (equation 8):

$$\mathbf{Equation8}: \qquad \theta = \frac{[P]}{K_d + [P]}$$

3.40 K_d fitting for recombinant His-tagged talin FERM

The purification of His-tagged talin FERM domain has been done before (Elliott et al., 2010). To measure recombinant protein binding to proteoliposomes, His-tagged talin FERM domain was labelled with Alexa-Fluor488-Maleimide (dye:protein ratio 1:10). This was done overnight in a buffer consisting of 50 mM Tris pH 7.0, 150 mM NaCl, 600 µM TCEP. To remove unbound dye, the labelled protein was dialyzed in a buffer consisting of 50 mM Tris pH 7.4, 150 mM, NaCl, 600 µM TCEP. To measure binding, labelled recombinant protein was let to bind to proteoliposomes 2 hours in room temperature before addition of streptavidin beads. The binding to both phosphoinositide-containing proteoliposomes and control liposomes was assessed using Fortessa FACS like before and background subtracted data was curve-fitted to assess the theoretical maximum fluorescence value (F_{max}) like in chapter 4.38. Occupancy values ($\theta = F / F_{max}$) were calculated like in chapter 4.38 and finally Hill's equation (equation 9) was used to assess dissociation constant (K_d):

$$\mathbf{Equation9}: \qquad \theta = \frac{[P]^n}{K_d + [P]^n}$$

Here [P] is the protein concentration and n is Hill's constant which in the best fit-scenario was 1.368.

3.41 Affinity capture of biotinylated proteins

Cell culture plates were pre-coated with 10 µg/ml fibronectin like described before and BioID-construct expressing U2-OS cells were seeded on fibronectin coated plates in a media containing 50 µM biotin for 20–24 hours. After washing cells with cold PBS, cells were lysed and debris was removed by centrifugation at 13 000 x g at +4°C for 2 minutes. Biotinylated proteins were let to bind to prewashed streptavidin beads (MyOne Streptavidin C1, Invitrogen) for 1–1.5 hours while in

rotation in +4°C. Beads were washed using a panel of different washing buffers like described previously in Roux et al., 2012. Briefly, panel consisted of four washing buffers: buffer 1 (2% SDS in dH_2O), buffer 2 (0.1% deoxycholate, 1% Triton X-100, 500 mM NaCl, 1 mM EDTA, and 50 mM Hepes, pH 7.5), buffer 3 (250 mM LiCl, 0.5% NP-40, 0.5% deoxycholate, 1 mM EDTA, and 10 mM Tris, pH 8.1), buffer 4 (50 mM Tris, pH 7.4, and 50 mM NaCl). After washing, beads were resuspended in Laemmli sample buffer and bound proteins were eluted by heating for 5–10 minutes at +90°C

3.42 Mass-spectrometry analysis of biotin-enriched proteins

Affinity captured biotinylated proteins were separated on a SDS-PAGE gel (Mini-PROTEAN TGXTM precast gels, 30 µl wells, Bio-Rad) and stained using Instant Blue Protein Stain (Expedeon) for 15–30 minutes. To ease peptide detection, samples were first separated on a gel and the whole lane consisting of each sample was cut into equal size slices. The slices were washed using a solution of 50% 100 mM ammonium bicarbonate and 50% acetonitrile until all blue color was vanished. Gel slices were washed with 100% acetonitrile for 5–10 minutes and then rehydrated in a reducing buffer containing 20 mM dithiothreitol in 100 mM ammonium bicarbonate for 30 min at 56°C. Proteins in gel pieces were then alkylated by washing the slices with 100% acetonitrile for 5–10 minutes and rehydrated using an alkylating buffer consisting of 55 mM iodoacetamide in 100 mM ammonium bicarbonate solution (covered from light, 20 min). Finally, gel pieces were washed with 100% acetonitrile followed by washes with 100 µl 100 mM ammonium bicarbonate after which slices were dehydrated using 100% acetonitrile and fully dried using a vacuum centrifuge. 0.01 µg/µl trypsin solution was used to digest the proteins (37°C overnight). After trypsinization, an equal amount of 100% acetonitrile was added and gel pieces were further incubated in 37°C for 15 minutes followed by peptide extraction using a buffer consisting of 50% acetonitrile and 5% formic acid. The buffer with peptides was collected and the sample was dried using a vacuum centrifuge. Extracted, dried peptides were stored in -20°C. Prior to LC-ESI-MS/MS analysis, dried peptides were dissolved in 0.1% formic acid. Samples dissolved in formic acid were analyzed using a nanoflow HPLC system (Easy-nLCII; Thermo Fisher Scientific) connected to a Q Exactive mass spectrometer (Thermo Fisher Scientific) with a nano-electrospray ionization source. Peptides were first loaded into a trapping column and separated in a C18 column (75 µm × 15 cm, ReproSil-Pur 5 µm 200 Å C18-AQ; Dr. Maisch HPLC GmbH) by using a mobile phase of 0.1% formic acid in water and 0.1% formic acid in acetonitrile/water in 4:1 volumetric ratio. To elute peptides a linear acetonitrile gradient from 6% to 39% was applied

for 20 minutes 0.1% formic acid as a solvent. With a mass-range of 300–2000 m/z, a survey full-scan MS spectra was acquired and the ten most intense peptide ions in each survey in a scan were isolated and further fragmented using higher energy collision dissociation (HCD). Mascot search engine was used to cross-reference sample data against human proteome. Total spectrum counts were normalized to the molecular weight of the protein and to the total detected spectra in the sample and protein enrichment was assessed by comparing samples to control.

4 Results

4.1 Myosin-X and talin modulate integrin activity at filopodia tips (original publication I)

4.1.1 Myosin motor coupled FERM domain is an essential requirement for integrin activity at filopodia tips

Although integrin-positive adhesions have been known to exist in filopodia, only a few studies have looked at them indirectly using tools such as optical tweezers. We set out to map the requirements for integrin activation in filopodia by coupling super-resolution microscopy with well documented integrin antibodies targeting either active or inactive integrin species. We carefully mapped the distribution of active and inactive integrin species along the base-to-tip axis in myosin-X positive filopodia. As documented before, these filopodia showed pronounced numbers of active integrins towards their tips whereas inactive integrin was distributed more or less equally along the filopodia covering the plasma membrane (Figure 1). Although the striking localization of active integrin in filopodia tips was to be expected, as integrin receptors have been considered as Myosin-X cargo and thus hypothesized being actively trafficked unidirectionally towards filopodia tips, the uniform distribution of inactive integrin was surprising (Figure 1).

Since the myosin-X's integrin binding site has been documented to reside inside the FERM domain, we wanted to assess the effects of deleting FERM region in myosin-X for integrin distribution in filopodia. There exists two good quality crystallography structures of myosin-X MyTH-FERM domains so by comparing the crystal structures with myosin-X cDNA sequence, we deleted the MyTH-FERM region entirely (Figure 3A). Unexpectedly, cells expressing the new Myo10^{dFERM} were completely devoid of active integrin receptors at filopodia tips whereas the inactive pool of integrin remained unchanged (Figure 3F–G).

U2-OS cell line is a convenient model for filopodia research as normally these cells don't extend any filopodia after completion of their initial spreading on fibronectin matrix. However, overexpression of myosin-X expression induces prominent filopodia in these cells. This is opposite to many other cell lines, such as MDA-MB-231 or DCIS.com cells that express myosin-X at higher levels and readily

make filopodia after spreading on fibronectin. Nonetheless, because the U2-OS cell line does express small amounts of myosin-X, we wanted to make sure the endogenous myosin-X expression does not hamper our analysis of integrin activation in filopodia in a rescue experiment where we expressed Myo10 or Myo10^{dFERM} in U2-OS cell line silenced for endogenous myosin-X. Reassuringly, expressing Myo10 or Myo10^{dFERM} against silenced Myo10 background did not change any of the findings but a comparison between siCTRL versus siMyo10 showed a slight reduction in integrin activation in filopodia tips indicating that integrin activation in filopodia would be dose dependent (Figure S3).

Since myosin-X MyTH4-FERM region has four subdomains we wanted to narrow down which subdomains are needed for integrin activity in filopodia. Again, by taking advantage of existing crystal structures of myosin-X's MyTH4-FERM, we were able to engineer subdomain deletion mutants for myosin-X (Figure S5A). By doing this we found that the deletion of F3 subdomain in the FERM region showed a marked decrease in integrin activity in filopodia (Figure S5D). Because the F3 subdomain also harbours the β integrin binding site, we expected that the loss in integrin activity would be due to diminished integrin binding by myosin-X. Because the exact binding site was not known, we decided to superimpose myosin-X MyTH-FERM structure with talin FERM, whose integrin binding function has been well studied in the past. By introducing two single amino acid mutations into myosin-X, we were finally able to interfere with myosin-X's integrin binding function (Figure 4B-C). The mutant, named Myo10^{ITGBD}, also showed a marked decrease in its ability to support activate integrin receptors at filopodia tips (Figure 4G-H) indicating that myosin-X's integrin binding is essential for integrin activation at filopodia tips.

4.1.2 Myosin-X FERM domain has a unique capacity to bind both α and β integrin tails

The interaction between myosin-X and β integrin tails, mainly β-5 and β-1 was first discovered using myosin-X FERM domain as a bait in a yeast 2 hybrid screen (Hongquan Zhang et al. 2004). Since myosin-X's integrin binding function is essential for integrin activation at filopodia, we wanted to study this interaction in detail. By using a highly sensitive method, microscale thermophoresis, we tested how a panel of integrin tail peptides interact with either myosin-X or talin FERM domain. We purified a recombinant myosin-X MyTH-FERM domain and talin FERM domain with affinity chromatography and labeled its 6xHis tag with a fluorescent dye (Figure S6C). We then titrated a panel of different integrin tail peptides and tested their binding with either of the purified domains in solution. Interestingly, although myosin-X binds β integrin tails with moderate affinity (25.1 μM), talin showed higher affinity towards β integrin tails indicating that it can

outcompete myosin-X at β integrin tails (Figure 6A-B). This is credible especially as it is well documented how talin FERM domain makes contacts with the plasma membrane via positively charged patch on its surface further increasing the binding avidity (Gingras et al. 2019; Franceschi et al. 2019; Goult et al. 2010). Unexpectedly, myosin-X's MyTH-FERM domain also bound to α-integrin tails indicating that myosin-X could potentially crosslink both α and β integrin tails (Figure 6C). Although by using the previously characterized integrin binding deficient myosin-X mutant was unable to discriminate between α and β integrin tail binding, we were able to find that myosin-X binds GFFKR motif in α integrin tails as mutations in this area in α2 integrin (GAAKR mutation) showed diminished myosin-X binding (Figure 6D–E). We compared α2 wild-type integrin with GAAKR mutant in CHO cells with null endogenous expression of collagen binding integrins and saw a remarked decrease in filopodia formation upon GAAKR mutation indicating that this region of α2 integrin is crucial for filopodia formation (Figure 6F). How myosin-X supports filopodia function via its double integrin tail binding function remains unclear and will hopefully be a topic for a follow-up structural analysis of myosin-X MyTH-FERM coupled with both α and β integrin tails.

4.1.3 Only a minimal set of proteins are recruited to filopodia tips via Myosin-X FERM domain

Although, we have shown that myosin-X supports integrin activity via its integrin binding function, an alternative hypothesis would have been that instead of direct integrin binding, myosin-X would support integrin activity by recruiting important cargo molecules to filopodia tips via its MyTH-FERM domain. The FERM domain of myosin-X has been described as a protein-protein interaction hub and a cargo binding site of myosin-X. By over-expressing a panel of known filopodia tip localizing together with myosin-X wild-type or myosin-X with MyTH-FERM deletion, we wanted to assess whether myosin-X FERM domain deletion has an impact on the filopodial proteome. Unexpectedly, from the six filopodia-tip localizing proteins, none showed altered localization when compared in myosin-X wild-type or myosin-X FERM domain deleted expressing cells (Figure S4). Even the localization of VASP, that has been previously described as a myosin-X cargo molecule together with Mena (Tokuo and Ikebe 2004), didn't change indicating that either the Mena/Vasp complex binds elsewhere in myosin-X or it has alternative ways to get recruited to filopodia tips.

Since the deletion of MyTH-FERM domain in myosin-X had minimal effects on filopodia proteome, we wanted to study myosin-X FERM interactors by using proximity proteomics. We generated a myosin-X-BioID where BioID part was inserted to the C-terminus of myosin-X next to myosin-X's FERM domain in an

attempt to characterize better the cargo molecules that make contact with myosin-X FERM (Figure 7A). We confirmed that the fusion protein localizes to filopodia tips similarly to wild-type protein (Figure 7B) and that it can biotinylate cellular proteins (Figure 7C-D). Although not indicated in any of the publications in this thesis, we were able to analyze biotinylated proteins using mass spectrometry yielding a hitlist for potential myosin-X FERM interactors. From these, we focused on lamellipodin, a RIAM family member. By imaging lamellipodin and myosin-X in live cells, it was obvious that the two punctae move together during filopodia elongation and retraction, indicating that these two proteins form a stable complex (Figure 7E). We confirmed the interaction between lamellipodin with myosin-X FERM domain in pull-down experiments using different myosin-X constructs (Figure 7F-G). Collectively, these data indicate that Lamellipodin forms a complex of high affinity with myosin-X FERM domain, as these two proteins seem to form a stronger complex than previously documented lamellipodin/talin (Figure 7F). Moreover, pulldown experiments indicated that myosin-X/lamellipodin interaction is lost upon FERM deletion which was further confirmed by microscopy (Figure 7G). Altogether, our unpublished data shows that myosin-X FERM forms a stable complex with Lamellipodin and that myosin-X FERM domain is essential for Lamellipodin recruitment to filopodia tips.

Figure 7. ► Proximity proteomics identifies Lamellipodin as a novel Myosin-X FERM binding cargo. A) Cartoon showing the structure of EGFP-Myo10-BioID construct. BioID was inserted into C-terminal end of Myo10 gene, next to Myo10 FERM domain. **B)** Transient transfection of either EGFP-Myo10 or the BioID variant. U2-OS cells expressing these plasmids were plated on fibronectin in the presence of 50 µM Biotin and fixed using paraformaldehyde. Samples were stained for biotin using Streptavidin-Alexa conjugate and DAPI. **C)** Cells treated similarly than in A) were lysed and the lysis was analyzed on western blot for biotinylation of cellular proteins. Streptavidin-Alexa conjugate was used for staining. **D)** Biotinylated proteins from EGFP-Myo10-BioID lysate were enriched by adding streptavidin beads. The pull-downs were analyzed on a westernblot by staining for biotin using Streptavidin-Alexa conjugate. **E)** EGFP-Lamellipodin (Lpd) and mScarlet-Myo10 were transfected into U2-OS cells, plated on fibronectin and imaged live using Zeiss880 confocal. **F)** EGFP-tagged FERM domains from talin1 or Myo10 (and EGFP control) were transfected into U2-OS cells. Cells expressing these plasmids were lysed and EGFP-tagged proteins together with their binding partners were pulled down using GFP trap beads. Binding with Lamellipodin was assessed in a western blot. **G)** Similarly to F), full-length EGFP-Myo10 plasmid or plasmid with a FERM deletion were expressed in U2-OS cells. EGFP-tagged proteins were pulled down and the binding to Lamellipodin was assessed using western blot. **H)** EGFP-Lamellipodin (Lpd) was transfected into U2-OS cells together with WT mScarlet-Myo10 or FERM deletion plasmid. Cells were plated on fibronectin in DMEM media supplemented with serum, let spread for 2 hours, fixed using paraformaldehyde and followed by permeabilization using 0.5% Triton-X100. Lamellipodin recruitment to filopodia tips was assessed by an antibody staining for endogenous Lamellipodin (Lpd). Cells were imaged with a structured-illumination microscope (SIM) microscope.

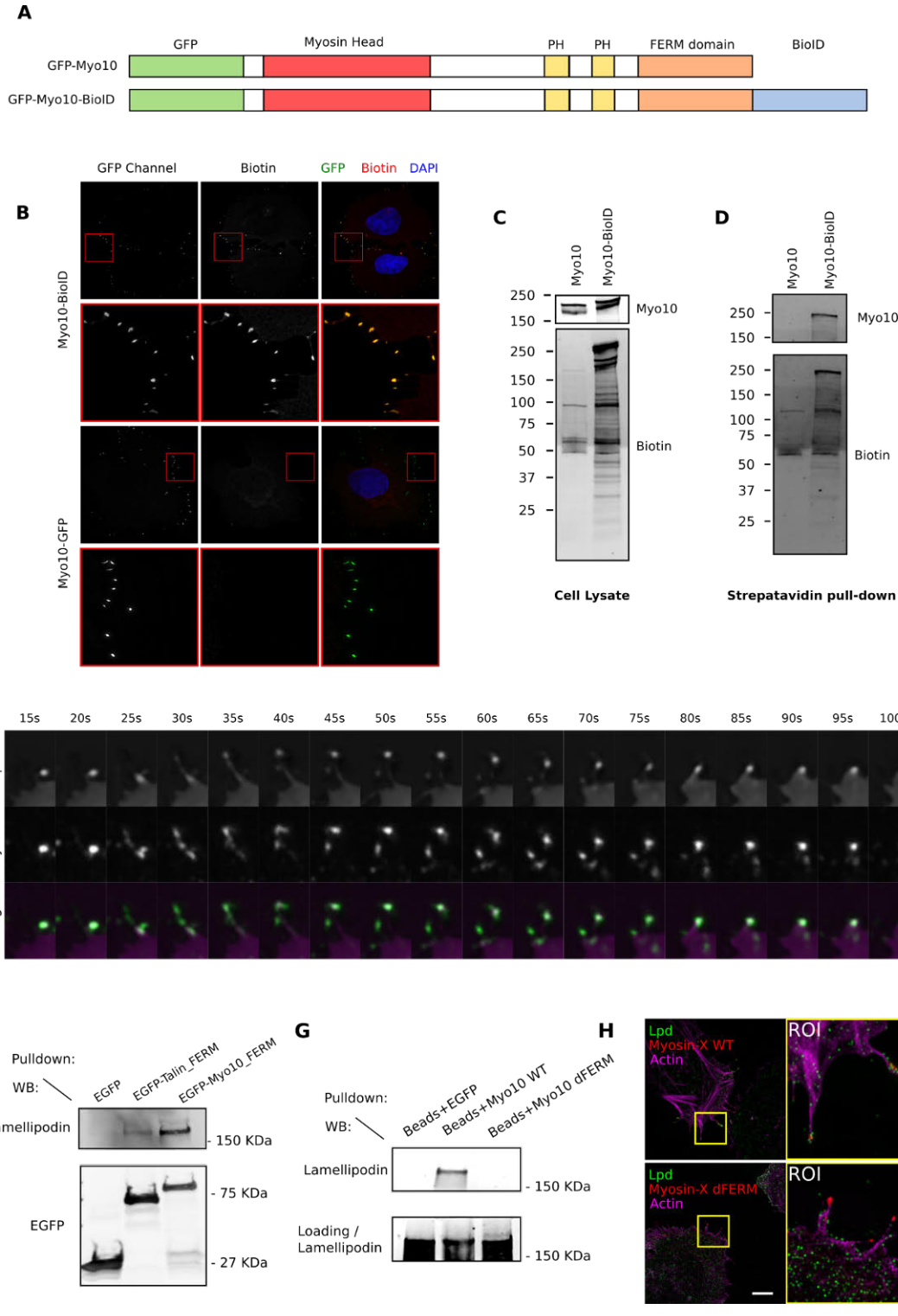
A
GFP
Myosin Head
PH
PH
FERM domain
BioID
GFP-Myo10
GFP-Myo10-BioID
B
GFP Channel
Biotin
GFP Biotin DAPI
Myo10-BioID
Myo10-GFP
C
Myo10
Myo10-BioID
250
150
Myo10
250
150
100
75
50
37
25
Biotin
Cell Lysate
D
Myo10
Myo10-BioID
250
150
Myo10
250
150
100
75
50
37
25
Biotin
Strepatavidin pull-down
E
15s 20s 25s 30s 35s 40s 45s 50s 55s 60s 65s 70s 75s 80s 85s 90s 95s 100s
Lpd
Myo10
Merge
F
Pulldown:
WB:
EGFP
EGFP-Talin_FERM
EGFP-Myo10_FERM
Lamellipodin
- 150 KDa
EGFP
- 75 KDa
- 27 KDa
G
Pulldown:
WB:
Beads+EGFP
Beads+Myo10 WT
Beads+Myo10 dFERM
Lamellipodin
- 150 KDa
Loading /
Lamellipodin
- 150 KDa
H
Lpd
Myosin-X WT
Actin
ROI
Lpd
Myosin-X dFERM
Actin
ROI

4.1.4 Myosin-X FERM domain slightly inhibits integrin activity

Since myosin-X supports filopodial integrin activity via its integrin binding site, we wanted to address whether over-expression of myosin-X's MyTH-FERM could promote integrin activation. By using talin FERM with known integrin activity promoting function as a control, we performed FACS experiments designed to analyze integrin activity in suspended cells. Unexpectedly, expression of talin FERM domain significantly increased integrin activation in multiple cell lines whereas myosin-X's MyTH-FERM expression had a slight inhibitory effect on integrin activation (Figure 5A–C). To confirm our finding, we also performed spreading assays both with xCelligence and by plating cells and imaging the area they occupy (Figure 5D–F). As integrin activity is correlated with cell spreading, we saw decreased cell spreading upon myosin-X MyTH-FERM expression indicating inactivated integrin receptors. It is tempting to speculate that myosin-X could indeed keep integrin receptors inactive prior to their activation by talin also in filopodia tips. This, however, is difficult to study as there exists a large pool of inactive integrin receptors already even in filopodia generated by other filopodia-inducing proteins such as FMNL3 (Figure S2).

4.2 Filopodome mapping identifies BCAR1 as a mechanosensitive regulator of filopodia stability (original publication II)

4.2.1 Filopodia-mapping defines classes of core and accessory filopodia proteins

Given the abundance of lipidic membranes around filopodia tip adhesion, we mapped 80 putative regulators of either filopodia tip adhesion or protein-lipid association on their ability to localize to filopodia. To effectively screen for filopodia localization, a large library of GFP-tagged proteins were co-transfected together with Myo10 into U2-OS cells that were later plated on fibronectin and imaged by using structural illumination microscopy (SIM). The localization of GFP-tagged protein in filopodia was assessed by obtaining a base-to-tip line intensity profile from each recorded filopodium. Strikingly, only 15 of 38 adhesion-linked proteins described before in the consensus adhesome (Horton et al. 2015) localized to filopodia (Figure 1C, Data S2), however, multiple established filopodia-tip complex proteins such as Lamellipodin (RAPH1) and talin (TLN1/2) showed remarked localization towards filopodia tips validating the model system and image analyses setup (Figure 1C, Figure 2). Whereas some of the established filopodia-linked proteins such as myosin-

X (Myo10) and talin-1 (TLN1) occupy filopodia tip almost 100% of time, roughly half of the proteins detected in filopodia did not either localize to filopodia or only localized to filopodia fraction of the time (Figure 1C). Based on this analysis of probabilities, there exists three subclasses of proteins 1) not localizing to filopodia 2) localizing to filopodia most of the time and 2) accessory proteins that can localize to a subset of filopodia generated by cells. This indicates versatility in the mechanisms of how these proteins are recruited to filopodia. Interestingly, paxillin (PXN), a key adaptor for focal adhesions, only occupies filopodia ~30% of the time and seems to be recruited there later during the filopodium life-cycle (Video S2).

4.2.2 Filopodia are enriched with phosphoinositides

To analyse domain architecture of filopodia-localizing proteins, a protein domain enrichment analysis was performed by using DAVID platform (Figure 3A) (D. W. Huang, Sherman, and Lempicki 2009). Interestingly, a protein domain enrichment analysis indicated that Pleckstrin homology (PH) domain, FERM domain and Src homology 3 domain (SH3) were enriched in proteins localizing to filopodia tips. The strong enrichment of lipid binding PH domain among filopodia-linked proteins mapped here led us to hypothesize that phosphoinositide metabolism could be a key orchestrator for normal filopodia function.

PH-domains of PLC**γ,** FYVE, P4M, BTK and TAPP have strong preference for $PI(4,5)P_2$, PI(3)P, PI(4)P, $PI(3,4,5)P_3$, and $PI(3,4)P_2$, respectively. GFP-tagged versions of these domains were used to map distributions of different phosphoinositide species in filopodia similarly with previous analysis by coexpressing the GFP-tagged probes with myosin-X in a U2-OS cell model. To assess filopodia tip enrichment, plasma membrane dye was imaged as one control. Whereas PI(3)P and PI(4)P species were detected mainly at sites outside of filopodia such as vesicular structures, $PI(4,5)P_2$ and $PI(3,4,5)P_3$ showed marked localization to filopodia. This localization was, however, rather homogenous and similar to the plasma membrane indicating that these phosphoinositide species might not be differentially regulated in filopodia with respect to plasma membrane in general (Figure 3B-C). Interestingly, $PI(3,4)P_2$ phosphoinositide showed strong enrichment towards filopodia tips indicating that this species might be specifically generated in filopodia tips to regulate the function of these protrusions (Figure 3B-E). Importantly, the prominent enrichment of $PI(3,4)P_2$ phosphoinositide species was further confirmed in live cells and in cell lines expressing endogenous filopodia (RAT2 cells) (Figure 3D-E). Live cell imaging of $PI(3,4)P_2$ probe shows that this phosphoinositide species is quickly generated during filopodia elongation and stays at the filopodia tip throughout the life-cycle of the protrusion (Video S1). How

exactly PI(3,4)P_2 enrichment takes place at filopodia tips and how this might regulate the organization and function of the filopodia tip complex remains to be determined

4.2.3 Filopodia adhesion is different from other adhesion classes in a cell

Cell-ECM adhesions are highly dynamic and undergo force-dependent changes as the cell moves forward. The advancement of an adhesion from nascent adhesion to fibrillar adhesion are well visualized by the cytoplasmic protein assemblies that associate with these adhesions. To form an adhesion, integrin receptors need to first be activated by talin even in filopodia (original publication I). The mapping of filopodia localizing proteins clearly indicated the presence of multiple proteins known to directly or indirectly be key integrin activity regulators (talin1/2, kindlin1/2, ICAP-1), indicating that these proteins are either required for integrin activation or fine-tune integrin activation at filopodia tips. This was further supported by the high probability of these proteins to localize to filopodia tips and labelled here as filopodia core proteins (Figure 1C). However, proteins known to associate with more mature adhesions with high force transmission seem to be absent from filopodia that are known to be "low force" regions when compared with regions with bigger and more mature adhesions. TNS1–3 PDLIM1/5/7, TRIP6, zyxin (ZYX), and palladin (PALLD) all known to associate with bigger adhesions were all classified as non-filopodia localizing proteins or accessory proteins (Figure 1C, Figure 2). As nascent adhesions closely resemble filopodia adhesions by their small size, proteins known to accumulate at nascent adhesions were of specific interest. Importantly, we found that nascent adhesion proteins such as paxillin (PXN), FAK (PTK2), or arp3 (ACTR3) only to be classified as accessory proteins in filopodia. This indicates that filopodia tip adhesions are more simplistic than nascent adhesions and could maturate into nascent adhesions after appropriate cell signals. In fact, live cell imaging reveals that unstable filopodia are devoid of paxillin and paxillin is only detected in filopodia tips after filopodia get stabilized onto the substrate (Figure 5A; Video S2). Followed by filopodia stabilization and paxillin detection at the filopodia tip, paxillin forms clusters in filopodia shafts which will then give rise to focal adhesions once the lamellipodia beneath advances (Figure 5A; Video S2).

4.2.4 BCAR1 is a novel mechanosensitive component of filopodia tip complex

BCAR1 (protein name p130Cas) is an adaptor protein known to localize to focal adhesions. Whereas BCAR1 has been suggested to get recruited to FAs via PXN or PTK2 (Donato et al. 2010; Y. Wang and McNiven 2012), both of these proteins are

absent from most filopodia whereas BCAR1 seems to be a stable filopodia-tip complex protein occupying >90% of filopodia measured (Figure 1C). It also seems to localize strongly to filopodia tips in live cells regardless of filopodia stability (Video S3). Importantly, to rule out any over-expression artefacts, we stained for endogenous BCAR1 indicating that it highly localizes to filopodia tips together with myosin-X (Figure S3A). BCAR1 has been implicated as a mechanosensitive protein that gets phosphorylated by Src upon mechanical stretch (Sawada et al. 2006). However, BCAR1's filopodia tip enrichment seemed unaltered upon Src, PTK2 or cellular contractility inhibition (Figure S3C). Although, the filopodia-tip localization is not dependent on Src activity, phospho-specific antibodies against BCAR1 detect the phosphorylated protein at filopodia tips indicating that the phosphorylation status may play a role in ECM recognition by filopodial adhesions.

BCAR1 constructs lacking either SH3 or CCHD (C-terminal Cas Homology Domain) domains have been reported localizing poorly to focal adhesions. We tested a panel of SH3 and/or CCHD deletion constructs for their ability to localize at filopodia tips. Importantly, whereas SH3 domain seems unimportant for filopodia tip localization, constructs missing CCHD domain were completely absent from filopodia tips (Figure 5F). To confirm the filopodia-tip targeting role of BCAR1 CCHD domain, we fused the domain with a fluorescent protein. As expected, BCAR1 CCHD domain exhibited strong filopodia tip enrichment whereas its structural homolog, PTK2 FAT domain was absent from filopodia (Figure 5F). Data here strongly indicate that BCAR1 CCHD domain is needed for both focal adhesion and filopodia tip targeting of BCAR1.

We next wanted to analyze how BCAR1 silencing would affect filopodia function. Interestingly, silencing BCAR1 using siRNA resulted in strong increase in filopodia formation in two different cell lines indicating that BCAR1 could negatively affect filopodia formation (Figure 6A–C). This increase in filopodia formation was rescued by overexpression of full-length BCAR1 protein but not protein missing CCHD domain (Figure 6D). Filopodia in siBCAR1 cells were also more dynamic with a significant increase in short-lived filopodia and reduction of stable, long lived filopodia (Figure 6E). How filopodia can react to mechanical stimuli is not known, but an increase in substrate stiffness does downregulate filopodia formation (Figure 6G). Interestingly, phosphorylation status of BCAR1 at filopodia is stiffness dependent indicating that BCAR1 could be a key player in how filopodia sense and respond to changes in environmental stiffness. The exact kinases and downstream proteins in filopodia responding to BCAR1 phosphorylation, however, remain to be determined.

4.3 Conformational dynamics regulate SHANK3 actin and Rap1 binding (original publication III)

4.3.1 SHANK3 regulates filopodia and nests an actin binding site in its SPN domain

Scaffolding protein SHANK3 is required for normal actin regulation in neuronal cells via its binding with multiple actin binding proteins. Previously, SHANK3 has been shown to regulate neuronal filopodia possibly via its N-terminally located SPN domain which also regulates integrin activity. We tested the effects of full-length SHANK3 and SHANK3 SPN domain with known integrin regulatory function on filopodia formation in U2-OS cancer cells induced to form filopodia by over-expressing myosin-X. While SHANK3 expression dampened filopodia formation potentially by re-organizing actin networks in these cells (Figure 1B-C), SHANK3 SPN domain alone exhibited strong and unexpected localization to stress fibers not evident for full length protein (Figure 1F–G). Since SHANK3 SPN domain adopts a similar fold to kindlin F0 domain with a known actin binding site (Figure 2A–B), we thus hypothesized that the strong F-actin colocalization of the SHANK3 SPN domain would be due to its previously unmapped F-actin binding site. In line with our previous observations, EGFP-tagged SPN domain pelleted with F-actin while an engineered SPN domain with designed Q37A/R38A mutation stayed in solution, indicating that these residues are essential for SHANK3 SPN actin binding (Figure 2F). This was further supported by experiments where a loss of actin colocalization was clearly seen upon Q37A/R38A mutation (FIgure 2C–E). Finally, a recombinant wild-type GST-SPN pelleted with F-actin which could be significantly reduced by introducing recombinant protein with the actin binding deficient Q37A/R38A double mutation (Figure 2G–H). Altogether, the data strongly supports that SPN domain in isolation can directly bind F-actin and that residues Q37 and R38 are important for SPN F-actin binding. Furthermore, the data here shows that SHANK3 is a filopodia regulator not only in neuronal but in cancer cells as well.

4.3.2 SHANK3 forms a closed structure where its actin binding site is tucked away at the interface formed by SPN and ARR

Since SHANK3 SPN domain but not full length SHANK3 co-localize with F-actin structures (Figure 1), we hypothesized that F-actin binding site in full length SHANK3 is cryptic and available only under right conditions. SHANK3 has been previously described to regulate integrin activity indirectly by binding and sequestering Rap1 and the structure for SPN-ARR domains together has been

published. By inspecting the structure it is evident that the F-actin binding residues Q37 and R38 are hidden in the interface between SPN and ARR domain (Lilja et al. 2017). To access the hidden F-actin binding site in SPN-ARR, we were able to pinpoint a key residue, N52, in the SPN-ARR interface that seemed to maintain the stability of the closed SPN-ARR conformation. Molecular dynamics simulations using an engineered SPN-ARR with a N52R mutation confirmed that this mutation was able to artificially destabilize the closed conformation and open the structure (Figure 4A–E). In lines with our thinking, opening the SPN-ARR structure through introduction of the N52R mutation led into a dramatic increase in actin colocalization (Figure 4F–G) and binding (Figure 4H-I). Since SPN domain is known to bind and sequester Rap1 GTPase to limit integrin activity, we performed molecular dynamics simulations of destabilized SPN-ARR N52R with and without Rap1. In the molecular dynamics simulations performed, Rap1 supported the maintenance of the closed conformation (Figure 4J–K). Together these data indicate that there exists crosstalk between SHANK3 integrin binding and F-actin binding function and that the presence of Rap1 GTPase could favour the closed conformation of SHANK3 restricting its F-actin binding.

4.3.3 SHANK3 GTPase and actin binding functions compete with each other

Although residues necessary for Rap1 binding such as R12 (Lilja et al. 2017) reside on the other edge of the domain than actin binding Q37/R38 residues, we sought to find if F-actin binding affects integrin activation limiting function of this domain. By using an established FACS-based integrin activity measurements where cells expressing wild-type or Q37A/R38A SHANK3 SPN domain are stained for active and total integrin receptors, we saw that SPN domain not binding to F-actin (Q37A/R38A) more strongly inhibits integrin activity when compared to wild-type control (Figure 3A). We next sought to clarify whether adding Rap1 could compete with SPN's ability to bind F-actin. Importantly, F-actin binding of SHANK3 SPN was largely lowered upon addition of Rap1 indicating that Rap1 binding to SPN can prevent SPN/F-actin interaction (Figure 3B–C). To conclude, the data here indicate that Rap1 binding to SPN can prevent SHANK3 SPN domain's association with F-actin and actin binding can somewhat restrict Rap1-mediated integrin activity modulation. Altogether it seems that although located at different sides of SPN domain, F-actin binding and Rap1 binding compete with each other for binding to SPN domain.

4.3.4 Shank3 actin binding regulates neuronal development

While mechanistic studies show cross-talk between SHANK3 actin binding and its integrin regulatory functions, we wanted to test whether disrupting the actin binding with Q37A/R38A mutation in the full length SHANK3 would have consequences *in vivo.* Since SHANK3 has known regulatory functions organizing F-actin network inside neuronal dendrites, we expressed full length SHANK3 or its SPN domain and F-actin deficient mutant in wild-type rat primary hippocampal neurons. Interestingly, while SHANK3 expression promoted the appearance of high spine density neurons, the expression of SPN domain alone had negative effects on spine density (Figure 6A-B) indicating that SPN domain alone exhibits dominant negative effects over full-length SHANK3 and the full-length SHANK3 is needed to support normal spine development.

To investigate how the SHANK3 actin binding affects neuronal development, we first expressed GFP-Shank3 N52R in wild-type rat hippocampal neurons. The expression of the mutant Shank3 with the actin-binding site exposed led to a dramatic increase of malformed spines appearing thin (filopodia-like) or stubby with the expense of downregulation of more mature, mushroom-shaped spines (Extended Data Fig.5D, Fig. 6D) indicating that the increased SHANK3 actin binding interferes with normal actin network regulation leading to malformed dendritic architecture.

To rule out any effects from endogenous SHANK3, we next expressed wild-type SHANK3 or SHANK3 Q37A/R38A in Shank3αβ−/− rat knockout neurons. While SHANK3 wild-type expressing neurons exhibited normal morphology with rounded spine heads, SHANK3 Q37A/R38A expressing neurons had a lower spine density (Figure 6E) with a high appearance of filopodia-like thin spines (Figure 6F–G) indicating a developmental delay upon the loss of SHANK3 F-actin binding. Together these data indicate that normal SHANK3 actin-binding is needed to support neuronal development.

Previous reports indicate that SHANK knockout in fish models lead to developmental defects that resemble ASD disorders as seen in humans (L. Wang et al. 2020; 2020). To take a step towards studying early neurodevelopment of animals, we expressed full-length SHANK3, SHANK3 Q37A/R38A or SHANK N52R in developing fish embryos with morpholino-silenced endogenous SHANK3. Whereas fish embryos expressing wild-type SHANK3, fish embryos with both mutants (Q37A/R38A and N52R) displayed dramatic loss in swim distance and abnormal swimming patterns (Figure 7C–D). Concordantly with rat and mouse neuronal cells, either impairing and enhancing SHANK3 actin binding had strong effects on neuronal development and animals expressing these SHANK3 mutants display a dramatic loss-of-function phenotype during early animal neurodevelopment.

4.4 ProLIF - quantitative integrin protein-protein interactions and synergistic membrane effects on proteoliposomes (original publication III)

4.4.1 ProLIF is a novel flow cytometry based method for detecting protein-lipid interactions

Methods to interrogate protein-protein interactions of transmembrane proteins in the context of the plasma membrane remain underdeveloped. We developed ProLIF, a highly quantitative method for simultaneous detection of protein-protein and protein-lipid interactions.

Classically, protein-lipid interactions are probed by combining liposomes with a protein of interest and sedimenting the liposomes with ultracentrifugation followed by detection using a standard SDS-gel and/or western blotting. Instead of using semi-quantitative detection from a gel, we wanted to take advantage of fluorescently labelled protein libraries common to a majority of cell biology labs. We hypothesized that by first letting a fluorescently labelled protein bind to a liposome surface and then coupling many of these protein-bound liposomes with a streptavidin bead, the fluorescent signal of a single streptavidin bead, when recorded using a flow cytometer, would be a result of the binding affinity between the fluorescent protein and lipid surface from the liposomes.

To confirm that liposomes with a small fraction (2%) of biotinylated lipids could be captured by streptavidin beads and detected using flow cytometry, we let Cy5 encapsulating liposomes with biotinylated lipids bind to streptavidin bead. The bead-liposome complex was assessed with a standard flow cytometry run detecting first the particles using forward vs side scatter plot (FSC vs SSC) followed by emission and detection of the Cy5 label in the liposomes. We were easily able to record liposomes bound with streptavidin beads and importantly, this signal could be outcompeted by addition of free biotin (Figure 1B). We noticed that the streptavidin beads alone do emit a significant amount of autofluorescence (Figure 1C) and thus in the further experiments, we decided to include a beads only -sample to be able to subtract for bead-accounted autofluorescence.

Since many proteins have lipid-binding PH domains with well characterized lipid-binding profiles, we wanted to test our hypothesis by letting different EGFP-tagged PH domains bind liposomes with different compositions in our system. To overcome any protein purification difficulties, we over-expressed EGFP-tagged PH domains or EGFP alone in HEK273 cells and though detergent-free lysis and removal of membrane compartments using ultracentrifuge isolated the cytoplasmic compartment of these cells. By combining the detergent-free lysates with liposomes with a specific phosphoinositide species and 2 % of biotinylated lipids, we were able

to systematically show how different PH domains have different binding specificities using ProLIF (Figure 1D-G).

4.4.2 The binding of cytosolic proteins to proteoliposomic surfaces can be quantitatively measured even with hard to purify proteins

The idea of using the cytoplasmic compartment as a surrogate for purified proteins together with ProLIF is simple and overcomes difficulties in purification steps with many proteins. However, to be able to draw quantitative values out of ProLIF experiments, knowing the concentration of our fluorescent protein alone in the lysate is essential. Fortunately, fluorescence is a well studied phenomenon and in low concentrations there exists a logarithmic relation between an observed fluorescence of a molecule and its concentration. We thus hypothesized that it would be possible to accurately estimate the concentration of a fluorescent protein in a lysate by taking advantage of an external standard. By measuring the fluorescence of a titration curve of any fluorescent molecule (with known quantum yield, extinction coefficient and concentration) it is possible to accurately estimate the concentration of a fluorescent protein in a lysate. Via an elimination of variables from a system of equations depicting fluorescent properties of both the external standard and protein of interest, we arrive at a relatively simple linear equation described in the methods section.

Because we wanted to show our calculations match experimental values, we next measured and calculated the concentration of recombinant GFP protein from its fluorescence intensity (Figure 3A). Importantly, the mathematical estimation based on fluorescence intensity can yield a standard curve closely resembling a standard curve measured experimentally (fluorescence vs concentration). By being able to estimate concentrations of fluorescent proteins in a lysate, lysates could be now titrated down and the binding of differing amounts of fluorescent protein to liposomes could be measured (Figure 3B-C). By measuring the binding of EGFP tagged BTK PH domain or 2xFYVE to PIP3 or PI(3)P, respectively, we were able to draw dissociation constants (K_d) values by fitting the data against Hill's function. Importantly, the values yielded using ProLIF closely resembled values mentioned previously in literature further justifying our approach.

4.4.3 Introduction of synthetic integrin receptors into ProLIF

To make ProLIF suited for interaction studies for studies with membrane receptors, we designed synthetic integrin receptors that could be introduced into liposomes as integral membrane proteins. In these constructs the extracellular integrin domains were replaced with purification tags to aid purification of synthetic integrin receptors

from *E. coli* membranes. Put shortly, we were able to purify synthetic α5 and β1 integrin receptors and incorporate them into liposomes yielding proteoliposomes (Figure 3A–D). We confirmed the existence of proteoliposomes with a gradient flotation assay where particles of different sizes are separated in a sucrose gradient. Importantly, we saw correctly sized particles that stained positively for integrin α5 or β1 tail recognizing antibodies (Figure 3E).

To take advantage of the integrin-positive proteoliposomes, and the modularity of the system, we wanted to know how the binding of talin head domain with integrin tails is affected by the surrounding plasma membrane. As suspected, talin head domain bound strongly with liposomes having β1 integrin but not with the ones having α5 integrin receptor as this domain has been documented binding β-integrin tails alone. Furthermore, as documented before, the addition of phosphoinositides into the proteoliposomes increased talin head binding to β1-positive proteoliposomes as this protein has a positively-charged surface (Figure 4A–D). Finally, we recorded the dissociation constant of talin head to β1-integrin containing proteoliposomes by using a recombinantly produced Talin head tagged with a fluorescent label (K_d = 0.77 μM, Figure 4E). It is important to note, that significantly weaker K_d values have been reported for talin/β1-integrin interaction when measured in solution (i.e. K_d 490 μM for β1A binding to talin1 F3; Anthis et al., 2009). Thus, the presence of the plasma membrane can highly increase the binding avidity of proteins when binding to receptor tails. These results together indicate that ProLIF is a quantitative and unprecedentedly modular in vivo assay that can be used even with proteins that are difficult to purify or proteins whose activity depends on proper post-translational modifications.

5 Discussion (I–IV)

Recognition of the ECM guides cellular behaviour during a variety of biological processes (Frantz, Stewart, and Weaver 2010). While it seems clear that cells achieve ECM recognition by expressing subsets of the 24 possible integrin heterodimers, how these receptors distribute and function in a cell is still not evident. A single cell spread on a simple fibronectin matrix displays multiple different adhesion types that vastly differ in their architecture and intracellular protein assemblies implying distinct functionalities for these adhesions. Although much resources and time have been invested into studying adhesive structures, such as the focal adhesion, a disproportionately little knowledge exists for smaller adhesions such as the one at the filopodium tip. In this thesis work, we have uncovered new regulatory mechanisms for 1) how adhesions at filopodia tips form, 2) which proteins and lipids occupy filopodia tip to regulate adhesion formation and integrin downstream signalling 3) how a specific set of cytoplasmic integrin-linked proteins define filopodial adhesions and 4) how neuronal cells shape their cytoskeleton during synapse formation when filopodia protrusions maturate into synapses. The work also presents a novel high-end binding assay for biochemical analysis of plasma membrane proteins.

The essentials of filopodia tip adhesion (original publication I)

While filopodia seem relatively simple protrusions, different cell types ranging from cancer cells to neurons will extend filopodia causing different cellular outcomes. It appears that filopodia induced in different ways have different characteristics that will affect their function, such as the evident lack of integrin activity in FMNL3-positive filopodia (publication I, figure S2). Due to their lack in integrin activation, these filopodia seem unable to probe and adhere the surrounding ECM matrix (publication I-II). Integrin activation has been mainly studied in adhesions that are easily visualized, e.g. in focal adhesions where talin binding to integrin tails and to the plasma membrane will activate integrin receptor in a Rap1-mediated or independent manner - all depending on the cell type (Sun, Costell, and Fässler 2019b). When viewed against this conviction, the requirement for Myosin-X in integrin activation at filopodia tips is surprising, as it represents the adhesion field a

previously unappreciated component required for integrin activity in filopodial adhesions (publication I). Most likely Myosin-X supports integrin activation via tethering the receptor to filopodium tip so that talin can then bind the tethered receptor. While it is true that filopodia tip is a unique compartment, it is tempting to speculate that perhaps the need for a tethering protein is a general requirement for integrin activation but only observed so far in filopodial adhesions. To study the requirements for cell adhesion initiation, filopodia tips could offer a great platform due to their narrow proteome when compared to cytoplasm (Spence et al. 2019). Although, we show that myosin-X/talin axis is crucial for integrin activation in filopodia (publication I), many other adhesion-linked proteins localize at filopodia tips as well (publication II). Kindlin, often termed as integrin co-activator, localizes at filopodia tips together with myosin-X and talin (publication II). Although, we saw no effects after kindlin1/2 silencing on filopodia number (publication I, Figure S1), whether kindlin silencing affects integrin activity in filopodia was not directly recorded. Kindlin's role in filopodia would be an interesting topic for a further study, since, when compared to talin, little is known about how kindlin interacts with integrin tails (H. Li et al. 2017).

Previous reports suggest that integrin activity can define cellular protrusiveness (Arjonen et al. 2014; Jacquemet et al. 2016). While global integrin inhibition does indeed seem to hinder filopodia formation, mutating myosin-X integrin binding site can lead to loss in integrin activity at filopodia tip without altering protrusiveness (publication I, Figure 4). This directly implies that adhesion at the filopodia tip is not required for filopodia formation or extension. Likely inhibition of integrin activity leads to decrease in focal adhesions that seem to be hot-spots for filopodia formation as individual filopodium seem to orientate according to the focal adhesion at their base (Stubb et al. 2020). Expanding on this ideology, inhibition of known focal adhesion regulators, such as CDK1 or myosin II, did not negatively affect filopodial adhesions further implying distinct regulation and function between filopodial and other cellular adhesions. It should thus be plausible to interfere with filopodial adhesions without affecting other cell-ECM contacts. The engineered mutant version of myosin-X provided here (publication I) does offer an exciting tool to interfere with filopodial integrin function and will hopefully be used further to interrogate filopodial adhesions. Introduction of this mutant to developing organisms or to cancer cells, should bring more insight into how filopodial adhesions regulate development and disease. It should also make it possible to study integrin downstream signaling in filopodia. Although we did not quantify if the engineered myosin-X designed to decrease integrin binding affects focal adhesion formation, a visual inspection of cells expressing this mutant implies that cells expressing the mutated form of myosin-X can very well form focal adhesions. Also, the highly punctate filopodial localization of myosin-X protein would indeed indicate that

myosin-X would regulate integrin receptors locally in filopodia. Although myosin-X does not localize to focal adhesions, it does interestingly localise to retraction fibers (Lock et al. 2018). In mitotic cells, there exists a specific subset of adhesions, coined as reticular adhesion, that mediates cell-adhesion during mitosis. Since the emergence of these adhesions tether retraction fibers to the ECM substrate, it is plausible that myosin-X would regulate the activation status of αvβ5 integrin in these adhesions. This, however, remains to be confirmed, albeit that the interaction between myosin-X and β5 integrin tail has been already reported (Hongquan Zhang et al. 2004).

We showed that myosin-X can unexpectedly bind both α and β integrin tails with high affinity (publication I, figure 6). This newly reported interaction with the α-integrin tail was mediated by the highly conserved GFFKR motif present in most of the α-integrin tails (Thinn, Wang, and Zhu 2018). Related to reticular adhesions, also αv-integrin nests the GFFKR motif in its cytoplasmic tail indicating that myosin-X could also bind both integrin tails in these adhesions. Although, we were able to show that an intact GFFKR motif in the α-integrin tail is essential for filopodia formation (publication I, figure 6), future structural work will likely pinpoint the exact binding site for both integrin tails in myosin-X FERM domain as well as their consequences for filopodia function. It is possible that Myosin-X could stay attached with the α-integrin tail even during the events where talin binds β-integrin tail of the integrin. If α-integrin binding of myosin-X is a requirement for integrin activity in filopodia will be an interesting topic for a future study but in theory this kind of integrin/talin/myosin-X complex could further separate integrin tails and lead to fully active integrin receptor. Given these unique and novel properties of myosin-X, whether other unconventional myosins (Myo7 & Myo15) could also support integrin activation at filopodia tips remain to be resolved. However, it would appear that in the case of myosin-X alone, integrin activity at filopodia tips might be dose dependent (publication I, Figure S3D). Although, myosin-X expression level alone seems to correlate invasiveness in cancer, it would be interesting to study whether low levels of all three unconventional myosins would support cancer related processes similar to what has been described for myosin-X alone.

Filopodia tip adhesion components (original publication II)

Although it seems that filopodia induced in different ways can have different functionalities, stemming from the small size of these protrusions, there currently exists no road-maps to classify different filopodia over different cell types. However, integrin activation level alone draws a clear distinction between different filopodia and could potentially be used as a marker for ECM-sensing filopodia (publication I). Other proteins localising to filopodia tips, the filopodia-tip complex, would also offer

a basis of how filopodia could be classified. To make this generalizable, we performed a massive super-resolution microscopy screen to map proteins localizing at filopodia tips (publication II). Based on observations from this mapping, it seems that proteins can be recruited to filopodia tips in a filopodia-stability dependent manner. This indicates many different pathways for protein recruitment to filopodia tips. Our unpublished observations show that lamellipodin, a component of the filopodia-tip complex, forms a complex with myosin-X FERM domain resulting in lamellipodin's punctate filopodial localization (Figure 7). Although not yet directly measured, this indicates that non-myosin induced filopodia, would not contain lamellipodin at their tips as a mere FERM deletion in myosin-X can prevent Lamellipodin's filopodia tip localisation (Figure 7). Therefore, the filopodia-tip complex is likely a changing entity and a direct consequence of the pathways leading to filopodia initiation. Although, much work needs to be done to fully characterize the molecular compositions of different filopodia over different cell types, staining for active integrin and lamellipodin alongside with actin binding proteins such as formins and unconventional myosins would offer a good starting point for filopodia classification. Future work will hopefully take advantage of proximity proteomics to compare filopodia in different model systems such as in cancer cells, neuronal dendrites or in cell types where filopodia have been described as a basis to form specialized structures such as tunneling nanotubes (Gousset et al. 2013). Although we have not defined functional consequences of myosin-X/lamellipodin interaction, both MYO10 and Lamellipodin KO mice exhibit white belly patches due to imperfect melanoblast migration (Heimsath et al. 2017; Law et al. 2013), indicating that myosin-X dependent Lamellipodin recruitment to filopodia tips might be an important factor for the migration in this cell system.

Filopodia can sense both ECM stiffness and topography (Chan and Odde 2008; Wong, Guo, and Wang 2014; Albuschies and Vogel 2013) but the molecular players in these events lack proper validation. In publication II we observed that paxillin gets recruited to filopodia tips after filopodia stabilization, slides down to filopodia shaft, eventually maturing into focal adhesion. It is tempting to speculate that paxillin spreading to filopodia shafts could be means for a cell to sense matrix alignment although highly speculative at this point. Related to ECM stiffness, mapping of filopodia-tip localizing proteins pinpointed BCAR1 (p130Cas) as a novel filopodia-tip complex protein with previously reported mechanosensitive roles where it has been described to be phosphorylated upon stretching of the molecule (Donato et al. 2010; Sawada et al. 2006). The presence of BCAR1 at filopodia, its stiffness sensitive phosphorylation status and filopodia's previously appreciated role as force mediators highly indicate that BCAR1 would be stretched and phosphorylated at filopodia tips upon mechanical stress, possibly due to actin retrograde flow. Although filopodia have been shown to exert forces up to 2 nN, BCAR1's force

requirement for stretching and activation are likely to be low making it potentially the first molecule at filopodia tips to respond to emerging forces (Hotta et al. 2014). Although we pinpointed CCHD domain as BCAR1 filopodia-tip targeting domain, later work will likely evaluate how BCAR1 protein stretching and phosphorylation affects filopodia function especially in the context of integrin activation.

Neuronal filopodia: SHANK3 F-actin binding is essential for neuronal development (original publication III)

Proper F-actin network function is essential during synaptogenesis where filopodia-like dendrites maturate into synapses. Interestingly, many integrin receptors have been described to enrich at synapses, particularly at the postsynaptic densities (Lilja and Ivaska 2018). SHANK3 has been previously described as a negative regulator for integrin activity as well as a regulator for filopodia formation in neurites (Lilja et al. 2017). We were able to confirm that both SHANK3 expression and the expression of SHANK3 SPN domain alone affect filopodia formation in cancer cells indicating that SPN domain in SHANK3 is essential in fine tuning filopodia formation (publication II, Figure 1). Interestingly, the SPN-domain retains a previously overlooked F-actin binding function that is masked by SHANK3 folding as the ARR domain next to SPN hides the F-actin binding site between the two domains (publication II, Figure 4). Since the N-terminal SPN-domain has been described as an integrin activity regulator (through its binding with Rap1), the domain presents an intriguing platform where F-actin binding and integrin activity regulation intersect. Since the F-actin binding site and GTPase binding site are located on different sides of the SPN domain (publication II, Figure 4J), competition between these two exist on two levels: First of all, Rap1 binding favours SPN-ARR interaction embedding the F-actin binding site between these two domains (publication II, Figure 4K). In addition, the release of SPN domain from F-actin filaments seems to further increment the inhibitory function SHANK3 SPN domain has on integrin receptors (publication II, Figure 3), indicating that F-actin bound SPN domain can less efficiently inhibit integrin function than its free cytosolic form.

Since SHANK3 can bind multiple actin binding proteins, SHANK3 has been thought to exert its effects on the F-actin network via these accessory proteins (Qualmann et al. 2004; Haeckel et al. 2008; L. Wang et al. 2020). Although we define and characterize the F-actin binding site in SHANK3 SPN domain, this raises a lot of questions, such as: What signals open the SPN-ARR fold? Although embedded between the domains or SPN and ARR, both SPN-ARR opening mutations N52R and F-actin binding mutation Q37A/R38A have effects on neuronal development indicating that proper control of SHANK3 actin binding is crucial for these processes (publication II, Figure 6). Unpublished data from us does indicate that a mere

phosphorylation does not regulate SPN-ARR interaction but the regulation of open-closed conformations of SPN-ARR domains would like to be more complex. Although, the exact nature of the signal that opens SPN-ARR domains is unclear, the full-length SHANK3 with an engineered SPN-ARR opening mutation (N52R) strongly localizes to alpha-actinin rich areas in stress fibers (publication II, Figure 5). This indicates that at least in these F-actin structures other cellular proteins can define how SHANK3 binds F-actin. Hypothetically, other F-actin binding proteins could first prime SHANK3 along an F-actin track and a correct SPN-ARR opening signal would then open the structure stabilizing the complex. Although a complex idea, cytoplasmic proteins can be highly orientation-sensitive when binding with the F-actin cytoskeleton. Thus, the guidance from accessory proteins would make F-actin binding more efficient. This type of orientation-sensitivity has been described for some of the essential F-actin binding proteins such as fascin (Courson and Rock 2010). Whereas α-fodrin binds closer to SHANK3 N-terminus, cortactin binding site is more C-terminally located (Böckers et al. 2001; Naisbitt et al. 1999). This type of double-binding from both ends of the molecule could potentially orient individual SHANK3 molecules in developing dendrites for proper F-actin binding function. Other opening signals such as mechanical stimuli might also play a role in SHANK3 actin binding. Here, the double-bound, stretched SHANK3 would be forced to open, releasing its F-actin binding site from the cleft between SPN and ARR domains. Unfortunately, neuronal mechanobiology seems only to be an emerging field and how mechanics of the brain would regulate synaptogenesis or cognitive function are not known. However, a theory has been proposed where mechanically stretched actin-binding molecules would offer a place for memory storage in the brain due to their binary open/closed nature (Goult 2021). It is to be noted that although synapses are essential structures in memory formation, how memories are stored in the brain is still not understood.

We have provided evidence how SHANK3 can function as an intersection of integrin and F-actin regulation. Importantly, like F-actin network function, integrin receptors have been implicated in synapse formation as well. At least α5-integrin has been described to be targeted to synapses upon glutamate stimulation whereas its depletion negatively affects the formation of dendritic protrusions, spines and synapses (Webb et al. 2007) and although the role of integrin activation in nervous system is still understudied, activation of integrin receptors seems to favour synapse formation by increasing the number of filopodia in post-synaptic apical dendrites of CA1 pyramidal neurons (Y. Shi and Ethell 2006). It is important to note that Myosin-X, a filopodial integrin activator, has been described to localize to filopodia tips in emerging filopodia-like dendrites (Lin et al. 2013). The localization of integrin receptors and myosin-X in these structures suggests that myosin-X dependent integrin activation can impact synaptogenesis. Since synaptogenesis occurs after

dendritic filopodia recognize a suitable presynaptic partner cell, the role, however, is likely different than in migrating cells. However, it is entirely possible that integrin activation in this system would function as a negative regulator for synaptogenesis, preventing dendrite maturation until a suitable presynaptic terminal is found. In this hypothetical model, myosin-X and SHANK3 could counterbalance each other leading to tightly regulated integrin activity in developing neuronal dendrites. Although this is highly hypothetical, the reported co-existence of these proteins in neuronal filopodia would indicate that SHANK3 and myosin-X associate with the same signaling network necessary with synapse development. Whether myosin-X dependent integrin activity is a requirement for normal synaptic development would be an interesting topic to study in adult neurons or during synaptic pruning in young animals. To my knowledge, whether successful synaptic pruning involves integrin activity regulation or SHANK3 is not known. Since myosin-X has been previously described to support dendritic filopodia by trafficking proteins such as VASP to filopodial tips (Lin et al. 2013), the notion how myosin-X might support integrin activation to counterbalance SHANK3 function will hopefully open new angles to address how integrins function during synaptogenesis. Although there do exist MYO10 knockout mice (Heimsath et al. 2017), any testing to define the cognitive abilities such as memory retention of these mice have not to my knowledge been done.

ProLIF assay (original publication IV)

Integrin activity regulates filopodia function and synaptogenesis, but much of integrin activity itself is fine-tuned by regulatory proteins that bind integrin cytoplasmic tails (Morse, Brahme, and Calderwood 2014). Although plasma membrane does affect integrin function, the assays that take this into consideration are underdeveloped. The ability to measure how plasma membrane affects cellular events led us to develop a novel method to accurate measure protein binding to lipidic membranes (called ProLIF, publication III). We selected flow cytometry as a detection method due to its supreme specificity and sensitivity over standard methods such as detection by western blot. Although we have demonstrated the sensitivity and accuracy of the method by using mere liposomes, the potential of the system is underlined in experiments where binding of fluorescently labelled cytosolic protein is probed against a proteoliposomic surface where synthetic integrin receptors are embedded in lipid surface. We introduced synthetic integrin receptors into proteoliposomes to be able to probe interactions in the adhesome field, where binding events are characterized by often weak interactions and clustering of complexes rather than strong interactions between two components alone. In addition, most of integrin biology has been researched using biochemical tools where

binding events with integrins are interrogated in solution without the presence of plasma membrane even though plasma membrane supports even the most rudimentary interactions e.g. integrin binding with talin (Anthis et al. 2009). Here, a part of talin FERM domain has been reported to make contacts with the plasma membrane via a positively-charged patch on the protein surface, strongly enhancing the overall avidity of the interaction. Thus, it is important to develop tools that allow the researcher to both tweak the membrane composition and integral proteins.

Although we concluded that the system can be used with recombinant proteins, we took a step towards mammalian expression systems to preserve post-translational modifications as present in mammalian cells. By expressing fluorescently labelled proteins in HEK293 cells, we were easily able to generate enough protein for measurements with the system and by exploiting standard properties that fluorescent molecules have, we were able to make accurate predictions of the amount (concentration) of fluorescent protein we have in order to quantitatively measure binding of variety of different lipid-lipid and/or protein/lipid interactions of even synergistic nature. To further provide proof of the system's modularity, we showed how talin-β1-integrin binding was strongly enhanced by the presence of either negatively charged phospholipids, β1-integrin tails or both at the proteoliposomes.

The abundance of the plasma membrane is especially evident in filopodia where the plasma membrane area / cytoplasm ratio is perhaps the greatest in a cell. Maybe not surprisingly, over ⅓ of filopodia localizing cell-adhesion molecules have a lipid-binding PH domain indicating that plasma membrane binding is an important feature of these protein's function (original publication II). In addition, I hypothesize that once a cell adhesion complex starts forming in filopodia or elsewhere around an activated integrin receptor, many of the proteins would stay attached to the membrane while participating in the complex. In addition to integrin-linked proteins having a specific lipid-binding domain, talin is a good example of how a mere positive patch on the protein surface can provide more avidity for binding supporting integrin function. Although plasma membrane lipids support the function of essentially all receptors at the cell surface, the topic remains understudied. Over time, the modularity of ProLIF will hopefully be applied with other important receptors types such as growth factor receptors that, like integrins, also span the membrane only once. ProLIF could also be expanded into a multiplexed assay by taking advantage of different fluorophores along with a flow cytometry device with multiple channels to detect emission. Outside this detection system, ProLIF offers a proof-of-concept of how integrin receptors could be introduced into lipidic membranes and the use of such membranes could then be exploited with together mass-spectrometry techniques or potentially even with cryo-EM microscopy to yield atomic resolution images of complexes forming around integrin tails at the plasma membrane.

6 Conclusions

The aim of this thesis in general was to investigate how integrin receptors and actin cytoskeleton come together to form a functional filopodia. By taking different approaches to study filopodia in different systems we were able to reach significant conclusions about how F-actin and integrin adhesions are regulated in filopodia in different model systems. I hope that the well conducted and documented studies will be used to further understand filopodia-linked biological processes and their regulation. This thesis book presents highly detailed studies of myosin-X (integrin binding protein) and SHANK3 (integrin regulatory protein) and integrin adhesion, all in the context of filopodia. The experiments provide new insight into integrin and F-actin network regulation in filopodia. The last publication displays a novel and modular binding assay that allows for quantitative detection of cytoplasmic proteins into integrin receptor tails in the context of plasma membrane.

Original publication I

We illustrate how activated integrins are mainly localized at filopodia tips although a large pool of inactive integrin receptors are situated throughout the filopodia shaft-tip region. We further go on to show that Myosin-X FERM domain is crucial for localizing integrin activation to filopodia tips and that a full integrin activation at filopodia tips is only observed in the presence of talin and myosin-X. Based on high-resolution imaging and detailed biochemical analysis we arrive at a conclusion where myosin-X tethers integrin receptors to filopodia tips in order for talin to activate the receptors. Importantly, talin can not activate integrin receptors at filopodia tips without the presence of myosin-X FERM domain. The study brings forward myosin-X as a novel and essential component that's needed for integrin activation in filopodia.

Based on these results, we suggest a two-step model for integrin activation at filopodia tips: Myosin-X -dependent tethering of integrin receptors to filopodia tips, followed by integrin activation by talin. Unlike in other adhesions in a cell, the strong actin retrograde flow can be counterbalanced by myosin-X's unidirectional motor activity tethering integrin receptors at filopodia tip and providing stability for talin to replace myosin-X at integrin tail.

Original publication II

Integrin tail molecular interactions define cellular adhesion types. We aimed at classifying filopodial cell-ECM adhesions by mapping filopodia localizing cell adhesion molecules in a massive super-resolution screen.

The study provides a road map to classify filopodial adhesions based on the filopodia-tip localizing proteins (the filopodome) and highlights the fact that not all proteins capable of localizing to filopodia tips equally do so. For example, paxillin is only recruited to filopodia tips after filopodia stabilization, whereas other proteins such as myosin-X or BCAR1 occupy filopodia tips regardless of filopodia stability. The study also reveals BCAR1 as a novel filopodia tip-localizing protein with a mechanosensitive role. In conclusion, filopodia mechanosensing can be orchestrated via proteins at filopodia tips and there likely exists multiple pathways of how different proteins are recruited to filopodia tips. The study provides the first ever extensive classification of filopodial proteins and will be an important resource for further filopodial and cell-ECM research.

Original publication III

We sought to investigate filopodia function via a known integrin regulatory protein, SHANK3. By using either SPN domain SPN-ARR domains together or full-length shank in cells or in vitro, we defined SHANK3 as a novel actin binding protein that binds F-actin via a hidden binding site in its SPN domain. Whereas the F-actin binding site is normally embedded between SPN and ARR domains, it does regulate F-actin as mutating this site in full length SHANK3 interferes with synaptogenesis by preventing dendrite maturation.

This work provides evidence of how SHANK3 actin binding is modulated conformationally and how it directly affects F-actin network organization in developing dendrites. In addition, developing fish models show how point-mutations in the actin binding site of SHANK3 cause autism-linked phenotypes, congruent with data from in vitro and neuronal cell experiments.

Original publication IV

Plasma membrane is an abundant constituent that regulates function of all receptors embedded in it. We wanted to develop an accurate binding assay where the receptor would be embedded in its native plasma membrane lipidic environment. By engineering a synthetic integrin receptors without extracellular domain, we build a modular system where synthetic integrin receptors are reconstituted into proteoliposomes and probed with fluorescently-tagged proteins purified using prokaryotic expression systems or maybe more simply, just extracted from

mammalian cell lysate. We use known talin integrin interaction as means to show the functionality of our system where introducing either b-integrin or negatively charged phospholipids into the modular binding assay increases talin FERM domain binding as previously reported. We also provide vast evidence how the system can be quantitatively used to draw values such as dissociation constant for almost any bi-molecular interaction measured with ProLIF.

Acknowledgements

This thesis work was performed at the Faculty of Medicine, Department of Cell biology and Anatomy, University of Turku and Turku Bioscience. Conducting this type of research would not have been possible without the excellent core services at the Turku Bioscience, run by extremely dedicated and talented staff with substantial knowledge in their respective fields.

Beyond the fantastic bioscience infrastructure built and run in Turku, I owe my deepest gratitude to my supervisors, Johanna Ivaska and Guillaume Jacquemet for teaching me how to navigate in the wild jungle that is the scientific world. I came into the lab wanting to learn how to use microscopes for biological research but ended up learning much more than that. Some might argue that the scientific method is the greatest invention humankind ever made and teaching me so much about this is something I deeply value. Thank you for always having time for your students, in the busy academic world this is nothing but obvious. The both of you are brilliant scientists and there is so much I value and respect in the work you do. Thank you for the opportunity to learn, I don't believe I could be any more prepared for the next challenges and I think this is highly important.

At the very beginning of my PhD studies, I was fortunate enough to get accepted into University of Turku graduate school, Drug Research Doctoral programme (DPDP). Thank you for believing in me and in my project I proposed at the time. DRDP has been a place for great peer support and new friends for me. I would especially like to thank Eeva Valve, Ullamari Pesonen and Eriika Savontaus. I really appreciate how the events and various gatherings have aimed at helping the students in their journey. Furthermore, I want to acknowledge Outi Irjala for the support throughout the thesis submission formalities. There are many steps to this and figuring out how the bureaucracy works is difficult. Thank you for helping me and many others with the home stretch of things.

Any PhD thesis needs to be checked by external examiners before the actual dissertation. It takes a lot of time to go through a scientific book like this. I would like to thank my pre-examiners, Jenny Gallop and Vesa Hytönen for their work on this matter. Again, in the busy academic world this is highly appreciated. I would also like to thank professor Staffan Strömblad for accepting the invitation to be my

opponent. I feel the work done in previous years in his research group has opened many avenues for my own research. Because of this I feel privileged going towards the doctoral dissertation on the 8th of October.

There are no words for how much I appreciate my fellow lab members from the past years. The joyful atmosphere in the lab has made it a cozy place to work. I have enjoyed the humour in the lab tremendously and it has been absolutely fantastic to follow how all the other people in the lab have worked hard on their own projects, overcoming failures, shining brightly. There is no question that the lab is full of talented people, and I know that with excitement I will be following what everyone is doing next. I feel really lucky to have been working in this kind of environment and I know the friendships from this time will last. I am not going to go into details how much I appreciate everyone, but I do want to mention Jenni and Petra for making the lab run so smoothly. I have known for a long time that doing a PhD is something I absolutely want to do. It is incredibly hard work and receiving help every day, a year after a year really does sum up. Frankly, I would not have been able to do half the things without your help. This has been *really*, *really* important for me.

While I am excited and happy reaching a milestone like this, I'm also really sad that for the past years I have not been able to spend as much time with my friends and family as I wanted. Although I know all the people in my life have understood this, it has still been the biggest sorrow in my life through this time. My friends and family have always supported me no matter what and given me so much for free. As a result of this, I've now reached a goal that I set for myself a long time ago. I appreciate and love each of you.

Lastly, I would like to thank Tuulia for supporting me throughout my whole PhD. You are the kindest person I know and we have grown so much together. Life is never ready or perfect but this is also what makes it so interesting. I am already looking forward to what happens next.

20.9.2021,
Mitro Miihkinen

References

Abe, Tomoyuki, Masayoshi Kato, Hiroaki Miki, Tadaomi Takenawa, and Takeshi Endo. 2003. "Small GTPase Tc10 and Its Homologue RhoT Induce N-WASP-Mediated Long Process Formation and Neurite Outgrowth." *Journal of Cell Science* 116 (Pt 1): 155–68. https://doi.org/10.1242/jcs.00208.

Abercrombie, M., J. E. Heaysman, and S. M. Pegrum. 1970. "The Locomotion of Fibroblasts in Culture. II. 'RRuffling.'" *Experimental Cell Research* 60 (3): 437–44. https://doi.org/10.1016/0014-4827(70)90537-9.

Aguilera-Gomez, Angelica, and Catherine Rabouille. 2017. "Membrane-Bound Organelles versus Membrane-Less Compartments and Their Control of Anabolic Pathways in Drosophila." *Developmental Biology*, Hubrecht Institute centennial, from embryos to stem cells, 428 (2): 310–17. https://doi.org/10.1016/j.ydbio.2017.03.029.

Alajlouni R, Drahos KE, Finkielstein CV, Capelluto DG. Lipid-mediated membrane binding properties of Disabled-2. Biochim Biophys Acta. 2011;1808(11):2734-2744. doi:10.1016/j.bbamem.2011.07.029

Albuschies, Jörg, and Viola Vogel. 2013. "The Role of Filopodia in the Recognition of Nanotopographies." *Scientific Reports* 3 (1): 1658. https://doi.org/10.1038/srep01658.

Alday-Parejo, Begoña, Roger Stupp, and Curzio Rüegg. 2019. "Are Integrins Still Practicable Targets for Anti-Cancer Therapy?" *Cancers* 11 (7). https://doi.org/10.3390/cancers11070978.

Alieva, N. O., A. K. Efremov, S. Hu, D. Oh, Z. Chen, M. Natarajan, H. T. Ong, et al. 2019. "Myosin IIA and Formin Dependent Mechanosensitivity of Filopodia Adhesion." *Nature Communications* 10 (1): 3593. https://doi.org/10.1038/s41467-019-10964-w.

Almagro, Sébastien, Claire Durmort, Adeline Chervin-Pétinot, Stephanie Heyraud, Mathilde Dubois, Olivier Lambert, Camille Maillefaud, et al. 2010. "The Motor Protein Myosin-X Transports VE-Cadherin along Filopodia to Allow the Formation of Early Endothelial Cell-Cell Contacts." *Molecular and Cellular Biology* 30 (7): 1703–17. https://doi.org/10.1128/MCB.01226-09.

Amit, Moran, Shorook Na'ara, and Ziv Gil. 2016. "Mechanisms of Cancer Dissemination along Nerves." *Nature Reviews. Cancer* 16 (6): 399–408. https://doi.org/10.1038/nrc.2016.38.

Anderson, D. W., F. J. Probst, I. A. Belyantseva, R. A. Fridell, L. Beyer, D. M. Martin, D. Wu, et al. 2000. "The Motor and Tail Regions of Myosin XV Are Critical for Normal Structure and Function of Auditory and Vestibular Hair Cells." *Human Molecular Genetics* 9 (12): 1729–38. https://doi.org/10.1093/hmg/9.12.1729.

Anthis, Nicholas J., Kate L. Wegener, Feng Ye, Chungho Kim, Benjamin T. Goult, Edward D. Lowe, Ioannis Vakonakis, et al. 2009. "The Structure of an Integrin/Talin Complex Reveals the Basis of inside-out Signal Transduction." *The EMBO Journal* 28 (22): 3623–32. https://doi.org/10.1038/emboj.2009.287.

Arjonen, Antti, Riina Kaukonen, and Johanna Ivaska. 2011. "Filopodia and Adhesion in Cancer Cell Motility." *Cell Adhesion & Migration* 5 (5): 421–30. https://doi.org/10.4161/cam.5.5.17723.

Arjonen, Antti, Riina Kaukonen, Elina Mattila, Pegah Rouhi, Gunilla Högnäs, Harri Sihto, Bryan W. Miller, et al. 2014. "Mutant P53–Associated Myosin-X Upregulation Promotes Breast Cancer Invasion and Metastasis." *The Journal of Clinical Investigation* 124 (3): 1069–82. https://doi.org/10.1172/JCI67280.

Atherton, Paul, Franziska Lausecker, Alexandre Carisey, Andrew Gilmore, David Critchley, Igor Barsukov, and Christoph Ballestrem. 2019. “Relief of Talin Autoinhibition Triggers a Force-Independent Association with Vinculin.” *Journal of Cell Biology* 219 (e201903134). https://doi.org/10.1083/jcb.201903134.

Azioune, Ammar, Marko Storch, Michel Bornens, Manuel Théry, and Matthieu Piel. 2009. “Simple and Rapid Process for Single Cell Micro-Patterning.” *Lab on a Chip* 9 (11): 1640–42. https://doi.org/10.1039/B821581M.

Bachmann, Michael, Sampo Kukkurainen, Vesa P. Hytönen, and Bernhard Wehrle-Haller. 2019. “Cell Adhesion by Integrins.” *Physiological Reviews* 99 (4): 1655–99. https://doi.org/10.1152/physrev.00036.2018.

Balzer, Connor J., Andrew R. Wagner, Luke A. Helgeson, and Brad J. Nolen. 2019. “Single-Turnover Activation of Arp2/3 Complex by Dip1 May Balance Nucleation of Linear versus Branched Actin Filaments.” *Current Biology: CB* 29 (19): 3331-3338.e7. https://doi.org/10.1016/j.cub.2019.08.023.

Baumann, Petra, Wilko Thiele, Natascha Cremers, Santoshi Muppala, Justyna Krachulec, Markus Diefenbacher, Olivier Kassel, et al. 2012. “CD24 Interacts with and Promotes the Activity of C-Src within Lipid Rafts in Breast Cancer Cells, Thereby Increasing Integrin-Dependent Adhesion.” *Cellular and Molecular Life Sciences* 69 (3): 435–48. https://doi.org/10.1007/s00018-011-0756-9.

Baumgart, Tobias, Adam T. Hammond, Prabuddha Sengupta, Samuel T. Hess, David A. Holowka, Barbara A. Baird, and Watt W. Webb. 2007. “Large-Scale Fluid/Fluid Phase Separation of Proteins and Lipids in Giant Plasma Membrane Vesicles.” *Proceedings of the National Academy of Sciences* 104 (9): 3165–70. https://doi.org/10.1073/pnas.0611357104.

Berridge, Michael J. 2016. “The Inositol Trisphosphate/Calcium Signaling Pathway in Health and Disease.” *Physiol Rev* 96: 36.

Bledzka K, Bialkowska K, Nie H, Qin J, Byzova T, Wu C, Plow EF, Ma YQ. Tyrosine phosphorylation of integrin beta3 regulates kindlin-2 binding and integrin activation. J Biol Chem. 2010 Oct 1;285(40):30370-4. doi: 10.1074/jbc.C110.134247. Epub 2010 Aug 11. PMID: 20702409; PMCID: PMC2945529.

Bouaouina M, Goult BT, Huet-Calderwood C, et al. A conserved lipid-binding loop in the kindlin FERM F1 domain is required for kindlin-mediated αIIbβ3 integrin coactivation. J Biol Chem. 2012;287(10):6979-6990. doi:10.1074/jbc.M111.330845

Bu W, Levitskaya Z, Loh ZY, Jin S, Basu S, Ero R, Yan X, Wang M, Ngan SFC, Sze SK, Tan SM, Gao YG. Structural basis of human full-length kindlin-3 homotrimer in an auto-inhibited state. PLoS Biol. 2020 Jul 9;18(7):e3000755. doi: 10.1371/journal.pbio.3000755. PMID: 32644996; PMCID: PMC7373317.

Böckers, T. M., M. G. Mameza, M. R. Kreutz, J. Bockmann, C. Weise, F. Buck, D. Richter, E. D. Gundelfinger, and H. J. Kreienkamp. 2001. “Synaptic Scaffolding Proteins in Rat Brain. Ankyrin Repeats of the Multidomain Shank Protein Family Interact with the Cytoskeletal Protein Alpha-Fodrin.” *The Journal of Biological Chemistry* 276 (43): 40104–12. https://doi.org/10.1074/jbc.M102454200.

Bohil, Aparna B., Brian W. Robertson, and Richard E. Cheney. 2006. “Myosin-X Is a Molecular Motor That Functions in Filopodia Formation.” *Proceedings of the National Academy of Sciences of the United States of America* 103 (33): 12411–16. https://doi.org/10.1073/pnas.0602443103.

Breitsprecher, Dennis, and Bruce L. Goode. 2013. “Formins at a Glance.” *Journal of Cell Science* 126 (1): 1–7. https://doi.org/10.1242/jcs.107250.

Bridgewater, Rebecca E., Jim C. Norman, and Patrick T. Caswell. 2012. “Integrin Trafficking at a Glance.” *Journal of Cell Science* 125 (16): 3695–3701. https://doi.org/10.1242/jcs.095810.

Budczies, Jan, Moritz von Winterfeld, Frederick Klauschen, Michael Bockmayr, Jochen K. Lennerz, Carsten Denkert, Thomas Wolf, et al. 2015. “The Landscape of Metastatic Progression Patterns across Major Human Cancers.” *Oncotarget* 6 (1): 570–83. https://doi.org/10.18632/oncotarget.2677.

Byron, Adam, Jonathan D. Humphries, Janet A. Askari, Sue E. Craig, A. Paul Mould, and Martin J. Humphries. 2009. “Anti-Integrin Monoclonal Antibodies.” *Journal of Cell Science* 122 (22): 4009–11. https://doi.org/10.1242/jcs.056770.

Campbell, Melody G., Anthony Cormier, Saburo Ito, Robert I. Seed, Andrew J. Bondesson, Jianlong Lou, James D. Marks, Jody L. Baron, Yifan Cheng, and Stephen L. Nishimura. 2020. "Cryo-EM Reveals Integrin-Mediated TGF-β Activation without Release from Latent TGF-β." *Cell* 180 (3): 490-501.e16. https://doi.org/10.1016/j.cell.2019.12.030.

Cao, R., J. Chen, X. Zhang, Y. Zhai, X. Qing, W. Xing, L. Zhang, Y. S. Malik, H. Yu, and X. Zhu. 2014. "Elevated Expression of Myosin X in Tumours Contributes to Breast Cancer Aggressiveness and Metastasis." *British Journal of Cancer* 111 (3): 539–50. https://doi.org/10.1038/bjc.2014.298.

Casares, Doralicia, Pablo V. Escribá, and Catalina Ana Rosselló. 2019. "Membrane Lipid Composition: Effect on Membrane and Organelle Structure, Function and Compartmentalization and Therapeutic Avenues." *International Journal of Molecular Sciences* 20 (9). https://doi.org/10.3390/ijms20092167.

Casimiro, Sandra, Khalid S. Mohammad, Ricardo Pires, Joana Tato-Costa, Irina Alho, Rui Teixeira, António Carvalho, et al. 2013. "RANKL/RANK/MMP-1 Molecular Triad Contributes to the Metastatic Phenotype of Breast and Prostate Cancer Cells in Vitro." *PloS One* 8 (5): e63153. https://doi.org/10.1371/journal.pone.0063153.

Castillo-Kauil, Alejandro, Irving García-Jiménez, Rodolfo Daniel Cervantes-Villagrana, Sendi Rafael Adame-García, Yarely Mabell Beltrán-Navarro, J. Silvio Gutkind, Guadalupe Reyes-Cruz, and José Vázquez-Prado. 2020. "Gαs Directly Drives PDZ-RhoGEF Signaling to Cdc42." *Journal of Biological Chemistry* 295 (50): 16920–28. https://doi.org/10.1074/jbc.AC120.015204.

Chan, Clarence E., and David J. Odde. 2008. "Traction Dynamics of Filopodia on Compliant Substrates." *Science* 322 (5908): 1687–91. https://doi.org/10.1126/science.1163595.

Chang, Yu-Chung, Wenjuan Su, Eun-ah Cho, Hao Zhang, Qingqiu Huang, Mark R. Philips, and Jinhua Wu. 2019. "Molecular Basis for Autoinhibition of RIAM Regulated by FAK in Integrin Activation." *Proceedings of the National Academy of Sciences* 116 (9): 3524–29. https://doi.org/10.1073/pnas.1818880116.

Chastney, Megan R., Craig Lawless, Jonathan D. Humphries, Stacey Warwood, Matthew C. Jones, David Knight, Claus Jorgensen, and Martin J. Humphries. 2020. "Topological Features of Integrin Adhesion Complexes Revealed by Multiplexed Proximity Biotinylation." *Journal of Cell Biology* 219 (e202003038). https://doi.org/10.1083/jcb.202003038.

Chen SX, Tari PK, She K, Haas K. Neurexin-neuroligin cell adhesion complexes contribute to synaptotropic dendritogenesis via growth stabilization mechanisms in vivo. Neuron. 2010 Sep 23;67(6):967-83. doi: 10.1016/j.neuron.2010.08.016. PMID: 20869594.

Chen, Wenjing, Andrew D. Hoffmann, Huiping Liu, and Xia Liu. 2018. "Organotropism: New Insights into Molecular Mechanisms of Breast Cancer Metastasis." *Npj Precision Oncology* 2 (1): 1–12. https://doi.org/10.1038/s41698-018-0047-0.

Chinthalapudi, Krishna, Erumbi S. Rangarajan, and Tina Izard. 2018. "The Interaction of Talin with the Cell Membrane Is Essential for Integrin Activation and Focal Adhesion Formation." *Proceedings of the National Academy of Sciences* 115 (41): 10339–44. https://doi.org/10.1073/pnas.1806275115.

Choi, Sunkyu, Aditya M. Bhagwat, Rasha Al Mismar, Neha Goswami, Hisham Ben Hamidane, Lu Sun, and Johannes Graumann. 2018. "Proteomic Profiling of Human Cancer Pseudopodia for the Identification of Anti-Metastatic Drug Candidates." *Scientific Reports* 8 (1): 5858. https://doi.org/10.1038/s41598-018-24256-8.

Clark, Andrew G, and Danijela Matic Vignjevic. 2015. "Modes of Cancer Cell Invasion and the Role of the Microenvironment." *Current Opinion in Cell Biology*, Cell adhesion and migration, 36 (October): 13–22. https://doi.org/10.1016/j.ceb.2015.06.004.

Conway, James R. W., and Guillaume Jacquemet. 2019. "Cell Matrix Adhesion in Cell Migration." *Essays in Biochemistry* 63 (5): 535–51. https://doi.org/10.1042/EBC20190012.

Corbin JA, Evans JH, Landgraf KE, Falke JJ. Mechanism of specific membrane targeting by C2 domains: localized pools of target lipids enhance Ca2+ affinity. Biochemistry. 2007;46(14):4322-4336. doi:10.1021/bi062140c

Courson, David S., and Ronald S. Rock. 2010. “Actin Cross-Link Assembly and Disassembly Mechanics for α-Actinin and Fascin.” *The Journal of Biological Chemistry* 285 (34): 26350–57. https://doi.org/10.1074/jbc.M110.123117.

Dai, Xiaofeng, Ting Li, Zhonghu Bai, Yankun Yang, Xiuxia Liu, Jinling Zhan, and Bozhi Shi. 2015. “Breast Cancer Intrinsic Subtype Classification, Clinical Use and Future Trends.” *American Journal of Cancer Research* 5 (10): 2929–43.

De Arcangelis, A., M. Mark, J. Kreidberg, L. Sorokin, and E. Georges-Labouesse. 1999. “Synergistic Activities of Alpha3 and Alpha6 Integrins Are Required during Apical Ectodermal Ridge Formation and Organogenesis in the Mouse.” *Development (Cambridge, England)* 126 (17): 3957–68.

De Franceschi, Nicola, Antti Arjonen, Nadia Elkhatib, Konstantin Denessiouk, Antoni G. Wrobel, Thomas A. Wilson, Jeroen Pouwels, Guillaume Montagnac, David J. Owen, and Johanna Ivaska. 2016. “Selective Integrin Endocytosis Is Driven by Interactions between the Integrin α-Chain and AP2.” *Nature Structural & Molecular Biology* 23 (2): 172–79. https://doi.org/10.1038/nsmb.3161.

Dedden, Dirk, Stephanie Schumacher, Charlotte F. Kelley, Martin Zacharias, Christian Biertümpfel, Reinhard Fässler, and Naoko Mizuno. 2019. “The Architecture of Talin1 Reveals an Autoinhibition Mechanism.” *Cell* 179 (1): 120-131.e13. https://doi.org/10.1016/j.cell.2019.08.034.

Disanza, Andrea, Sara Bisi, Moritz Winterhoff, Francesca Milanesi, Dmitry S. Ushakov, David Kast, Paola Marighetti, et al. 2013. “CDC42 Switches IRSp53 from Inhibition of Actin Growth to Elongation by Clustering of VASP.” *The EMBO Journal* 32 (20): 2735–50. https://doi.org/10.1038/emboj.2013.208.

Dobramysl, Ulrich, Iris Katharina Jarsch, Yoshiko Inoue, Hanae Shimo, Benjamin Richier, Jonathan R. Gadsby, Julia Mason, et al. 2021. “Stochastic Combinations of Actin Regulatory Proteins Are Sufficient to Drive Filopodia Formation.” *Journal of Cell Biology* 220 (e202003052). https://doi.org/10.1083/jcb.202003052.

Dominguez, Roberto. 2016. “The WH2 Domain and Actin Nucleation: Necessary but Insufficient.” *Trends in Biochemical Sciences* 41 (6): 478–90. https://doi.org/10.1016/j.tibs.2016.03.004.

Donato, Dominique M., Larisa M. Ryzhova, Leslie M. Meenderink, Irina Kaverina, and Steven K. Hanks. 2010. “Dynamics and Mechanism of P130Cas Localization to Focal Adhesions*,.” *Journal of Biological Chemistry* 285 (27): 20769–79. https://doi.org/10.1074/jbc.M109.091207.

Dourdin, N., A. K. Bhatt, P. Dutt, P. A. Greer, J. S. Arthur, J. S. Elce, and A. Huttenlocher. 2001. “Reduced Cell Migration and Disruption of the Actin Cytoskeleton in Calpain-Deficient Embryonic Fibroblasts.” *The Journal of Biological Chemistry* 276 (51): 48382–88. https://doi.org/10.1074/jbc.M108893200.

Dozynkiewicz, Marta A., Nigel B. Jamieson, Iain MacPherson, Joan Grindlay, Peter V.E. van den Berghe, Anne von Thun, Jennifer P. Morton, et al. 2012. “Rab25 and CLIC3 Collaborate to Promote Integrin Recycling from Late Endosomes/Lysosomes and Drive Cancer Progression.” *Developmental Cell* 22 (1): 131–45. https://doi.org/10.1016/j.devcel.2011.11.008.

D’Souza, Ryan S, Jun Y Lim, Alper Turgut, Kelly Servage, Junmei Zhang, Kim Orth, Nisha G Sosale, Matthew J Lazzara, Jeremy Allegood, and James E Casanova. 2020. “Calcium-Stimulated Disassembly of Focal Adhesions Mediated by an ORP3/IQSec1 Complex.” Edited by Maddy Parsons and Anna Akhmanova. *ELife* 9 (April): e54113. https://doi.org/10.7554/eLife.54113.

Ebrahim, Seham, Matthew R. Avenarius, M’hamed Grati, Jocelyn F. Krey, Alanna M. Windsor, Aurea D. Sousa, Angela Ballesteros, et al. 2016. “Stereocilia-Staircase Spacing Is Influenced by Myosin III Motors and Their Cargos Espin-1 and Espin-Like.” *Nature Communications* 7 (1): 10833. https://doi.org/10.1038/ncomms10833.

Fiala JC, Feinberg M, Popov V, Harris KM. Synaptogenesis via dendritic filopodia in developing hippocampal area CA1. J Neurosci. 1998 Nov 1;18(21):8900-11. doi: 10.1523/JNEUROSCI.18-21-08900.1998. PMID: 9786995; PMCID: PMC6793554.

Font-Clos, Francesc, Stefano Zapperi, and Caterina A. M. La Porta. 2020. “Blood Flow Contributions to Cancer Metastasis.” *IScience* 23 (5): 101073. https://doi.org/10.1016/j.isci.2020.101073.

Franceschi, Nicola De, Hellyeh Hamidi, Jonna Alanko, Pranshu Sahgal, and Johanna Ivaska. 2015. "Integrin Traffic – the Update." *Journal of Cell Science* 128 (5): 839–52. https://doi.org/10.1242/jcs.161653.

Franceschi, Nicola De, Mitro Miihkinen, Hellyeh Hamidi, Jonna Alanko, Anja Mai, Laura Picas, Camilo Guzmán, et al. 2019. "ProLIF – Quantitative Integrin Protein–Protein Interactions and Synergistic Membrane Effects on Proteoliposomes." *Journal of Cell Science* 132 (4). https://doi.org/10.1242/jcs.214270.

Frantz, Christian, Kathleen M. Stewart, and Valerie M. Weaver. 2010. "The Extracellular Matrix at a Glance." *Journal of Cell Science* 123 (24): 4195–4200. https://doi.org/10.1242/jcs.023820.

Gagnoux-Palacios, Laurent, Michael Dans, Wouter van't Hof, Agnese Mariotti, Angela Pepe, Guerrino Meneguzzi, Marilyn D. Resh, and Filippo G. Giancotti. 2003. "Compartmentalization of Integrin Alpha6beta4 Signaling in Lipid Rafts." *The Journal of Cell Biology* 162 (7): 1189–96. https://doi.org/10.1083/jcb.200305006.

Galbraith, Catherine G., Kenneth M. Yamada, and James A. Galbraith. 2007. "Polymerizing Actin Fibers Position Integrins Primed to Probe for Adhesion Sites." *Science* 315 (5814): 992–95. https://doi.org/10.1126/science.1137904.

Gallop, J. L. 2020. "Filopodia and Their Links with Membrane Traffic and Cell Adhesion." *Seminars in Cell & Developmental Biology*, SI: Actin_15 June 2019, 102 (June): 81–89. https://doi.org/10.1016/j.semcdb.2019.11.017.

Gallop, Jennifer L., Astrid Walrant, Lewis C. Cantley, and Marc W. Kirschner. 2013. "Phosphoinositides and Membrane Curvature Switch the Mode of Actin Polymerization via Selective Recruitment of Toca-1 and Snx9." *Proceedings of the National Academy of Sciences of the United States of America* 110 (18): 7193–98. https://doi.org/10.1073/pnas.1305286110.

Geiger, Benjamin, and Kenneth M. Yamada. 2011. "Molecular Architecture and Function of Matrix Adhesions." *Cold Spring Harbor Perspectives in Biology* 3 (5): a005033. https://doi.org/10.1101/cshperspect.a005033.

Georgiadou, Maria, Johanna Lilja, Guillaume Jacquemet, Camilo Guzmán, Maria Rafaeva, Charlotte Alibert, Yan Yan, et al. 2017. "AMPK Negatively Regulates Tensin-Dependent Integrin Activity." *The Journal of Cell Biology* 216 (4): 1107–21. https://doi.org/10.1083/jcb.201609066.

Gerhardt, Holger, Matthew Golding, Marcus Fruttiger, Christiana Ruhrberg, Andrea Lundkvist, Alexandra Abramsson, Michael Jeltsch, et al. 2003. "VEGF Guides Angiogenic Sprouting Utilizing Endothelial Tip Cell Filopodia." *The Journal of Cell Biology* 161 (6): 1163–77. https://doi.org/10.1083/jcb.200302047.

Gerratana, L., V. Fanotto, M. Bonotto, S. Bolzonello, A. M. Minisini, G. Fasola, and F. Puglisi. 2015. "Pattern of Metastasis and Outcome in Patients with Breast Cancer." *Clinical & Experimental Metastasis* 32 (2): 125–33. https://doi.org/10.1007/s10585-015-9697-2.

Ghashghaei, H. Troy, Cary Lai, and E. S. Anton. 2007. "Neuronal Migration in the Adult Brain: Are We There Yet?" *Nature Reviews Neuroscience* 8 (2): 141–51. https://doi.org/10.1038/nrn2074.

Gingras, Alexandre R., Frederic Lagarrigue, Monica N. Cuevas, Andrew J. Valadez, Marcus Zorovich, Wilma McLaughlin, Miguel Alejandro Lopez-Ramirez, et al. 2019. "Rap1 Binding and a Lipid-Dependent Helix in Talin F1 Domain Promote Integrin Activation in Tandem." *Journal of Cell Biology* 218 (6): 1799–1809. https://doi.org/10.1083/jcb.201810061.

Giorgione JR, Lin JH, McCammon JA, Newton AC. Increased membrane affinity of the C1 domain of protein kinase Cdelta compensates for the lack of involvement of its C2 domain in membrane recruitment. J Biol Chem. 2006;281(3):1660-1669. doi:10.1074/jbc.M510251200

Goh, Wah Ing, Thankiah Sudhaharan, Kim Buay Lim, Kai Ping Sem, Chew Ling Lau, and Sohail Ahmed. 2011. "Rif-MDia1 Interaction Is Involved in Filopodium Formation Independent of Cdc42 and Rac Effectors." *The Journal of Biological Chemistry* 286 (15): 13681–94. https://doi.org/10.1074/jbc.M110.182683.

Gordon, Ana, and Karine Gousset. 2021. “Utilization of Laser Capture Microdissection Coupled to Mass Spectrometry to Uncover the Proteome of Cellular Protrusions.” *Methods in Molecular Biology (Clifton, N.J.)* 2259: 25–45. https://doi.org/10.1007/978-1-0716-1178-4_3.

Goult, Benjamin T. 2021. “The Mechanical Basis of Memory – the MeshCODE Theory.” *Frontiers in Molecular Neuroscience* 14. https://doi.org/10.3389/fnmol.2021.592951.

Goult, Benjamin T., Neil Bate, Nicholas J. Anthis, Kate L. Wegener, Alexandre R. Gingras, Bipin Patel, Igor L. Barsukov, Iain D. Campbell, Gordon C. K. Roberts, and David R. Critchley. 2009. “The Structure of an Interdomain Complex That Regulates Talin Activity.” *The Journal of Biological Chemistry* 284 (22): 15097–106. https://doi.org/10.1074/jbc.M900078200.

Goult, Benjamin T, Mohamed Bouaouina, Paul R Elliott, Neil Bate, Bipin Patel, Alexandre R Gingras, J Günter Grossmann, et al. 2010. “Structure of a Double Ubiquitin-like Domain in the Talin Head: A Role in Integrin Activation.” *The EMBO Journal* 29 (6): 1069–80. https://doi.org/10.1038/emboj.2010.4.

Gousset, Karine, Ludovica Marzo, Pierre-Henri Commere, and Chiara Zurzolo. 2013. “Myo10 Is a Key Regulator of TNT Formation in Neuronal Cells.” *Journal of Cell Science* 126 (Pt 19): 4424–35. https://doi.org/10.1242/jcs.129239.

Gozani O, Karuman P, Jones DR, et al. The PHD finger of the chromatin-associated protein ING2 functions as a nuclear phosphoinositide receptor. Cell. 2003;114(1):99-111. doi:10.1016/s0092-8674(03)00480-x

Haeckel, Akvile, Rashmi Ahuja, Eckart D. Gundelfinger, Britta Qualmann, and Michael M. Kessels. 2008. “The Actin-Binding Protein Abp1 Controls Dendritic Spine Morphology and Is Important for Spine Head and Synapse Formation.” *The Journal of Neuroscience* 28 (40): 10031–44. https://doi.org/10.1523/JNEUROSCI.0336-08.2008.

Hamidi, Hellyeh, and Johanna Ivaska. 2018. “Every Step of the Way: Integrins in Cancer Progression and Metastasis.” *Nature Reviews. Cancer* 18 (9): 533–48. https://doi.org/10.1038/s41568-018-0038-z.

Han, Xianlin. 2016. “Lipidomics for Studying Metabolism.” *Nature Reviews Endocrinology* 12 (11): 668–79. https://doi.org/10.1038/nrendo.2016.98.

Hanahan, Douglas, and Robert A. Weinberg. 2011. “Hallmarks of Cancer: The Next Generation.” *Cell* 144 (5): 646–74. https://doi.org/10.1016/j.cell.2011.02.013.

Hankins, Hannah M., Ryan D. Baldridge, Peng Xu, and Todd R. Graham. 2015. “Role of Flippases, Scramblases, and Transfer Proteins in Phosphatidylserine Subcellular Distribution.” *Traffic (Copenhagen, Denmark)* 16 (1): 35–47. https://doi.org/10.1111/tra.12233.

Hartman MA, Spudich JA. The myosin superfamily at a glance. J Cell Sci. 2012 Apr 1;125(Pt 7):1627-32. doi: 10.1242/jcs.094300. PMID: 22566666; PMCID: PMC3346823.

Hashimoto, Yosuke, Tetsuo Ito, Harutaka Inoue, Tomoyuki Okumura, Eiji Tanaka, Shigeru Tsunoda, Motoshige Higashiyama, Go Watanabe, Masayuki Imamura, and Yutaka Shimada. 2005. “Prognostic Significance of Fascin Overexpression in Human Esophageal Squamous Cell Carcinoma.” *Clinical Cancer Research: An Official Journal of the American Association for Cancer Research* 11 (7): 2597–2605. https://doi.org/10.1158/1078-0432.CCR-04-1378.

Hashiya, Naotaka, Nobuo Jo, Motokuni Aoki, Kunio Matsumoto, Toshikazu Nakamura, Yasufumi Sato, Nahoko Ogata, Toshio Ogihara, Yasufumi Kaneda, and Ryuichi Morishita. 2004. “In Vivo Evidence of Angiogenesis Induced by Transcription Factor Ets-1: Ets-1 Is Located Upstream of Angiogenesis Cascade.” *Circulation* 109 (24): 3035–41. https://doi.org/10.1161/01.CIR.0000130643.41587.DB.

Heimsath, Ernest G., Yang-In Yim, Mirna Mustapha, John A. Hammer, and Richard E. Cheney. 2017. “Myosin-X Knockout Is Semi-Lethal and Demonstrates That Myosin-X Functions in Neural Tube Closure, Pigmentation, Hyaloid Vasculature Regression, and Filopodia Formation.” *Scientific Reports* 7 (1): 17354. https://doi.org/10.1038/s41598-017-17638-x.

Heuser, Vanina D., Aida Kiviniemi, Laura Lehtinen, Sune Munthe, Bjarne Winther Kristensen, Jussi P. Posti, Jussi O. T. Sipilä, Ville Vuorinen, Olli Carpén, and Maria Gardberg. 2020. “Multiple Formin Proteins Participate in Glioblastoma Migration.” *BMC Cancer* 20 (1): 710. https://doi.org/10.1186/s12885-020-07211-7.

Heuser, Vanina D, Naziha Mansuri, Jasper Mogg, Samu Kurki, Heli Repo, Pauliina Kronqvist, Olli Carpén, and Maria Gardberg. 2018. “Formin Proteins FHOD1 and INF2 in Triple-Negative Breast Cancer: Association With Basal Markers and Functional Activities.” *Breast Cancer : Basic and Clinical Research* 12 (August). https://doi.org/10.1177/1178223418792247.

Hille, Bertil, Eamonn J. Dickson, Martin Kruse, Oscar Vivas, and Byung-Chang Suh. 2015. “Phosphoinositides Regulate Ion Channels.” *Biochimica et Biophysica Acta (BBA) - Molecular and Cell Biology of Lipids*, Phosphoinositides, 1851 (6): 844–56. https://doi.org/10.1016/j.bbalip.2014.09.010.

Horton, Edward R., Adam Byron, Janet A. Askari, Daniel H. J. Ng, Angélique Millon-Frémillon, Joseph Robertson, Ewa J. Koper, et al. 2015. “Definition of a Consensus Integrin Adhesome and Its Dynamics during Adhesion Complex Assembly and Disassembly.” *Nature Cell Biology* 17 (12): 1577–87. https://doi.org/10.1038/ncb3257.

Horton, Edward R., Jonathan D. Humphries, Jenny James, Matthew C. Jones, Janet A. Askari, and Martin J. Humphries. 2016. “The Integrin Adhesome Network at a Glance.” *Journal of Cell Science* 129 (22): 4159–63. https://doi.org/10.1242/jcs.192054.

Horwitz, Rick, and Donna Webb. 2003. “Cell Migration.” *Current Biology* 13 (19): R756–59. https://doi.org/10.1016/j.cub.2003.09.014.

Hotta, Kinya, Soumya Ranganathan, Ruchuan Liu, Fei Wu, Hiroaki Machiyama, Rong Gao, Hiroaki Hirata, et al. 2014. “Biophysical Properties of Intrinsically Disordered P130Cas Substrate Domain — Implication in Mechanosensing.” *PLOS Computational Biology* 10 (4): e1003532. https://doi.org/10.1371/journal.pcbi.1003532.

Howe, Alan K., Linda C. Baldor, and Brian P. Hogan. 2005. “Spatial Regulation of the CAMP-Dependent Protein Kinase during Chemotactic Cell Migration.” *Proceedings of the National Academy of Sciences* 102 (40): 14320–25. https://doi.org/10.1073/pnas.0507072102.

Huang, Da Wei, Brad T. Sherman, and Richard A. Lempicki. 2009. “Systematic and Integrative Analysis of Large Gene Lists Using DAVID Bioinformatics Resources.” *Nature Protocols* 4 (1): 44–57. https://doi.org/10.1038/nprot.2008.211.

Huang, Fang-Ke, Shaoqin Han, Bowen Xing, Jianyun Huang, Bingqian Liu, Francois Bordeleau, Cynthia A. Reinhart-King, J. Jillian Zhang, and Xin-Yun Huang. 2015. “Targeted Inhibition of Fascin Function Blocks Tumour Invasion and Metastatic Colonization.” *Nature Communications* 6 (1): 7465. https://doi.org/10.1038/ncomms8465.

Humphries, Jonathan D., Adam Byron, and Martin J. Humphries. 2006. “Integrin Ligands at a Glance.” *Journal of Cell Science* 119 (19): 3901–3. https://doi.org/10.1242/jcs.03098.

Humphries, Jonathan D., Pengbo Wang, Charles Streuli, Benny Geiger, Martin J. Humphries, and Christoph Ballestrem. 2007. “Vinculin Controls Focal Adhesion Formation by Direct Interactions with Talin and Actin.” *The Journal of Cell Biology* 179 (5): 1043–57. https://doi.org/10.1083/jcb.200703036.

Huttenlocher, A., S. P. Palecek, Q. Lu, W. Zhang, R. L. Mellgren, D. A. Lauffenburger, M. H. Ginsberg, and A. F. Horwitz. 1997. “Regulation of Cell Migration by the Calcium-Dependent Protease Calpain.” *The Journal of Biological Chemistry* 272 (52): 32719–22. https://doi.org/10.1074/jbc.272.52.32719.

Huttenlocher, Anna, and Alan Rick Horwitz. 2011. “Integrins in Cell Migration.” *Cold Spring Harbor Perspectives in Biology* 3 (9): a005074. https://doi.org/10.1101/cshperspect.a005074.

Huttenlocher PR. Synaptic density in human frontal cortex - developmental changes and effects of aging. Brain Res. 1979 Mar 16;163(2):195-205. doi: 10.1016/0006-8993(79)90349-4. PMID: 427544.

Hynes RO, Naba A. Overview of the matrisome--an inventory of extracellular matrix constituents and functions. Cold Spring Harb Perspect Biol. 2012 Jan 1;4(1):a004903. doi: 10.1101/cshperspect.a004903. PMID: 21937732; PMCID: PMC3249625.

Hwang, Priscilla Y., Audrey Brenot, Ashley C. King, Gregory D. Longmore, and Steven C. George. 2019. “Randomly Distributed K14+ Breast Tumor Cells Polarize to the Leading Edge and Guide

Collective Migration in Response to Chemical and Mechanical Environmental Cues." *Cancer Research* 79 (8): 1899–1912. https://doi.org/10.1158/0008-5472.CAN-18-2828.

Ikeda, Mika, Akio Kihara, and Yasuyuki Igarashi. 2006. "Lipid Asymmetry of the Eukaryotic Plasma Membrane: Functions and Related Enzymes." *Biological & Pharmaceutical Bulletin* 29 (8): 1542–46. https://doi.org/10.1248/bpb.29.1542.

Ivaska, Johanna, and Jyrki Heino. 2011. "Cooperation between Integrins and Growth Factor Receptors in Signaling and Endocytosis." *Annual Review of Cell and Developmental Biology* 27: 291–320. https://doi.org/10.1146/annurev-cellbio-092910-154017.

Iwamoto, Takayuki, Naoki Niikura, Rin Ogiya, Hiroyuki Yasojima, Ken-Ichi Watanabe, Chizuko Kanbayashi, Michiko Tsuneizumi, et al. 2019. "Distinct Gene Expression Profiles between Primary Breast Cancers and Brain Metastases from Pair-Matched Samples." *Scientific Reports* 9 (1): 13343. https://doi.org/10.1038/s41598-019-50099-y.

Jacquemet, Guillaume, Habib Baghirov, Maria Georgiadou, Harri Sihto, Emilia Peuhu, Pierre Cettour-Janet, Tao He, et al. 2016. "L-Type Calcium Channels Regulate Filopodia Stability and Cancer Cell Invasion Downstream of Integrin Signalling." *Nature Communications* 7 (1): 13297. https://doi.org/10.1038/ncomms13297.

Jacquemet, Guillaume, David M. Green, Rebecca E. Bridgewater, Alexander von Kriegsheim, Martin J. Humphries, Jim C. Norman, and Patrick T. Caswell. 2013. "RCP-Driven A5β1 Recycling Suppresses Rac and Promotes RhoA Activity via the RacGAP1–IQGAP1 Complex." *Journal of Cell Biology* 202 (6): 917–35. https://doi.org/10.1083/jcb.201302041.

Jacquemet, Guillaume, Ilkka Paatero, Alexandre F. Carisey, Artur Padzik, Jordan S. Orange, Hellyeh Hamidi, and Johanna Ivaska. 2017. "FiloQuant Reveals Increased Filopodia Density during Breast Cancer Progression." *Journal of Cell Biology* 216 (10): 3387–3403. https://doi.org/10.1083/jcb.201704045.

Jacquemet, Guillaume, Aki Stubb, Rafael Saup, Mitro Miihkinen, Elena Kremneva, Hellyeh Hamidi, and Johanna Ivaska. 2019. "Filopodome Mapping Identifies P130Cas as a Mechanosensitive Regulator of Filopodia Stability." *Current Biology* 29 (2): 202-216.e7. https://doi.org/10.1016/j.cub.2018.11.053.

Jakobsson, Lars, Claudio A. Franco, Katie Bentley, Russell T. Collins, Bas Ponsioen, Irene M. Aspalter, Ian Rosewell, et al. 2010. "Endothelial Cells Dynamically Compete for the Tip Cell Position during Angiogenic Sprouting." *Nature Cell Biology* 12 (10): 943–53. https://doi.org/10.1038/ncb2103.

Jarsch IK, Gadsby JR, Nuccitelli A, Mason J, Shimo H, Pilloux L, Marzook B, Mulvey CM, Dobramysl U, Bradshaw CR, Lilley KS, Hayward RD, Vaughan TJ, Dobson CL, Gallop JL. A direct role for SNX9 in the biogenesis of filopodia. J Cell Biol. 2020 Apr 6;219(4):e201909178. doi: 10.1083/jcb.201909178. PMID: 32328641; PMCID: PMC7147113.

Ji, Zhi-Min, Li-Li Yang, Juan Ni, San-Peng Xu, Cheng Yang, Pei Duan, Li-Ping Lou, and Qiu-Rong Ruan. 2018. "Silencing Filamin A Inhibits the Invasion and Migration of Breast Cancer Cells by Up-Regulating 14-3-3σ." *Current Medical Science* 38 (3): 461–66. https://doi.org/10.1007/s11596-018-1901-6.

John, Alison E., Rebecca H. Graves, K. Tao Pun, Giovanni Vitulli, Ellen J. Forty, Paul F. Mercer, Josie L. Morrell, et al. 2020. "Translational Pharmacology of an Inhaled Small Molecule Avβ6 Integrin Inhibitor for Idiopathic Pulmonary Fibrosis." *Nature Communications* 11 (1): 4659. https://doi.org/10.1038/s41467-020-18397-6.

Kanchanawong, Pakorn, Gleb Shtengel, Ana M. Pasapera, Ericka B. Ramko, Michael W. Davidson, Harald F. Hess, and Clare M. Waterman. 2010. "Nanoscale Architecture of Integrin-Based Cell Adhesions." *Nature* 468 (7323): 580–84. https://doi.org/10.1038/nature09621.

Kast, David J., and Roberto Dominguez. 2019. "Mechanism of IRSp53 Inhibition by 14-3-3." *Nature Communications* 10 (1): 483. https://doi.org/10.1038/s41467-019-08317-8.

Kayser MS, Nolt MJ, Dalva MB. EphB receptors couple dendritic filopodia motility to synapse formation. Neuron. 2008 Jul 10;59(1):56-69. doi: 10.1016/j.neuron.2008.05.007. PMID: 18614029; PMCID: PMC2617787.

Kechagia, Jenny Z., Johanna Ivaska, and Pere Roca-Cusachs. 2019. “Integrins as Biomechanical Sensors of the Microenvironment.” *Nature Reviews Molecular Cell Biology* 20 (8): 457–73. https://doi.org/10.1038/s41580-019-0134-2.

Ketschek, Andrea, and Gianluca Gallo. 2010. “Nerve Growth Factor Induces Axonal Filopodia through Localized Microdomains of Phosphoinositide 3-Kinase Activity That Drive the Formation of Cytoskeletal Precursors to Filopodia.” *The Journal of Neuroscience* 30 (36): 12185–97. https://doi.org/10.1523/JNEUROSCI.1740-10.2010.

Khan, Rejina B., and Benjamin T. Goult. 2019. “Adhesions Assemble!—Autoinhibition as a Major Regulatory Mechanism of Integrin-Mediated Adhesion.” *Frontiers in Molecular Biosciences* 6 (December). https://doi.org/10.3389/fmolb.2019.00144.

Khurana, Seema, and Sudeep P George. 2011. “The Role of Actin Bundling Proteins in the Assembly of Filopodia in Epithelial Cells.” *Cell Adhesion & Migration* 5 (5): 409–20. https://doi.org/10.4161/cam.5.5.17644.

Kim, Seong M., Saurabh G. Roy, Bin Chen, Tiffany M. Nguyen, Ryan J. McMonigle, Alison N. McCracken, Yanling Zhang, et al. 2016. “Targeting Cancer Metabolism by Simultaneously Disrupting Parallel Nutrient Access Pathways.” *The Journal of Clinical Investigation* 126 (11): 4088–4102. https://doi.org/10.1172/JCI87148.

Krugmann, Sonja, Ingrid Jordens, Kris Gevaert, Mariëtte Driessens, Joel Vandekerckhove, and Alan Hall. 2001. “Cdc42 Induces Filopodia by Promoting the Formation of an IRSp53:Mena Complex.” *Current Biology* 11 (21): 1645–55. https://doi.org/10.1016/S0960-9822(01)00506-1.

Kukkurainen S, Azizi L, Zhang P, Jacquier MC, Baikoghli M, von Essen M, Tuukkanen A, Laitaoja M, Liu X, Rahikainen R, Orłowski A, Jänis J, Määttä JAE, Varjosalo M, Vattulainen I, Róg T, Svergun D, Cheng RH, Wu J, Hytönen VP, Wehrle-Haller B. The F1 loop of the talin head domain acts as a gatekeeper in integrin activation and clustering. J Cell Sci. 2020 Oct 12;133(19):jcs239202. doi: 10.1242/jcs.239202. PMID: 33046605.

Kühn, Sonja, and Matthias Geyer. 2014. “Formins as Effector Proteins of Rho GTPases.” *Small GTPases* 5 (June). https://doi.org/10.4161/sgtp.29513.

Kwakwa, Kristin A., and Julie A. Sterling. 2017. “Integrin Avβ3 Signaling in Tumor-Induced Bone Disease.” *Cancers* 9 (7). https://doi.org/10.3390/cancers9070084.

Labernadie A, Kato T, Brugués A, Serra-Picamal X, Derzsi S, Arwert E, Weston A, González-Tarragó V, Elosegui-Artola A, Albertazzi L, Alcaraz J, Roca-Cusachs P, Sahai E, Trepat X. A mechanically active heterotypic E-cadherin/N-cadherin adhesion enables fibroblasts to drive cancer cell invasion. Nat Cell Biol. 2017 Mar;19(3):224-237. doi: 10.1038/ncb3478. Epub 2017 Feb 20. PMID: 28218910; PMCID: PMC5831988.

Ladoux, Benoit, and René-Marc Mège. 2017. “Mechanobiology of Collective Cell Behaviours.” *Nature Reviews Molecular Cell Biology* 18 (12): 743–57. https://doi.org/10.1038/nrm.2017.98.

Lagarrigue, Frederic, Chungho Kim, and Mark H. Ginsberg. 2016. “The Rap1-RIAM-Talin Axis of Integrin Activation and Blood Cell Function.” *Blood* 128 (4): 479–87. https://doi.org/10.1182/blood-2015-12-638700.

Lagarrigue, Frederic, Praju Vikas Anekal, Ho-Sup Lee, Alexia I. Bachir, Jailal N. Ablack, Alan F. Horwitz, and Mark H. Ginsberg. 2015. “A RIAM/Lamellipodin–Talin–Integrin Complex Forms the Tip of Sticky Fingers That Guide Cell Migration.” *Nature Communications* 6 (1): 8492. https://doi.org/10.1038/ncomms9492.

Law, Ah-Lai, Anne Vehlow, Maria Kotini, Lauren Dodgson, Daniel Soong, Eric Theveneau, Cristian Bodo, et al. 2013. “Lamellipodin and the Scar/WAVE Complex Cooperate to Promote Cell Migration in Vivo.” *The Journal of Cell Biology* 203 (4): 673–89. https://doi.org/10.1083/jcb.201304051.

Lee, Joycelyn JX, Kiley Loh, and Yoon-Sim Yap. 2015. “PI3K/Akt/MTOR Inhibitors in Breast Cancer.” *Cancer Biology & Medicine* 12 (4): 342–54. https://doi.org/10.7497/j.issn.2095-3941.2015.0089.

Leondaritis G, Eickholt BJ. Short Lives with Long-Lasting Effects: Filopodia Protrusions in Neuronal Branching Morphogenesis. PLoS Biol. 2015 Sep 3;13(9):e1002241. doi: 10.1371/journal.pbio.1002241. PMID: 26334727; PMCID: PMC4559444.

Levental, Ilya, Kandice R. Levental, and Frederick A. Heberle. 2020. "Lipid Rafts: Controversies Resolved, Mysteries Remain." *Trends in Cell Biology* 30 (5): 341–53. https://doi.org/10.1016/j.tcb.2020.01.009.

Li, Ang, John C. Dawson, Manuel Forero-Vargas, Heather J. Spence, Xinzi Yu, Ireen König, Kurt Anderson, and Laura M. Machesky. 2010. "The Actin-Bundling Protein Fascin Stabilizes Actin in Invadopodia and Potentiates Protrusive Invasion." *Current Biology* 20 (4): 339–45. https://doi.org/10.1016/j.cub.2009.12.035.

Li, Ang, Jennifer P. Morton, YaFeng Ma, Saadia A. Karim, Yan Zhou, William J. Faller, Emma F. Woodham, et al. 2014. "Fascin Is Regulated by Slug, Promotes Progression of Pancreatic Cancer in Mice, and Is Associated With Patient Outcomes." *Gastroenterology* 146 (5): 1386-1396.e17. https://doi.org/10.1053/j.gastro.2014.01.046.

Li, Huadong, Yi Deng, Kang Sun, Haibin Yang, Jie Liu, Meiling Wang, Zhang Zhang, et al. 2017. "Structural Basis of Kindlin-Mediated Integrin Recognition and Activation." *Proceedings of the National Academy of Sciences* 114 (35): 9349–54. https://doi.org/10.1073/pnas.1703064114.

Li X, Zheng H, Hara T, Takahashi H, Masuda S, Wang Z, Yang X, Guan Y, Takano Y. Aberrant expression of cortactin and fascin are effective markers for pathogenesis, invasion, metastasis and prognosis of gastric carcinomas. Int J Oncol. 2008 Jul;33(1):69-79. PMID: 18575752.

Lilja, Johanna, and Johanna Ivaska. 2018. "Integrin Activity in Neuronal Connectivity." *Journal of Cell Science* 131 (12). https://doi.org/10.1242/jcs.212803.

Lilja, Johanna, Thomas Zacharchenko, Maria Georgiadou, Guillaume Jacquemet, Nicola De Franceschi, Emilia Peuhu, Hellyeh Hamidi, et al. 2017. "SHANK Proteins Limit Integrin Activation by Directly Interacting with Rap1 and R-Ras." *Nature Cell Biology* 19 (4): 292–305. https://doi.org/10.1038/ncb3487.

Lin, Wan-Hsin, Joshua T. Hurley, Alexander N. Raines, Richard E. Cheney, and Donna J. Webb. 2013. "Myosin X and Its Motorless Isoform Differentially Modulate Dendritic Spine Development by Regulating Trafficking and Retention of Vasodilator-Stimulated Phosphoprotein." *Journal of Cell Science* 126 (Pt 20): 4756–68. https://doi.org/10.1242/jcs.132969.

Liu, Jianmin, Mitali Das, Jun Yang, Sujay Subbayya Ithychanda, Valentin P. Yakubenko, Edward F. Plow, and Jun Qin. 2015. "Structural Mechanism of Integrin Inactivation by Filamin." *Nature Structural & Molecular Biology* 22 (5): 383–89. https://doi.org/10.1038/nsmb.2999.

Liu, Ming, Fengshen Kuo, Kristelle J. Capistrano, Davina Kang, Briana G. Nixon, Wei Shi, Chun Chou, et al. 2020. "TGF-β Suppresses Type 2 Immunity to Cancer." *Nature* 587 (7832): 115–20. https://doi.org/10.1038/s41586-020-2836-1.

Liu, Rong, Neil Billington, Yi Yang, Charles Bond, Amy Hong, Verl Siththanandan, Yasuharu Takagi, and James R. Sellers. 2021. "A Binding Protein Regulates Myosin-7a Dimerization and Actin Bundle Assembly." *Nature Communications* 12 (1): 563. https://doi.org/10.1038/s41467-020-20864-z.

Liu, Tsung-Li, Srigokul Upadhyayula, Daniel E. Milkie, Ved Singh, Kai Wang, Ian A. Swinburne, Kishore R. Mosaliganti, et al. 2018. "Observing the Cell in Its Native State: Imaging Subcellular Dynamics in Multicellular Organisms." *Science* 360 (6386). https://doi.org/10.1126/science.aaq1392.

Liu, X. Z., J. Walsh, P. Mburu, J. Kendrick-Jones, M. J. Cope, K. P. Steel, and S. D. Brown. 1997. "Mutations in the Myosin VIIA Gene Cause Non-Syndromic Recessive Deafness." *Nature Genetics* 16 (2): 188–90. https://doi.org/10.1038/ng0697-188.

Liu, Yan-Jun, Maël Le Berre, Franziska Lautenschlaeger, Paolo Maiuri, Andrew Callan-Jones, Mélina Heuzé, Tohru Takaki, Raphaël Voituriez, and Matthieu Piel. 2015. "Confinement and Low Adhesion Induce Fast Amoeboid Migration of Slow Mesenchymal Cells." *Cell* 160 (4): 659–72. https://doi.org/10.1016/j.cell.2015.01.007.

Llorens-Bobadilla, Enric, Sheng Zhao, Avni Baser, Gonzalo Saiz-Castro, Klara Zwadlo, and Ana Martin-Villalba. 2015. “Single-Cell Transcriptomics Reveals a Population of Dormant Neural Stem Cells That Become Activated upon Brain Injury.” *Cell Stem Cell* 17 (3): 329–40. https://doi.org/10.1016/j.stem.2015.07.002.

Lock, John G., Matthew C. Jones, Janet A. Askari, Xiaowei Gong, Anna Oddone, Helene Olofsson, Sara Göransson, Melike Lakadamyali, Martin J. Humphries, and Staffan Strömblad. 2018. “Reticular Adhesions Are a Distinct Class of Cell-Matrix Adhesions That Mediate Attachment during Mitosis.” *Nature Cell Biology* 20 (11): 1290–1302. https://doi.org/10.1038/s41556-018-0220-2.

Machesky, Laura M., and Ang Li. 2010. “Fascin.” *Communicative & Integrative Biology* 3 (3): 263–70. https://doi.org/10.4161/cib.3.3.11556.

Maletic-Savatic M, Malinow R, Svoboda K. Rapid dendritic morphogenesis in CA1 hippocampal dendrites induced by synaptic activity. Science. 1999 Mar 19;283(5409):1923-7. doi: 10.1126/science.283.5409.1923. PMID: 10082466.

Manno, Sumie, Yuichi Takakuwa, and Narla Mohandas. 2002. “Identification of a Functional Role for Lipid Asymmetry in Biological Membranes: Phosphatidylserine-Skeletal Protein Interactions Modulate Membrane Stability.” *Proceedings of the National Academy of Sciences* 99 (4): 1943–48. https://doi.org/10.1073/pnas.042688399.

Mao, Yu-Ting, Julia X. Zhu, Kenji Hanamura, Giuliano Iurilli, Sandeep R. Datta, and Matthew B. Dalva. 2018. “Filopodia Conduct Target Selection in Cortical Neurons Using Differences in Signal Kinetics of a Single Kinase.” *Neuron* 98 (4): 767-782.e8. https://doi.org/10.1016/j.neuron.2018.04.011.

Masters, Thomas A., and Folma Buss. 2017. “Filopodia Formation and Endosome Clustering Induced by Mutant Plus-End–Directed Myosin VI.” *Proceedings of the National Academy of Sciences* 114 (7): 1595–1600. https://doi.org/10.1073/pnas.1616941114.

Matsuoka, Satomi, and Masahiro Ueda. 2018. “Mutual Inhibition between PTEN and PIP3 Generates Bistability for Polarity in Motile Cells.” *Nature Communications* 9 (1): 4481. https://doi.org/10.1038/s41467-018-06856-0.

McDole, Katie, Léo Guignard, Fernando Amat, Andrew Berger, Grégoire Malandain, Loïc A. Royer, Srinivas C. Turaga, Kristin Branson, and Philipp J. Keller. 2018. “In Toto Imaging and Reconstruction of Post-Implantation Mouse Development at the Single-Cell Level.” *Cell* 175 (3): 859-876.e33. https://doi.org/10.1016/j.cell.2018.09.031.

Meer, Gerrit van, and Anton I. P. M. de Kroon. 2011. “Lipid Map of the Mammalian Cell.” *Journal of Cell Science* 124 (1): 5–8. https://doi.org/10.1242/jcs.071233.

Meer, Gerrit van, Dennis R. Voelker, and Gerald W. Feigenson. 2008. “Membrane Lipids: Where They Are and How They Behave.” *Nature Reviews. Molecular Cell Biology* 9 (2): 112–24. https://doi.org/10.1038/nrm2330.

Meyen, Dana, Katsiaryna Tarbashevich, Torsten U Banisch, Carolina Wittwer, Michal Reichman-Fried, Benoît Maugis, Cecilia Grimaldi, Esther-Maria Messerschmidt, and Erez Raz. n.d. “Dynamic Filopodia Are Required for Chemokine-Dependent Intracellular Polarization during Guided Cell Migration in Vivo.” *ELife* 4. Accessed February 15, 2021. https://doi.org/10.7554/eLife.05279.

Milloud, Rachel, Olivier Destaing, Richard de Mets, Ingrid Bourrin-Reynard, Christiane Oddou, Antoine Delon, Irène Wang, Corinne Albigès-Rizo, and Martial Balland. 2017. “Avβ3 Integrins Negatively Regulate Cellular Forces by Phosphorylation of Its Distal NPXY Site.” *Biology of the Cell* 109 (3): 127–37. https://doi.org/10.1111/boc.201600041.

Minn, Andy J., Gaorav P. Gupta, Peter M. Siegel, Paula D. Bos, Weiping Shu, Dilip D. Giri, Agnes Viale, Adam B. Olshen, William L. Gerald, and Joan Massagué. 2005. “Genes That Mediate Breast Cancer Metastasis to Lung.” *Nature* 436 (7050): 518–24. https://doi.org/10.1038/nature03799.

Mogilner, A., and B. Rubinstein. 2005. “The Physics of Filopodial Protrusion.” *Biophysical Journal* 89 (2): 782–95. https://doi.org/10.1529/biophysj.104.056515.

Monteiro, Ana Carolina, Ana Carolina Leal, Triciana Gonçalves-Silva, Ana Carolina T. Mercadante, Fabiola Kestelman, Sacha Braun Chaves, Ricardo Bentes Azevedo, João P. Monteiro, and Adriana Bonomo. 2013. "T Cells Induce Pre-Metastatic Osteolytic Disease and Help Bone Metastases Establishment in a Mouse Model of Metastatic Breast Cancer." *PloS One* 8 (7): e68171. https://doi.org/10.1371/journal.pone.0068171.

Morse, ElizabethM., Nina N. Brahme, and David A. Calderwood. 2014. "Integrin Cytoplasmic Tail Interactions." *Biochemistry* 53 (5): 810–20. https://doi.org/10.1021/bi401596q.

Muller, Patricia A. J., Patrick T. Caswell, Brendan Doyle, Marcin P. Iwanicki, Ee H. Tan, Saadia Karim, Natalia Lukashchuk, et al. 2009. "Mutant P53 Drives Invasion by Promoting Integrin Recycling." *Cell* 139 (7): 1327–41. https://doi.org/10.1016/j.cell.2009.11.026.

Nacke, Marisa, Emma Sandilands, Konstantina Nikolatou, Álvaro Román-Fernández, Susan Mason, Rachana Patel, Sergio Lilla, et al. 2021. "An ARF GTPase Module Promoting Invasion and Metastasis through Regulating Phosphoinositide Metabolism." *Nature Communications* 12 (1): 1623. https://doi.org/10.1038/s41467-021-21847-4.

Naisbitt, Scott, Eunjoon Kim, Jian Cheng Tu, Bo Xiao, Carlo Sala, Juli Valtschanoff, Richard J. Weinberg, Paul F. Worley, and Morgan Sheng. 1999. "Shank, a Novel Family of Postsynaptic Density Proteins That Binds to the NMDA Receptor/PSD-95/GKAP Complex and Cortactin." *Neuron* 23 (3): 569–82. https://doi.org/10.1016/S0896-6273(00)80809-0.

Nawrotek, Agata, Sarah Benabdi, Supaporn Niyomchon, Marie-Hélène Kryszke, Christophe Ginestier, Tatiana Cañeque, Livia Tepshi, et al. 2019. "PH-Domain-Binding Inhibitors of Nucleotide Exchange Factor BRAG2 Disrupt Arf GTPase Signaling." *Nature Chemical Biology* 15 (4): 358–66. https://doi.org/10.1038/s41589-019-0228-3.

Nelson JC, Stavoe AK, Colón-Ramos DA. The actin cytoskeleton in presynaptic assembly. Cell Adh Migr. 2013 Jul-Aug;7(4):379-87. doi: 10.4161/cam.24803. Epub 2013 Apr 29. PMID: 23628914; PMCID: PMC3739815.

Notni, Johannes, Dominik Reich, Oleg V. Maltsev, Tobias G. Kapp, Katja Steiger, Frauke Hoffmann, Irene Esposito, Wilko Weichert, Horst Kessler, and Hans-Jürgen Wester. 2017. "In Vivo PET Imaging of the Cancer Integrin Avβ6 Using 68Ga-Labeled Cyclic RGD Nonapeptides." *Journal of Nuclear Medicine: Official Publication, Society of Nuclear Medicine* 58 (4): 671–77. https://doi.org/10.2967/jnumed.116.182824.

Obenauf, Anna C., and Joan Massagué. 2015. "Surviving at a Distance: Organ Specific Metastasis." *Trends in Cancer* 1 (1): 76–91. https://doi.org/10.1016/j.trecan.2015.07.009.

Omelchenko, Tatiana, Alan Hall, and Kathryn V. Anderson. 2020. "β-Pix-Dependent Cellular Protrusions Propel Collective Mesoderm Migration in the Mouse Embryo." *Nature Communications* 11 (1): 6066. https://doi.org/10.1038/s41467-020-19889-1.

Oxley, Camilla L., Nicholas J. Anthis, Edward D. Lowe, Ioannis Vakonakis, Iain D. Campbell, and Kate L. Wegener. 2008. "An Integrin Phosphorylation Switch: The Effect of Beta3 Integrin Tail Phosphorylation on Dok1 and Talin Binding." *The Journal of Biological Chemistry* 283 (9): 5420–26. https://doi.org/10.1074/jbc.M709435200.

Padrick, Shae B., Lynda K. Doolittle, Chad A. Brautigam, David S. King, and Michael K. Rosen. 2011. "Arp2/3 Complex Is Bound and Activated by Two WASP Proteins." *Proceedings of the National Academy of Sciences* 108 (33): E472–79. https://doi.org/10.1073/pnas.1100236108.

Pasapera, Ana M., Ian C. Schneider, Erin Rericha, David D. Schlaepfer, and Clare M. Waterman. 2010. "Myosin II Activity Regulates Vinculin Recruitment to Focal Adhesions through FAK-Mediated Paxillin Phosphorylation." *The Journal of Cell Biology* 188 (6): 877–90. https://doi.org/10.1083/jcb.200906012.

Pastushenko, Ievgenia, Audrey Brisebarre, Alejandro Sifrim, Marco Fioramonti, Tatiana Revenco, Soufiane Boumahdi, Alexandra Van Keymeulen, et al. 2018. "Identification of the Tumour Transition States Occurring during EMT." *Nature* 556 (7702): 463–68. https://doi.org/10.1038/s41586-018-0040-3.

Paul, Nikki R., Jennifer L. Allen, Anna Chapman, Maria Morlan-Mairal, Egor Zindy, Guillaume Jacquemet, Laura Fernandez del Ama, et al. 2015. “A5β1 Integrin Recycling Promotes Arp2/3-Independent Cancer Cell Invasion via the Formin FHOD3.” *The Journal of Cell Biology* 210 (6): 1013–31. https://doi.org/10.1083/jcb.201502040.

Pellegrin, Stéphanie, and Harry Mellor. 2005. “The Rho Family GTPase Rif Induces Filopodia through MDia2.” *Current Biology: CB* 15 (2): 129–33. https://doi.org/10.1016/j.cub.2005.01.011.

Pellinen, Teijo, Antti Arjonen, Karoliina Vuoriluoto, Katja Kallio, Jack A. M. Fransen, and Johanna Ivaska. 2006. “Small GTPase Rab21 Regulates Cell Adhesion and Controls Endosomal Traffic of Beta1-Integrins.” *The Journal of Cell Biology* 173 (5): 767–80. https://doi.org/10.1083/jcb.200509019.

Peng, Jun, Bradley J. Wallar, Akiko Flanders, Pamela J. Swiatek, and Arthur S. Alberts. 2003. “Disruption of the Diaphanous-Related Formin Drf1 Gene Encoding MDia1 Reveals a Role for Drf3 as an Effector for Cdc42.” *Current Biology* 13 (7): 534–45. https://doi.org/10.1016/S0960-9822(03)00170-2.

Peng, Xiao, Elke S. Nelson, Jessica L. Maiers, and Kris A. DeMali. 2011. “New Insights into Vinculin Function and Regulation.” *International Review of Cell and Molecular Biology* 287: 191–231. https://doi.org/10.1016/B978-0-12-386043-9.00005-0.

Petridou, Nicoletta I., and Paris A. Skourides. 2016. “A Ligand-Independent Integrin B1 Mechanosensory Complex Guides Spindle Orientation.” *Nature Communications* 7 (March). https://doi.org/10.1038/ncomms10899.

Petrie, Ryan J., and Kenneth M. Yamada. 2012. “At the Leading Edge of Three-Dimensional Cell Migration.” *Journal of Cell Science* 125 (24): 5917–26. https://doi.org/10.1242/jcs.093732.

Plantard, Laure, Antti Arjonen, John G. Lock, Ghasem Nurani, Johanna Ivaska, and Staffan Strömblad. 2010. “PtdIns(3,4,5)P3 Is a Regulator of Myosin-X Localization and Filopodia Formation.” *Journal of Cell Science* 123 (20): 3525–34. https://doi.org/10.1242/jcs.069609.

Pollard, Thomas D. 2016. “Actin and Actin-Binding Proteins.” *Cold Spring Harbor Perspectives in Biology* 8 (8). https://doi.org/10.1101/cshperspect.a018226.

Prestwich, Glenn D. 2004. “Phosphoinositide Signaling: From Affinity Probes to Pharmaceutical Targets.” *Chemistry & Biology* 11 (5): 619–37. https://doi.org/10.1016/j.chembiol.2004.03.025.

Prévost C, Zhao H, Manzi J, et al. IRSp53 senses negative membrane curvature and phase separates along membrane tubules. Nat Commun. 2015;6:8529. Published 2015 Oct 15. doi:10.1038/ncomms9529

Pyrgaki, Christina, Paul Trainor, Anna-Katerina Hadjantonakis, and Lee Niswander. 2010. “Dynamic Imaging of Mammalian Neural Tube Closure.” *Developmental Biology* 344 (2): 941–47. https://doi.org/10.1016/j.ydbio.2010.06.010.

Qualmann, Britta, Tobias M. Boeckers, Monika Jeromin, Eckart D. Gundelfinger, and Michael M. Kessels. 2004. “Linkage of the Actin Cytoskeleton to the Postsynaptic Density via Direct Interactions of Abp1 with the ProSAP/Shank Family.” *Journal of Neuroscience* 24 (10): 2481–95. https://doi.org/10.1523/JNEUROSCI.5479-03.2004.

Raab-Westphal, Sabine, John F. Marshall, and Simon L. Goodman. 2017. “Integrins as Therapeutic Targets: Successes and Cancers.” *Cancers* 9 (9). https://doi.org/10.3390/cancers9090110.

Rantala JK, Pouwels J, Pellinen T, Veltel S, Laasola P, Mattila E, Potter CS, Duffy T, Sundberg JP, Kallioniemi O, Askari JA, Humphries MJ, Parsons M, Salmi M, Ivaska J. SHARPIN is an endogenous inhibitor of β1-integrin activation. Nat Cell Biol. 2011 Sep 25;13(11):1315-24. doi: 10.1038/ncb2340. PMID: 21947080; PMCID: PMC3257806.

Ratcliffe, Colin D. H., Pranshu Sahgal, Christine A. Parachoniak, Johanna Ivaska, and Morag Park. 2016. “Regulation of Cell Migration and B1 Integrin Trafficking by the Endosomal Adaptor GGA3.” *Traffic (Copenhagen, Denmark)* 17 (6): 670–88. https://doi.org/10.1111/tra.12390.

Reardon, David A., and David Cheresh. 2011. “Cilengitide: A Prototypic Integrin Inhibitor for the Treatment of Glioblastoma and Other Malignancies.” *Genes & Cancer* 2 (12): 1159–65. https://doi.org/10.1177/1947601912450586.

Ren, X. D., W. B. Kiosses, D. J. Sieg, C. A. Otey, D. D. Schlaepfer, and M. A. Schwartz. 2000. "Focal Adhesion Kinase Suppresses Rho Activity to Promote Focal Adhesion Turnover." *Journal of Cell Science* 113 (Pt 20) (October): 3673–78.

Rhee, Sangmyung. 2009. "Fibroblasts in Three Dimensional Matrices: Cell Migration and Matrix Remodeling." *Experimental & Molecular Medicine* 41 (12): 858–65. https://doi.org/10.3858/emm.2009.41.12.096.

Riahi, Reza, Jian Sun, Shue Wang, Min Long, Donna D. Zhang, and Pak Kin Wong. 2015. "Notch1-Dll4 Signaling and Mechanical Force Regulate Leader Cell Formation during Collective Cell Migration." *Nature Communications* 6 (March): 6556. https://doi.org/10.1038/ncomms7556.

Richier, Benjamin, Yoshiko Inoue, Ulrich Dobramysl, Jonathan Friedlander, Nicholas H. Brown, and Jennifer L. Gallop. 2018. "Integrin Signaling Downregulates Filopodia during Muscle–Tendon Attachment." *Journal of Cell Science* 131 (jcs217133). https://doi.org/10.1242/jcs.217133.

Ridley, Anne J. 2011. "Life at the Leading Edge." *Cell* 145 (7): 1012–22. https://doi.org/10.1016/j.cell.2011.06.010.

Robles, Estuardo, Stephanie Woo, and Timothy M. Gomez. 2005. "Src-Dependent Tyrosine Phosphorylation at the Tips of Growth Cone Filopodia Promotes Extension." *The Journal of Neuroscience* 25 (33): 7669–81. https://doi.org/10.1523/JNEUROSCI.2680-05.2005.

Rohatgi, Rajat, Hsin-yi Henry Ho, and Marc W. Kirschner. 2000. "Mechanism of N-Wasp Activation by Cdc42 and Phosphatidylinositol 4,5-Bisphosphate." *The Journal of Cell Biology* 150 (6): 1299–1310.

Rottner K, Faix J, Bogdan S, Linder S, Kerkhoff E. Actin assembly mechanisms at a glance. J Cell Sci. 2017 Oct 15;130(20):3427-3435. doi: 10.1242/jcs.206433. PMID: 29032357.

Roux KJ, Kim DI, Burke B. BioID: a screen for protein-protein interactions. Curr Protoc Protein Sci. 2013 Nov 5;74:19.23.1-19.23.14. doi: 10.1002/0471140864.ps1923s74. PMID: 24510646.

Rozovsky S, Forstner MB, Sondermann H, Groves JT. Single molecule kinetics of ENTH binding to lipid membranes. J Phys Chem B. 2012;116(17):5122-5131. doi:10.1021/jp210045r

Runz, Steffen, Claudia T. Mierke, Safwan Joumaa, Jürgen Behrens, Ben Fabry, and Peter Altevogt. 2008. "CD24 Induces Localization of Beta1 Integrin to Lipid Raft Domains." *Biochemical and Biophysical Research Communications* 365 (1): 35–41. https://doi.org/10.1016/j.bbrc.2007.10.139.

Sahgal, Pranshu, Jonna Alanko, Jaroslav Icha, Ilkka Paatero, Hellyeh Hamidi, Antti Arjonen, Mika Pietilä, Anne Rokka, and Johanna Ivaska. 2019. "GGA2 and RAB13 Promote Activity-Dependent B1-Integrin Recycling." *Journal of Cell Science* 132 (11). https://doi.org/10.1242/jcs.233387.

Salles, Felipe T., Raymond C. Merritt, Uri Manor, Gerard W. Dougherty, Aurea D. Sousa, Judy E. Moore, Christopher M. Yengo, Andréa C. Dosé, and Bechara Kachar. 2009. "Myosin IIIa Boosts Elongation of Stereocilia by Transporting Espin 1 to the plus Ends of Actin Filaments." *Nature Cell Biology* 11 (4): 443–50. https://doi.org/10.1038/ncb1851.

Sawada, Yasuhiro, Masako Tamada, Benjamin J. Dubin-Thaler, Oksana Cherniavskaya, Ryuichi Sakai, Sakae Tanaka, and Michael P. Sheetz. 2006. "Force Sensing by Mechanical Extension of the Src Family Kinase Substrate P130Cas." *Cell* 127 (5): 1015–26. https://doi.org/10.1016/j.cell.2006.09.044.

Saxena, Mayur, Rishita Changede, James Hone, Haguy Wolfenson, and Michael P. Sheetz. 2017. "Force-Induced Calpain Cleavage of Talin Is Critical for Growth, Adhesion Development, and Rigidity Sensing." *Nano Letters* 17 (12): 7242–51. https://doi.org/10.1021/acs.nanolett.7b02476.

Sbrissa D, Ikonomov OC, Shisheva A. Phosphatidylinositol 3-phosphate-interacting domains in PIKfyve. Binding specificity and role in PIKfyve. Endomenbrane localization. J Biol Chem. 2002;277(8):6073-6079. doi:10.1074/jbc.M110194200

Scarpa, Elena, and Roberto Mayor. 2016. "Collective Cell Migration in Development." *The Journal of Cell Biology* 212 (2): 143–55. https://doi.org/10.1083/jcb.201508047.

Schäfer, Matthias, and Sabine Werner. 2007. "Transcriptional Control of Wound Repair." *Annual Review of Cell and Developmental Biology* 23 (1): 69–92. https://doi.org/10.1146/annurev.cellbio.23.090506.123609.

Schober, Markus, Srikala Raghavan, Maria Nikolova, Lisa Polak, H. Amalia Pasolli, Hilary E. Beggs, Louis F. Reichardt, and Elaine Fuchs. 2007. "Focal Adhesion Kinase Modulates Tension Signaling to Control Actin and Focal Adhesion Dynamics." *The Journal of Cell Biology* 176 (5): 667–80. https://doi.org/10.1083/jcb.200608010.

Schroeder, Avi, Daniel A. Heller, Monte M. Winslow, James E. Dahlman, George W. Pratt, Robert Langer, Tyler Jacks, and Daniel G. Anderson. 2012. "Treating Metastatic Cancer with Nanotechnology." *Nature Reviews Cancer* 12 (1): 39–50. https://doi.org/10.1038/nrc3180.

Sebé-Pedrós, Arnau, Xavier Grau-Bové, Thomas A. Richards, and Iñaki Ruiz-Trillo. 2014. "Evolution and Classification of Myosins, a Paneukaryotic Whole-Genome Approach." *Genome Biology and Evolution* 6 (2): 290–305. https://doi.org/10.1093/gbe/evu013.

Senning, Eric N., Marcus D. Collins, Anastasiia Stratiievska, Carmen A. Ufret-Vincenty, and Sharona E. Gordon. 2014. "Regulation of TRPV1 Ion Channel by Phosphoinositide (4,5)-Bisphosphate: The Role of Membrane Asymmetry." *The Journal of Biological Chemistry* 289 (16): 10999–6. https://doi.org/10.1074/jbc.M114.553180.

Shattil, Sanford J., Chungho Kim, and Mark H. Ginsberg. 2010. "The Final Steps of Integrin Activation: The End Game." *Nature Reviews. Molecular Cell Biology* 11 (4): 288–300. https://doi.org/10.1038/nrm2871.

Sheng C, Javed U, Gibbs M, Long C, Yin J, Qin B, Yuan Q. Experience-dependent structural plasticity targets dynamic filopodia in regulating dendrite maturation and synaptogenesis. Nat Commun. 2018 Aug 22;9(1):3362. doi: 10.1038/s41467-018-05871-5. PMID: 30135566; PMCID: PMC6105721.

Shi, Song-Hai, Lily Yeh Jan, and Yuh-Nung Jan. 2003. "Hippocampal Neuronal Polarity Specified by Spatially Localized MPar3/MPar6 and PI 3-Kinase Activity." *Cell* 112 (1): 63–75. https://doi.org/10.1016/s0092-8674(02)01249-7.

Shi, Yang, and Iryna M. Ethell. 2006. "Integrins Control Dendritic Spine Plasticity in Hippocampal Neurons through NMDA Receptor and Ca2+/Calmodulin-Dependent Protein Kinase II-Mediated Actin Reorganization." *Journal of Neuroscience* 26 (6): 1813–22. https://doi.org/10.1523/JNEUROSCI.4091-05.2006.

Shibue, Tsukasa, Mary W. Brooks, M. Fatih Inan, Ferenc Reinhardt, and Robert A. Weinberg. 2012. "The Outgrowth of Micrometastases Is Enabled by the Formation of Filopodium-like Protrusions." *Cancer Discovery* 2 (8): 706–21. https://doi.org/10.1158/2159-8290.CD-11-0239.

Shneyer, Boris I., Marko Ušaj, Naama Wiesel-Motiuk, Ronit Regev, and Arnon Henn. 2017. "ROS Induced Distribution of Mitochondria to Filopodia by Myo19 Depends on a Class Specific Tryptophan in the Motor Domain." *Scientific Reports* 7 (1): 11577. https://doi.org/10.1038/s41598-017-11002-9.

Solnica-Krezel, Lila, and Diane S. Sepich. 2012. "Gastrulation: Making and Shaping Germ Layers." *Annual Review of Cell and Developmental Biology* 28 (1): 687–717. https://doi.org/10.1146/annurev-cellbio-092910-154043.

Spence, Erin F., Shataakshi Dube, Akiyoshi Uezu, Margaret Locke, Erik J. Soderblom, and Scott H. Soderling. 2019. "In Vivo Proximity Proteomics of Nascent Synapses Reveals a Novel Regulator of Cytoskeleton-Mediated Synaptic Maturation." *Nature Communications* 10 (1): 386. https://doi.org/10.1038/s41467-019-08288-w.

Stubb, Aki, Camilo Guzmán, Elisa Närvä, Jesse Aaron, Teng-Leong Chew, Markku Saari, Mitro Miihkinen, Guillaume Jacquemet, and Johanna Ivaska. 2019. "Superresolution Architecture of Cornerstone Focal Adhesions in Human Pluripotent Stem Cells." *Nature Communications* 10 (1): 4756. https://doi.org/10.1038/s41467-019-12611-w.

Stubb, Aki, Romain F. Laine, Mitro Miihkinen, Hellyeh Hamidi, Camilo Guzmán, Ricardo Henriques, Guillaume Jacquemet, and Johanna Ivaska. 2020. "Fluctuation-Based Super-Resolution Traction Force Microscopy." *Nano Letters* 20 (4): 2230–45. https://doi.org/10.1021/acs.nanolett.9b04083.

Summerbell, Emily R., Janna K. Mouw, Joshua S. K. Bell, Christina M. Knippler, Brian Pedro, Jamie L. Arnst, Tala O. Khatib, et al. 2020. "Epigenetically Heterogeneous Tumor Cells Direct Collective

Invasion through Filopodia-Driven Fibronectin Micropatterning." *Science Advances* 6 (30). https://doi.org/10.1126/sciadv.aaz6197.

Sun, Zhiqi, Mercedes Costell, and Reinhard Fässler. 2019a. "Integrin Activation by Talin, Kindlin and Mechanical Forces." *Nature Cell Biology* 21 (1): 25–31. https://doi.org/10.1038/s41556-018-0234-9.

———. 2019b. "Integrin Activation by Talin, Kindlin and Mechanical Forces." *Nature Cell Biology* 21 (1): 25–31. https://doi.org/10.1038/s41556-018-0234-9.

Sun Y, Kaksonen M, Madden DT, Schekman R, Drubin DG. Interaction of Sla2p's ANTH domain with PtdIns(4,5)P2 is important for actin-dependent endocytic internalization. Mol Biol Cell. 2005;16(2):717-730. doi:10.1091/mbc.e04-08-0740

Stoeckli ET. Understanding axon guidance: are we nearly there yet? Development. 2018 May 14;145(10):dev151415. doi: 10.1242/dev.151415. PMID: 29759980.

Szabó, András, and Roberto Mayor. 2016. "Modelling Collective Cell Migration of Neural Crest." *Current Opinion in Cell Biology* 42 (October): 22–28. https://doi.org/10.1016/j.ceb.2016.03.023.

Szabó, András, Manuela Melchionda, Giancarlo Nastasi, Mae L. Woods, Salvatore Campo, Roberto Perris, and Roberto Mayor. 2016. "In Vivo Confinement Promotes Collective Migration of Neural Crest Cells." *Journal of Cell Biology* 213 (5): 543–55. https://doi.org/10.1083/jcb.201602083.

Tabariès S, Dupuy F, Dong Z, Monast A, Annis MG, Spicer J, Ferri LE, Omeroglu A, Basik M, Amir E, Clemons M, Siegel PM. Claudin-2 promotes breast cancer liver metastasis by facilitating tumor cell interactions with hepatocytes. Mol Cell Biol. 2012 Aug;32(15):2979-91. doi: 10.1128/MCB.00299-12. Epub 2012 May 29. PMID: 22645303; PMCID: PMC3434516.

Takagi, Junichi, Benjamin M. Petre, Thomas Walz, and Timothy A. Springer. 2002. "Global Conformational Rearrangements in Integrin Extracellular Domains in Outside-in and inside-out Signaling." *Cell* 110 (5): 599–511. https://doi.org/10.1016/s0092-8674(02)00935-2.

Takala, Heikki, Elisa Nurminen, Susanna M. Nurmi, Maria Aatonen, Tomas Strandin, Maarit Takatalo, Tiila Kiema, Carl G. Gahmberg, Jari Ylänne, and Susanna C. Fagerholm. 2008. "B2 Integrin Phosphorylation on Thr758 Acts as a Molecular Switch to Regulate 14-3-3 and Filamin Binding." *Blood* 112 (5): 1853–62. https://doi.org/10.1182/blood-2007-12-127795.

Thinn, Aye Myat Myat, Zhengli Wang, and Jieqing Zhu. 2018. "The Membrane-Distal Regions of Integrin α Cytoplasmic Domains Contribute Differently to Integrin inside-out Activation." *Scientific Reports* 8 (1): 5067. https://doi.org/10.1038/s41598-018-23444-w.

Thomas RJ, Guise TA, Yin JJ, Elliott J, Horwood NJ, Martin TJ, Gillespie MT. Breast cancer cells interact with osteoblasts to support osteoclast formation. Endocrinology. 1999 Oct;140(10):4451-8. doi: 10.1210/endo.140.10.7037. PMID: 10499498.

Tokuo, Hiroshi, and Mitsuo Ikebe. 2004. "Myosin X Transports Mena/VASP to the Tip of Filopodia." *Biochemical and Biophysical Research Communications* 319 (1): 214–20. https://doi.org/10.1016/j.bbrc.2004.04.167.

Tokuo, Hiroshi, Katsuhide Mabuchi, and Mitsuo Ikebe. 2007. "The Motor Activity of Myosin-X Promotes Actin Fiber Convergence at the Cell Periphery to Initiate Filopodia Formation." *The Journal of Cell Biology* 179 (2): 229–38. https://doi.org/10.1083/jcb.200703178.

Vignjevic, Danijela, Marie Schoumacher, Nancy Gavert, Klaus-Peter Janssen, Gloria Jih, Marick Laé, Daniel Louvard, Avri Ben-Ze'ev, and Sylvie Robine. 2007. "Fascin, a Novel Target of Beta-Catenin-TCF Signaling, Is Expressed at the Invasive Front of Human Colon Cancer." *Cancer Research* 67 (14): 6844–53. https://doi.org/10.1158/0008-5472.CAN-07-0929.

Wang, F. S., J. S. Wolenski, R. E. Cheney, M. S. Mooseker, and D. G. Jay. 1996. "Function of Myosin-V in Filopodial Extension of Neuronal Growth Cones." *Science (New York, N.Y.)* 273 (5275): 660–63. https://doi.org/10.1126/science.273.5275.660.

Wang, Li, Kaifang Pang, Kihoon Han, Carolyn J. Adamski, Wei Wang, Lingjie He, Jason K. Lai, et al. 2020. "An Autism-Linked Missense Mutation in SHANK3 Reveals the Modularity of Shank3 Function." *Molecular Psychiatry* 25 (10): 2534–55. https://doi.org/10.1038/s41380-018-0324-x.

Wang, Yu, and Mark A. McNiven. 2012. “Invasive Matrix Degradation at Focal Adhesions Occurs via Protease Recruitment by a FAK–P130Cas Complex.” *Journal of Cell Biology* 196 (3): 375–85. https://doi.org/10.1083/jcb.201105153.

Watt, Fiona M., and Hironobu Fujiwara. 2011. “Cell-Extracellular Matrix Interactions in Normal and Diseased Skin.” *Cold Spring Harbor Perspectives in Biology* 3 (4): a005124. https://doi.org/10.1101/cshperspect.a005124.

Webb, Donna J., Huaye Zhang, Devi Majumdar, and Alan F. Horwitz. 2007. “A5 Integrin Signaling Regulates the Formation of Spines and Synapses in Hippocampal Neurons *.” *Journal of Biological Chemistry* 282 (10): 6929–35. https://doi.org/10.1074/jbc.M610981200.

Welf, Erik S., Ulhas P. Naik, and Babatunde A. Ogunnaike. 2012. “A Spatial Model for Integrin Clustering as a Result of Feedback between Integrin Activation and Integrin Binding.” *Biophysical Journal* 103 (6): 1379–89. https://doi.org/10.1016/j.bpj.2012.08.021.

Wendel, Claudia, André Hemping-Bovenkerk, Julia Krasnyanska, Sören Torge Mees, Marina Kochetkova, Sandra Stoeppeler, and Jörg Haier. 2012. “CXCR4/CXCL12 Participate in Extravasation of Metastasizing Breast Cancer Cells within the Liver in a Rat Model.” *PLOS ONE* 7 (1): e30046. https://doi.org/10.1371/journal.pone.0030046.

Winograd-Katz, Sabina E., Reinhard Fässler, Benjamin Geiger, and Kyle R. Legate. 2014. “The Integrin Adhesome: From Genes and Proteins to Human Disease.” *Nature Reviews Molecular Cell Biology* 15 (4): 273–88. https://doi.org/10.1038/nrm3769.

Wolf, Katarina, Mariska te Lindert, Marina Krause, Stephanie Alexander, Joost te Riet, Amanda L. Willis, Robert M. Hoffman, Carl G. Figdor, Stephen J. Weiss, and Peter Friedl. 2013. “Physical Limits of Cell Migration: Control by ECM Space and Nuclear Deformation and Tuning by Proteolysis and Traction Force.” *Journal of Cell Biology* 201 (7): 1069–84. https://doi.org/10.1083/jcb.201210152.

Wolf, Katarina, Irina Mazo, Harry Leung, Katharina Engelke, Ulrich H. von Andrian, Elena I. Deryugina, Alex Y. Strongin, Eva-B. Bröcker, and Peter Friedl. 2003. “Compensation Mechanism in Tumor Cell Migration: Mesenchymal-Amoeboid Transition after Blocking of Pericellular Proteolysis.” *The Journal of Cell Biology* 160 (2): 267–77. https://doi.org/10.1083/jcb.200209006.

Wong, Stephanie, Wei-Hui Guo, and Yu-Li Wang. 2014. “Fibroblasts Probe Substrate Rigidity with Filopodia Extensions before Occupying an Area.” *Proceedings of the National Academy of Sciences* 111 (48): 17176–81. https://doi.org/10.1073/pnas.1412285111.

Wood, Megan N., Noboru Ishiyama, Indira Singaram, Connie M. Chung, Annette S. Flozak, Alex Yemelyanov, Mitsu Ikura, Wonhwa Cho, and Cara J. Gottardi. 2017. “α-Catenin Homodimers Are Recruited to Phosphoinositide-Activated Membranes to Promote Adhesion.” *Journal of Cell Biology* 216 (11): 3767–83. https://doi.org/10.1083/jcb.201612006.

Wu GY, Cline HT. Stabilization of dendritic arbor structure in vivo by CaMKII. Science. 1998 Jan 9;279(5348):222-6. doi: 10.1126/science.279.5348.222. PMID: 9422694.

Wu, Fei, Yannan Qin, Qiuyu Jiang, Jinyuan Zhang, Fang Li, Qian Li, Xiaofei Wang, et al. 2020. “MyoD1 Suppresses Cell Migration and Invasion by Inhibiting FUT4 Transcription in Human Gastric Cancer Cells.” *Cancer Gene Therapy* 27 (10): 773–84. https://doi.org/10.1038/s41417-019-0153-3.

Wu, Jia-shun, Jian Jiang, Bing-jun Chen, Ke Wang, Ya-ling Tang, and Xin-hua Liang. 2021. “Plasticity of Cancer Cell Invasion: Patterns and Mechanisms.” *Translational Oncology* 14 (1): 100899. https://doi.org/10.1016/j.tranon.2020.100899.

Wu, Xiaoyang, Atsuko Kodama, and Elaine Fuchs. 2008. “ACF7 Regulates Cytoskeletal-Focal Adhesion Dynamics and Migration and Has ATPase Activity.” *Cell* 135 (1): 137–48. https://doi.org/10.1016/j.cell.2008.07.045.

Wyckoff, Jeffrey B., Sophie E. Pinner, Steve Gschmeissner, John S. Condeelis, and Erik Sahai. 2006. “ROCK- and Myosin-Dependent Matrix Deformation Enables Protease-Independent Tumor-Cell Invasion in Vivo.” *Current Biology: CB* 16 (15): 1515–23. https://doi.org/10.1016/j.cub.2006.05.065.

Xia S, Yim EKF, Kanchanawong P. Molecular Organization of Integrin-Based Adhesion Complexes in Mouse Embryonic Stem Cells. ACS Biomater Sci Eng. 2019 Aug 12;5(8):3828-3842. doi: 10.1021/acsbiomaterials.8b01124. Epub 2019 Jan 29. PMID: 33438423.

Xu, Jian, Samy Lamouille, and Rik Derynck. 2009. "TGF-Beta-Induced Epithelial to Mesenchymal Transition." *Cell Research* 19 (2): 156–72. https://doi.org/10.1038/cr.2009.5.

Yamada, Kenneth M., and Michael Sixt. 2019. "Mechanisms of 3D Cell Migration." *Nature Reviews Molecular Cell Biology* 20 (12): 738–52. https://doi.org/10.1038/s41580-019-0172-9.

Yang, Changsong, and Tatyana Svitkina. 2011. "Filopodia Initiation: Focus on the Arp2/3 Complex and Formins." *Cell Adhesion & Migration* 5 (5): 402–8. https://doi.org/10.4161/cam.5.5.16971.

Yang, Yang, Hongmei Zheng, Yuting Zhan, and Songqing Fan. 2019. "An Emerging Tumor Invasion Mechanism about the Collective Cell Migration." *American Journal of Translational Research* 11 (9): 5301–12.

Yarar D, Surka MC, Leonard MC, Schmid SL. SNX9 activities are regulated by multiple phosphoinositides through both PX and BAR domains. Traffic. 2008;9(1):133-146. doi:10.1111/j.1600-0854.2007.00675.x

Yen, Hsin-Yung, Kin Kuan Hoi, Idlir Liko, George Hedger, Michael R. Horrell, Wanling Song, Di Wu, et al. 2018. "PtdIns(4,5)P 2 Stabilizes Active States of GPCRs and Enhances Selectivity of G-Protein Coupling." *Nature* 559 (7714): 423–27. https://doi.org/10.1038/s41586-018-0325-6.

Yoshihara, Masato, Yoshihiko Yamakita, Hiroaki Kajiyama, Takeshi Senga, Yoshihiro Koya, Mamoru Yamashita, Akihiro Nawa, and Fumitaka Kikkawa. 2020. "Filopodia Play an Important Role in the Trans-Mesothelial Migration of Ovarian Cancer Cells." *Experimental Cell Research* 392 (2): 112011. https://doi.org/10.1016/j.yexcr.2020.112011.

Yue B. Biology of the extracellular matrix: an overview. J Glaucoma. 2014 Oct-Nov;23(8 Suppl 1):S20-3. doi: 10.1097/IJG.0000000000000108. PMID: 25275899; PMCID: PMC4185430.

Yue, Jiping, Min Xie, Xuewen Gou, Philbert Lee, Michael D. Schneider, and Xiaoyang Wu. 2014. "Microtubules Regulate Focal Adhesion Dynamics through MAP4K4." *Developmental Cell* 31 (5): 572–85. https://doi.org/10.1016/j.devcel.2014.10.025.

Zhang, H., L. Xu, D. Xiao, J. Xie, H. Zeng, W. Cai, Y. Niu, Z. Yang, Z. Shen, and E. Li. 2006. "Fascin Is a Potential Biomarker for Early-Stage Oesophageal Squamous Cell Carcinoma." *Journal of Clinical Pathology* 59 (9): 958–64. https://doi.org/10.1136/jcp.2005.032730.

Zhang, Hongquan, Jonathan S. Berg, Zhilun Li, Yunling Wang, Pernilla Lång, Aurea D. Sousa, Aparna Bhaskar, Richard E. Cheney, and Staffan Strömblad. 2004. "Myosin-X Provides a Motor-Based Link between Integrins and the Cytoskeleton." *Nature Cell Biology* 6 (6): 523–31. https://doi.org/10.1038/ncb1136.

Zhang, Mei-Fang, Qiu-Li Li, Yu-Feng Yang, Yun Cao, and Chris Zhiyi Zhang. 2020. "FMNL1 Exhibits Pro-Metastatic Activity via CXCR2 in Clear Cell Renal Cell Carcinoma." *Frontiers in Oncology* 10: 564614. https://doi.org/10.3389/fonc.2020.564614.

Zhong, Banghua, Kewei Wang, Hao Xu, and Fanmin Kong. 2018. "Silencing Formin-like 2 Inhibits Growth and Metastasis of Gastric Cancer Cells through Suppressing Internalization of Integrins." *Cancer Cell International* 18 (June). https://doi.org/10.1186/s12935-018-0576-1.

Zhu, Xi-Ling, Li Liang, and Yan-Qing Ding. 2008. "Overexpression of FMNL2 Is Closely Related to Metastasis of Colorectal Cancer." *International Journal of Colorectal Disease* 23 (11): 1041–47. https://doi.org/10.1007/s00384-008-0520-2.

TURUN
YLIOPISTO
UNIVERSITY
OF TURKU

Painosalama, Turku, Finland 2021

ISBN 978-951-29-8626-2 (PRINT)
ISBN 978-951-29-8627-9 (PDF)
ISSN 0355-9483 (Print)
ISSN 2343-3213 (Online)